Combined fMRI and Electrical Microstimulation to Determine Functional Connections in Visual Areas of the Primate Brain

by

Leeland Bruce Ekstrom

B.Sc., Engineering Physics, Queen's University, 2002
B.Sc., Life Sciences, Queen's University, 2003

SUBMITTED TO THE HARVARD-MIT DIVISION OF HEALTH SCIENCES AND TECHNOLOGY AND DEPARTMENT OF NUCLEAR SCIENCE AND ENGINEERING IN PARTIAL FULFILLMENT OF THE REQUIREMENTS FOR THE DEGREE OF

ARCHIVES

DOCTOR OF PHILOSOPHY IN HEALTH SCIENCES AND TECHNOLOGY

AT THE
MASSACHUSETTS INSTITUTE OF TECHNOLOGY
FEBRUARY 2009
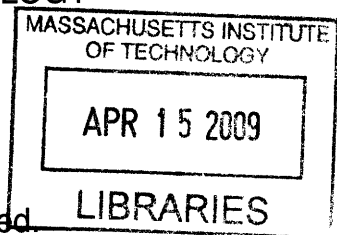
© Massachusetts Institute of Technology, 2009. All rights reserved.

Signature of Author: ___
Harvard-MIT Division of Health Sciences and Technology
Department of Nuclear Science and Engineering
November 5, 2008

Certified by: ___
Wim Vanduffel, Ph.D.
Assistant Professor in Radiology, Harvard Medical School
Thesis Supervisor

Certified by: ___
Alan P. Jasanoff, Ph.D.
Associate Professor of Biological Engineering, Nuclear Science & Engineering and Brain & Cognitive Sciences
Thesis Reader

Accepted by: ___
Director, Harvard-MIT Division of Health Sciences and Technology

Accepted by: ___
Jacquelyn C. Yanch, Ph.D.
Chair, Nuclear Science and Engineering Committee on Graduate Students

Combined fMRI and Electrical Microstimulation to Determine Functional Connections in Visual Areas of the Primate Brain

by

Leeland Bruce Ekstrom

Submitted to the Harvard-MIT Division of Health Sciences and Technology and
Department of Nuclear Science and Engineering on November 5, 2008,
in partial fulfillment of the requirements for the degree of
Doctor of Philosophy in Health Sciences and Technology

Abstract

The use of functional magnetic resonance imaging (fMRI) to study the non-human primate brain has been developed over the past decade. Primate fMRI has many attractive features: it allows validation of previous homology assumptions between humans and monkeys, provides a model to combine imaging with invasive techniques to directly manipulate the brain, and can guide other modalities, such as electrophysiology, to new areas of interest.

The frontal eye field (FEF) is a well-studied node in the oculomotor network, involved in visual target selection and saccade planning. Recent evidence has implicated FEF as a possible source of feedback signals that modulate visually-driven activity in posterior cortical areas, such as during the deployment of spatial attention. The goals of this thesis were extend the unique aspects of primate fMRI by combining it with simultaneous, intracortical microstimulation (EM), and to use these new methods to measure how local, artificially-increased FEF output could modulate visually-driven fMRI activity in earlier cortical regions.

The first outcome of this thesis was a novel form of functional tractography. FEF-EM below the threshold needed to evoke saccades yielded robust, focal fMRI activity in cortical and subcortical structures connected with FEF. The second outcome was a demonstration that sub-threshold FEF-EM produced retinotopically-specific enhancement and suppression of the representation of a stimulus presented at the saccadic endpoint, or movement field (MF), of the stimulated FEF site. Modulation occurred at multiple levels of the visual system and the signals presumably causing it appeared to be gated in the earliest cortical areas by bottom-up activity.

The third outcome was a characterization of how stimulus intensity altered these modulations. The luminance contrast of a stimulus presented in the MF was systematically varied to generate contrast response functions for many cortical areas, which were compared with existing data. Sub-threshold FEF-EM increased fMRI activity for the lowest contrasts and had little or even a suppressive influence at the highest contrasts, mainly in support of a contrast rather than activity gain effect. From these data, a simple spatial model explaining the interaction between bottom-up and top-down signals from the FEF was constructed, which could guide future psychophysical and electrophysiological experiments.

The final outcome was a demonstration that artificially-increased FEF output could alter stimulus selectivity in visual cortex independent of stimulus saliency. This suggests that FEF relays not only spatial but also feature-relevant information to specific visual cortical areas.

Supervisor: Wim Vanduffel, Ph.D.
Title: Assistant Professor of Radiology, Harvard Medical School

Acknowledgements

Looking back on the past 5+ years, I am amazed at how fast the time has elapsed and how many different memories and experiences have filled it. I remember thinking during that first semester at MIT that the concept of effectively writing a small book was incredibly intimidating and that I had no idea how I was going to produce a completed dissertation. As the years passed though, the intimidation subsided and particularly in the past few months I have been amazed at how the pieces have come together to generate this text.

The work presented in this thesis would simply not have been possible without the resources, ideas and team put in place by my adviser, Wim Vanduffel. Wim, over these years you have taught me how to hypothesize, analyze and criticize, and shared your great love of experimental neuroscience with me – for these lessons I am grateful. I have learned a tremendous amount about the primate brain and how to image it from you, and though I will not miss all of it (particularly the experiments that ended in the middle of the night), I will look back very fondly upon most of it. I also thank you for your patience and support during my various activities outside the lab. I have met many colleagues who were fearful of discussing such things with their advisers or of getting involved in extracurricular pursuits and invoking an adviser's wrath. With the environment you created in the lab, I never faced that and as a result have had an even more enjoyable and rewarding grad school experience.

Participation on a thesis committee seems not to garner many thanks from other sources, so I would like to acknowledge and thank each of the members of mine, Bruce Rosen, Alan Jasanoff and Chris Moore. Bruce, you were my first point of contact with the Martinos Center (not sure if you recall our first meeting in the summer of 2003, when I had no idea what research I wanted to pursue other than a vague notion of 'something that tied together physics, engineering and the life sciences'), helped me identify Wim as a supervisor and have been a trusted mentor through all stages of my Ph.D. since then. Alan, I am not sure I can count how many times you have had to listen to me present this material in departmental seminars, yet each time you had insightful questions or feedback and have been a great help navigating departmental requirements. Chris, you have added tremendous value to this thesis and the publication(s) that emerged from it with the conversations we have had, and I will keep my promise to remain informed of the goings on in the MIT neuroscience community going forward.

Anyone familiar with experimental monkey neuroscience knows that this work is not possible in isolation and so I would like to thank the entire monkey and magnet teams in Charlestown. Helen Deng has been absolutely essential to the success of this project, with seemingly tireless training of all the guys. John Arsenault, Timo van Kerkoerle, Mark Khachaturian, Bechir Jarraya, Reza Rajimehr, Hauke Kolster, Giorgio Bonmassar, Joe Mandeville, Francisca Leite, Kathryn Devaney, Natalia Bilenko, Justin Vincent, Tamara Knutsen, Roger Tootell and Dave Tuch have all contributed in ways both large and small (mostly large). Larry Wald and the rest of the folks in the Coil Lab have been invaluable, as has Gunjan Madan, who saved many a scanning session by diagnosing scanner problems over the phone, and the rest of the support and office staff that make the Martinos Center work (I will particularly note Linda Butler and Larry White, but there are many others). I take away fond memories of the other grad students, post-docs, RAs and lunch-list participants at the Center; some are already listed above, but other include Cherif Sahyoun (keep working on your monkey calls), Adrian KC Lee, Div Bolar, Thomas Witzel, Danny Joseph, Megan Hepler Blackwell, Jeremy Young and Anand 'too much work' Kumar, along with many more than space allows me to mention. Tom (MM1) and Dale (MM2) have been perhaps the most essential of all at CNY, and so I thank them too.

My time at MIT has been – in a word – incredible, and I am grateful for my years at the Institute. In large part, this is due to the rich mosaic of friends I have met and interacted with through classes, graduate housing and extracurricular activities. In my early years, I was fortunate to meet a fantastic group of people, including Kelly Klima, Bill Nadir, Paul Mitchell, and Mike Rinehart, who each contributed to the time passing so quickly. More recently, I have been fortunate to acquaint myself with Bruce Cameron, Neville Sanjana, Lucy Wong, Ankur Mani and Ron Tharp, who have each made the MIT experience memorable in multiple ways. I would like to thank my fellow members of graduate lunch seminar, Alex Ince-Cushman, Jamie Yang, Michael Henry and Johnathan Hodges, and hope that we can still gather at Sunny's occasionally, post-MIT. The time (perhaps too much time…) I spent working for the Graduate Student Council has taught me much about myself and about leading people, and afforded me an amazing view of the inner workings of MIT; I will hold those memories among my most cherished. There are too many from my GSC time to thank individually, so I will acknowledge my fellow officers, Johnna Powell, Oaz Nir and Mireille Akilian directly (the next time we dine

together, we will get something other than cheap takeout), and the rest of the friends, MIT Faculty, Administrators and Staff I met through the Council corporately.

The last group I must thank is the support network I have leaned most heavily upon these MIT years, and that is my family and my girlfriend. To my parents, Don and Wendy, you have been a wonderful source of inspiration from an early age, encouraging me to ask questions and undertake 'research projects' if you did not know the answer. You have nurtured my talents, always pushed me to produce the best work I am capable of and listened patiently while I explain why exactly we put monkeys in a scanner (and no doubt attempted to give that same explanation to curious / confused relatives and friends back home). Thank you for all the gifts you have given me. To my sister, Sherry, I occasionally like to think that I inspired you to a career working with animals, but if the truth is known you have shown those tendencies for as long as I can remember. I thank both you and Brad for your encouragement and support and hope that I can offer the same as you complete your studies. Lastly, to Sabrina, you have contributed the most to my personal success in this work and I am so glad that you have participated in this journey with me. You have been incredibly patient and supportive with all the late night experiments (and email-athons), an eager discusser of things scientific (both our own work and topics more general) and a fantastic dinner co-chef and companion; I am grateful for all these roles you have played.

I do not know exactly where the road ahead leads, but I am excited to find out.

Cambridge, MA
November, 2008

Contents

List of Figures

eye trace, and **(G, H)** mean vertical eye trace for MM2. The solid red line plots mean eye position across all sessions and contrasts during VEM and V epochs; the dashed black lines show +/- SEM across the four electrodes stimulated. Traces have been aligned to EM onset (VEM) or the matching time in epochs without stimulation (V); total duration of FEF-EM is indicated by the lower, dark grey bar (250 ms). The upper, light grey bar indicates the period of visual stimulation (VEM, V); visual onset, at -133 ms relative to EM onset, is not shown. Any run showing a significant difference between the two conditions at any time point was removed ($P > 0.05$, corrected for multiple comparisons across time points; two sample, two-tailed t-test across all acquired trials). These mean traces from the included runs show no significant difference at the aggregate level.. 107

signal change values at each contrast level; note the secondary y axis for red. An ROC area of 0.5 means an ideal observer could not distinguish the two distributions; larger deviations reflect greater distinguishability. To generate an ROC value for 0% contrast, all voxel values were shifted about the mean signal value of the voxel (across all conditions) rather than its baseline 0% V signal. Filled / hollow squares below the traces indicate a significant positive / negative interaction between factors EM and V at that contrast with respect to the 0% values, and correspond to the trace of matching color ($P < 0.05$; two-way ANOVA). **(C)** Fractional change in percent MR signal, determined by dividing the difference (black trace) in (B) by the underlying V signal change value. This fraction indicates the effective change in fMRI activity caused by FEF-EM relative to the visual-only activation level. Note that this parameter cannot be calculated for 0% contrast, because the 0% V condition was used as baseline. In all preceding panels, error bars indicate 1 SEM across epochs except for red in (B), which indicate 95% confidence intervals; some error bars are smaller than the symbol used. Note that all preceding x axes use a logarithmic scale. **(D)** ROC curves between the VEM and V MR signal change distributions for each contrast level.

a function of contrast, across both subjects and all visual voxels in the twelve visual areas defined in Figure 4. The mean was weighted by the number of voxels in each region. Vall represents all visual voxels ($P < 0.05$, uncorrected). V_{high} represents the best visually driven voxels ($P < 0.05$, corrected). V_{low} represents all remaining voxels from the visual voxels pool not included in V_{high} (0.05, corrected $< P < 0.05$, uncorrected); on the cortical surface, these voxels are primarily located in annuli surrounding the best driven population. The smooth curves show the best fitting Naka-Rushton model for that population. **(B)** Mean difference between VEM and V conditions in the twelve regions for the three populations identified above. Filled / hollow squares below the traces indicate a significant positive / negative interaction between factors EM and V at that contrast with respect to the 0% values, and correspond to the trace of matching color ($P < 0.05$; two-way ANOVA). **(C)** Fractional change in percent MR signal, determined by dividing the difference in VEM and V epochs by the underlying V signal change value at each contrast level for the three populations. In all panels, error bars indicate 1 SEM across epochs, and some error bars are smaller than the symbol used. Note that all x axes use a logarithmic scale. 127

List of Tables

Chapter 1

1 Introduction

The development of functional magnetic resonance imaging (fMRI) almost two decades ago (Belliveau et al., 1991; Ogawa et al., 1992; Kwong et al., 1992) produced a powerful tool to map functional activity in regions across, though by no means limited to, the human brain. fMRI represented the culmination of more than 100 years of work from the seemingly disparate fields of neuro-vascular physiology and nuclear magnetic resonance imaging to yield a non-invasive, highly repeatable technique that could capture dynamic, high-resolution snapshots of a brain at work.

One of the principal strengths of this tool is the ability to identify distributed functional networks of areas involved in the common processing of a sensory stimulus, a motor task, or a more complex cognitive function. For example within the visual system, fMRI can identify the network of areas responsible for processing and extracting the salient features from a particular visual stimulus presented to a human subject (Tootell et al., 1995). The local and global extent of activation, as well as the relative spatial relationships of these brain areas can be visualized and registered to the underlying anatomical features on a structural magnetic resonance (MR) image. An activation map produced from such a study is largely passive, however. It provides a

picture of the areas involved and, coupled with techniques such as diffusion weighted imaging (DWI), can suggest how these areas are interconnected, but offers little information about how these nodes interact functionally.

A logical next and very important step to unravel the workings of the brain then is to determine how such nodes communicate. Specific questions of relevance include: (i) how is information passed between different nodes in a functional network, (ii) how does a given node modulate activity in other network elements, and (iii) are certain nodes functionally more important, are all weighted equally or are some unnecessary? Computational approaches such as Dynamic Causal Modeling (Friston et al., 2003) and Structural Equation Modeling (McIntosh and Gonazlez-Lima, 1994) are one way to answer such questions. To do so physiologically though, and truly move the study of neural networks beyond something of a black-box or phrenological-like understanding, one needs to interfere with an intact network and determine the impact of this interference upon the remainder of the nodes at the functional, as well as behavioral, level. Example of this approach are already underway using traditional neurophysiological tools, such as recording neuronal signals simultaneously from multiple sites [see [e.g.] (Buschman and Miller, 2007)], electrically stimulating output from one node and recording the effects in other connected regions [see [e.g.] (Moore and Armstrong, 2003)], or transiently or permanently deactivating a particular node and measuring any deficits caused elsewhere in the system [see [e.g.] (Ponce et al., 2008)]. Combining one or more of these invasive techniques, such as electrical stimulation or metabolic deactivation, with functional imaging would further this approach by incorporating the specific advantages of fMRI, allowing the study of multiple nodes simultaneously and eliminating the needle-in-a-haystack problem of isolating distant but connected neurons.

Typically, fMRI has been a non-invasive imaging technique suitable for repeated use in the same subject, which makes it ideal for probing the human nervous system. The recent application of fMRI to other species, and in particular to one of the primary mammalian neurophysiological models of the past century, the rhesus macaque, (Logothetis et al., 1999; Vanduffel et al., 2001; Logothetis et al., 2001a; Tolias et al., 2001; Leite et al., 2002; Vanduffel et al., 2002; Sereno et al., 2002; Brewer et al., 2002; Orban et al., 2003; Fize et al., 2003; Tsao et al., 2003a; Tsao et al., 2003b; Kourtzi et al., 2003; Denys et al., 2004a; Denys et al., 2004b; Orban et al., 2004; Pinsk et al., 2005a; Pinsk et al., 2005b; Nelissen et al., 2005; Kayser et al., 2005; Sasaki et al., 2006; Nelissen et al., 2006; Shmuel et al., 2006; Durand et al., 2007; Hadj-Bouziane et al., 2008; Petkov et al., 2008), has expanded further the already broad spectrum of possible functional imaging experiments. One of the initial outcomes of 'monkey fMRI' was a more accurate comparison of the correspondence between the human and non-human primate nervous systems [[i.e.] clarifying homology issues previously confounded by differences in the technique used (Vanduffel et al., 2002; Tootell et al., 2003)]. Additionally, the combination of monkey fMRI with any of a number of invasive tools has produced exciting results, beyond what is possible in human subjects. Examples of this class of experiments include the localizing of activity for further study with electrophysiological electrodes (Tsao et al., 2006), the measurement of plasticity effects in an intentionally damaged brain (Smirnakis et al., 2005) and the observation of the overall neural response to highly addictive substances (Mandeville et al., 2005; Jarraya et al., 2007). The combination of an invasive tool with fMRI can further yield the ability to perturb, stimulate or disrupt specific nodes and then track the consequences at multiple other sites in the network to determine how these nodes functionally interact. Examples of these invasive techniques include electrical microstimulation (Tolias et al., 2005; Ekstrom et al., 2008;

Moeller et al., 2008) and reversible cortical deactivation through either cooling (Khachaturian et al., 2007a) or a pharmacological agent.

Within the rhesus monkey model, the visual system has historically proven itself a popular target for neuroscientific investigation. Reasons for this popularity include the large percentage (~50%) of the primate cortex involved in visual processing, known functional and anatomical homology with the human brain, the ease with which the system may be driven and the ability of monkeys to learn complex cognitive tasks. A number of visual cortical areas have been functionally defined in both humans and monkeys [see [e.g.] (Felleman and Van Essen, 1991)]. How these visual areas interact with each other and with other non-visual cortical regions remains largely unknown though, and is the subject of much active work across all modalities and both species.

In the visual system, a fronto-parieto-occipital network implicated in spatial attention, initially through the pre-motor theory of attention (Rizzolatti et al., 1987) and later on more generally (Kastner and Ungerleider, 2000; Corbetta and Shulman, 2002; Moore et al., 2003; Hamker, 2005), provides an ideal candidate for the type of multi-modal study proposed here. This network largely overlaps the well studied oculomotor control system, in which the nodes and anatomical interconnections are well known. More importantly, an easily observable behavioral output exists – purposeful saccadic eye movements – which can be used to calibrate any exogenous interference with this network. Spanning diverse cortical locations, spatial attention engages a network of areas including visual, parietal and prefrontal regions thought to be connected by feedforward, feedback and lateral connections. The functionality of all these connections, and certainly that of the feedback and lateral ones, remains poorly understood [though see [e.g.] (Vanduffel et al., 1997; Hupé et al., 1998; Hupé et al., 2001)]. This network

presents a ripe target for fMRI combined with one or more invasive techniques, to both develop

a general methodology for this type of study and to unravel previously unknown neurobiology.

1.1 Thesis Overview

1.1.1 Specific Aims

The overall goal of this thesis was to first develop methods that extended the unique

aspects of a primate functional imaging model and to then deploy those methods to better

understand how different nodes within a specific functional network interact. In particular, the

traditional invasive technique of intracortical electrical microstimulation (EM) was adapted for

simultaneous application during fMRI of an awake, behaving monkey.

To accomplish this goal, two broad specific aims were proposed. The first aim was

technical in nature: to develop a platform for simultaneous EM and primate fMRI. Using

chronically implanted electrodes, the frontal eye fields (FEF) in two awake macaques were

electrically stimulated in a MR compatible manner. Using contrast agent enhanced fMRI at

3.0T, the nodes of the network activated by artificially increasing the output of the FEF in

cortical and subcortical brain structures were identified.

The second aim was applied: to use this unique platform to study a network of areas

implicated in the modulation of incoming visual information. The ability of the FEF to modulate

visual representations in occipital, temporal and parietal cortex in a retinotopically-specific

manner was tested. The effects of manipulating parameters such as visual stimulation-EM

congruency, visual stimulus saliency and the feature information contained within the stimulus

were also explored.

1.1.2 Chapter Outlines

The remainder of this Introduction chapter presents relevant background information, including overviews of the motivations for primate fMRI, the FEF as a component of the oculomotor control system, the use of intracortical EM as a standalone and combination technique and the neural correlates of spatial attention.

Chapter 2 presents the seminal innovations of this thesis, namely the implementation of the simultaneous EM and awake monkey fMRI platform. The methodology employed is first described in detail, and then a series of five experiments presented and discussed. These experiments begin with the effects of FEF-EM alone, yielding a form of *in vivo* tractography or connectography to identify functionally connected nodes throughout the primate brain. Using simple colored gratings, the local and area-wide modulatory effects and specificity of FEF-EM are detailed in the next three experiments for a number of cortical visual areas. Finally, expanding on these initial results, the direct effects of manipulating visual saliency in area V4 are determined in two further experiments by adding distractor stimuli to the contralateral visual field and varying the luminance contrast of the ipsilateral stimuli. The data in this chapter was presented at two Society for Neuroscience Annual Meetings (Ekstrom et al., 2005; Ekstrom et al., 2006) and recently published in the journal *Science* (Ekstrom et al., 2008).

The third chapter expands upon this last set of experiments and data introduced in Chapter 2, by examining the effects of FEF-EM on contrast response throughout the visual system. Visual contrast response functions for twelve visual areas were measured for the first time using fMRI in monkeys. To facilitate comparison with previous studies in both the monkey and human, these data were fit with a common model used to describe contrast response. The effect of stimulating corresponding sites in the FEF on these response functions was also measured in each of these cortical areas, and compared against several proposed models for the

effects of attention in visual cortex. Links to a proposed model of dynamic cortical responses were also made, possibly as a mechanism underpinning the effects of FEF stimulation seen. The data in this chapter was presented at one Society for Neuroscience Annual Meeting (Ekstrom et al., 2007) and will be submitted for publication shortly.

In the fourth chapter, the effects of FEF stimulation on stimuli of vastly different feature content were explored to determine if FEF output could alter stimulus selectivity in addition to modulating spatial locations. Moving, mono-chromatic gratings (as used in Chapter 3) and static, monkey face stimuli were chosen as exemplars known to drive different regions of the visual cortices (i.e. dorsal stream, motion sensitive areas versus ventral stream, object sensitive areas) and positioned at the same spatial location. Modulatory effects were found to vary depending upon the underlying functional sensitivity of the cortical region in which they were observed. Several higher order visual areas were found to exhibit large shifts in selectivity towards their presumably favored stimulus during FEF-EM, while early areas showed very little change. Further, the use of an incongruent or unaligned stimulation condition confirmed the earlier specificity observation. Taken together, these results show that the modulatory effects of FEF output are determined by stimulus location and stimulus content. The data in this chapter is still preliminary and has not yet been presented externally.

The fifth chapter summarizes the findings and implications of this thesis and suggests several possible extensions for immediately continuing this work, on both the imaging front (i.e. combining EM-tractography with other connectivity measures) and the neurobiological front (i.e. validating that these observed modulations have behavioral relevancy by implementing an attention task).

1.2 Background

1.2.1 Motivation for Primate fMRI

The macaque monkey has been one of the workhorses of systems neuroscience for much of the past century. Much of what is currently known about how the primate brain processes sensory information, executes motor commands, and carries out higher order functions has its origins in primate neurophysiology. The rise and maturation of non-invasive neuroimaging technologies, first with electroencephalography and then more recently with magneto-encephalography, positron emission tomography, fMRI and optical imaging techniques, however, has allowed a shift to direct study of the human brain. Given these emerging capabilities, the question of continued and future need for non-human primate models is worth exploring, especially given the not insignificant challenges and ethics of working with them. In broad terms, the capability that non-human primates bring to the above neuroimaging techniques is a bridge to the existing body of neurobiological knowledge and a facilitation of classes of essential experiments that would otherwise be impossible in human subjects. Primate fMRI in particular already offers several compelling examples that illustrate these points.

Questions of homology lie at the base of any use of non-human primate models to understand human neural function, and are a fundamental assumption of past non-human work. Primate fMRI, more than any other technique, provides the opportunity to test such assumptions by allowing the same experiment to be done in both subject populations using the same methodology. Any observed divergences can then be recognized as true homological differences. One example of this direct comparison using fMRI was shown for the processing and reconstruction of three-dimensional shapes generated by motion (Vanduffel et al., 2002). The same visual stimulus package of three-dimensional shapes was shown to both human and

Fig. 1-1: Figures 1A and 2A from Vanduffel et al., (2002). The left cortical surface shows macaque activation to motion-defined, three-dimensional shapes and the right cortical surface human activation to the shape shapes. Early extrastriate areas show very similar activation patterns, whereas areas in the Intraparietal sulcus (IPS, pink dotted region) shows a divergent pattern of activation between species. Reprinted with permission from AAAS.

awake monkey subjects during fMRI acquisition. In this comparison, early extrastriate visual areas showed very similar patterns of activation across species (compare areas V2, V3 and V4 on the two cortical surfaces in Fig. 1-1), but human intraparietal areas showed a number of activations that were for the most part not, or at best barely, found in monkeys (compare purple outlined regions in Fig. 1-1). The common methodological platform allows this divergence to be attributed to a true inter-species difference in visuospatial processing.

The second class of essential experiments that primate fMRI unlocks is the combination of any of the invasive tools previously used in monkey neurophysiology with the neuroimaging platform. As noted above, these experiments are considerably more difficult, and in some cases impossible, to perform in humans, but with monkeys can provide critical insight into the functioning of networks of areas distributed across the brain as well as the mechanisms the underlie neuroimaging itself. One example of this capability is the investigation of reward

encoding and conditioning in the brain using a highly addictive substance (Jarraya et al., 2007), which for obvious reasons is ethically very difficult in a naïve human subject. Following a conditioning paradigm that first paired cocaine with one of two generic stimuli, prominent orbito-frontal activations were later found in response to the conditioned stimulus without drug reinforcement. Over a timecourse of several weeks, this activation could be extinguished and then reinforced, or temporarily quenched with an appropriate antagonistic agent. A simple test of behavioral preference followed this pattern as well, indicating the relevance of these observed activations. The possible clinical implications of this finding, especially in terms of reversing such an addiction, are tremendously exciting.

The combination of primate fMRI and electrophysiological recording has proven particularly fruitful, with two prominent examples demonstrating the utility of these tools together. The question of what exactly the hemodynamic signal of fMRI represents in terms of more traditional neuronal currency, such as the local field potential (LFP) or single or multi-unit firing rates, has existed since the origin of the technique and in many ways remains an open question. Answering it conclusively will have profound implications, given the breadth of fMRI studies now conducted. Logotheis et al., (2001a) put forward one of the most direct attempts to address this issue by recording LFPs and spiking activity from monkey visual cortex while simultaneously collecting high in-plane resolution fMRI of the same area for a direct comparison of the two techniques. They concluded that the blood oxygen level dependent (BOLD) fMRI signal correlated best with LFP activity, and suggested that fMRI therefore best reflects neuronal input and local processing rather than spiking output from a particular area. Though recent studies [(Nir et al., 2007), and see the comment piece (Nir et al., 2008)] have suggested this correlation is more variable than initially presented, the initial study demonstrated well what is

technically possible with primate fMRI and how it can contribute to studying the mechanisms underlying fMRI. Further, the probability of unlocking these mechanisms solely in human subjects is remote, which adds further value to the primate imaging model.

The second prominent primate-electrophysiology study example did not feature the technical challenge of simultaneous fMRI and recording, but rather presented a template for the role fMRI could play for the broader primate neuroscience community. An obvious advantage of fMRI with respect to cellular recording is the ability to survey large swaths of the brain simultaneously, while trading off temporal resolution and measuring only population level responses. Tsao et al., (2006) therefore capitalized on this advantage by first using fMRI to localize face-selective patches in the superior temporal sulcus (STS) of two macaques, and then compensated for those limitations by recording single cell responses within one of the identified patches (Fig. 1-2). They found in their penetrations that 97% of visually responsive neurons were face selective – a level of object selectivity previously unheard of in the relatively heterogeneous inferotemporal (IT) cortex. This use of monkey fMRI as a pilot tool to guide spatially limited techniques to new areas of functional interest shows tremendous potential for investigating the organization of brain regions for which relatively little is known. Further, fMRI could be particularly useful in overcoming the idiosyncratic differences that inevitably exist between primate subjects.
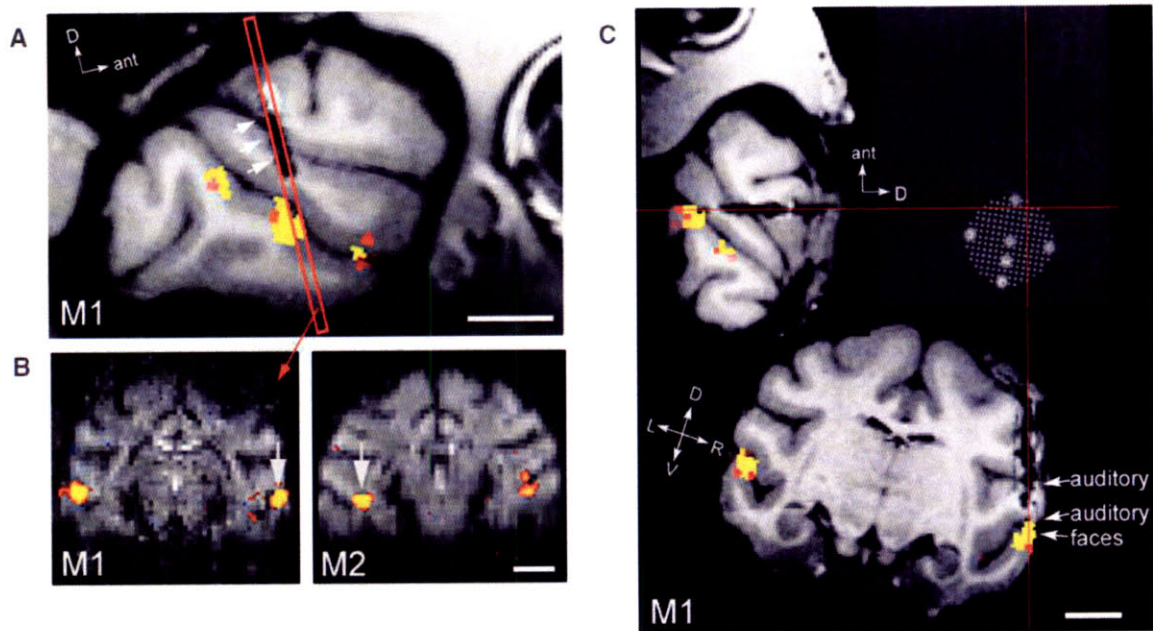
Fig. 1-2: Figure 1 from Tsao et al., (2006). Face selective patches were first identified along the lower bank of the STS using fMRI [raw EPI data in panel **(B)**, fMRI activation overlaid on higher resolution T1 image in panel **(A)**]. The coordinates of the middle activation patch were then transferred to a standard grid in a recording well positioned dorsal to the site of activation **(C)**, and single cell responses to a range of object stimuli recorded to test the degree of selectivity. Electrode penetration tracks are visible in both (A) and (C). Reprinted with permission from AAAS.

Lastly, as discussed above, the ability to interfere with nodes in a functional network should ultimately enable a deeper level of understanding of the interplay between nodes. Within this systems analysis framework, both stimulating and deactivating nodes is necessary to measure their contribution. While permanent deactivation via a lesion is relatively straightforward, the potential confounds of any long term neural or network reorganization would seem to favor a transient lesion technique. The use of intracortical cooling with primate fMRI [Fig. 1-3, (Khachaturian, 2007)] offers such an approach, with the added advantage, compared to pharmacological deactivation, of simultaneously measuring the extent of deactivation with a MR thermometry sequence (De Poorter et al., 1995). Intracortical cooling slows and eventually arrests cellular metabolism (Lomber et al., 1999) to create a confined lesion; rewarming the affected area in principle returns it to function with no permanent damage.
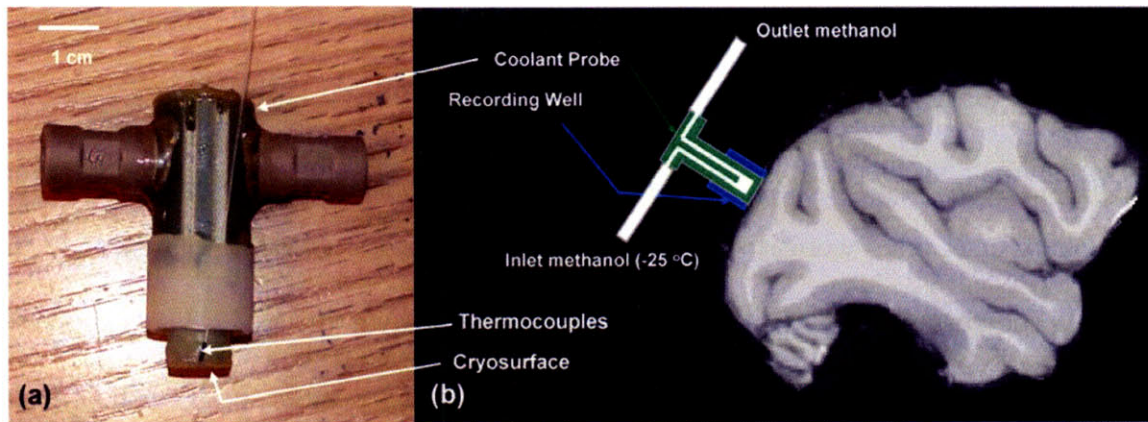
Fig. 1-3: Figure 5-1 from Khachaturian, (2007). A MR-compatible cryo-probe **(a)** was placed in contact with primary visual cortex through a standard recording well **(b)**. Both anesthetized and awake MRI sessions were collected to estimate metabolic contributions to the diffusion-weighted imaging signal and demonstrate proof-of-principle for transient fMRI lesions. Figure reprinted with author's permission.

Khachaturian, (2007) used this technique to estimate the relative contribution of cellular metabolism in diffusion-weighted MR images compared to the passive diffusion of water, and also showed how it could be applied during fMRI acquisition to eliminate visually driven activity. The eventual combination of such a deactivation tool with the stimulation approach described in this thesis would then represent an incredibly powerful technique for investigating neural network function, and primate fMRI is the platform that enables it.

1.2.2 Frontal Eye Fields

The FEF are a well documented component of the oculomotor control network responsible for converting visual information into saccadic motor commands (Schall, 1995). When the primate visual system observes a visual scene the eye-movement strategy employed is active, consisting of a constantly repeated pattern of discrete jumps and transient pauses. These discrete jumps are known as saccades; they are rapid, ballistic shifts in fixation that reorient the fovea, or highest-acuity part of the eye, on objects of interest previously in the retinal periphery (Yarbus, 1961). Specifically, the FEF are thought to be involved in both the selection of relevant

targets in a visual scene and the planning of appropriate eye movements to fixate these targets (Schall, 2002). This contention stands on the presence of both visually responsive and motor signaling neurons in the FEF. Further, these two processes have been shown to occur independently, or in other words that visual target selection does not depend on saccade signal production (Thompson et al., 1997). Ablation studies have shown that the FEF are necessary for saccade production, although such a post-lesion deficit gradually diminishes over time to some degree due to plasticity (Schiller et al., 1987).

In the macaque monkey, the FEF are located in each hemisphere in the prefrontal cortex along the rostral bank of the arcuate sulcus (Schall, 1997), some 2 - 6 mm below the dorsal surface of the brain. This anatomical location makes the FEF relatively accessible for recording and stimulation experiments. Identification is most commonly made in functional terms by defining the cortical region from which saccades can be elicited through low-current electrical stimulation [< 50 µA through acute electrodes (Bruce et al., 1985), somewhat larger values for chronic ones due to the possible growth of fibrous material following implantation (Bartlett et al., 2005)]. Several different topographical organizations have been characterized in the FEF, including maps of visual receptive field eccentricity, receptive field size, and saccade amplitude (Schall, 1997). Rostral to the arcuate sulcus, receptive field eccentricity increases along an axis running from lateral to medial, (Suzuki and Azuma, 1983). Receptive field size roughly follows a similar organization, increasing at more medial locations, though also showing a slight gradient along the caudal-rostral axis (Suzuki and Azuma, 1983). The saccade amplitude map generally mirrors the eccentricity map: stimulating more ventro-lateral regions of the FEF produces short, near-foveal saccades, while moving to more dorso-medial regions gradually elicits longer eye movements (Robinson and Fuchs, 1969; Bruce et al., 1985). A map of saccade direction is not

as readily apparent, but there does appear to be some systematic organization beyond the basic relationship of saccades to the visual hemi-field contralateral to the FEF stimulated (Bruce et al., 1985). The location in visual space to which a saccade is made following stimulation of a particular site in the FEF is defined as the movement field (MF) of that site (Moore and Fallah, 2004).

The anatomical connections of the macaque FEF are well studied and well known, at least in terms of which areas it projects to and which areas project back to it. Broadly, connections to and from FEF can be divided into sub-cortical and cortical. Sub-cortical sites receiving FEF efferents [see (Huerta et al., 1986; Stanton et al., 1988), or (Schall, 1997) for an overview] include all layers of the ipsilateral superior colliculus (though primarily the intermediate layers), the ipsilateral sub-thalamic nucleus and striatum of the basal ganglia, and a number of brainstem nuclei known to be directly involved in saccade production. Reciprocally connected sites within the ipsilateral thalamus include the mediodorsal and ventroanterior nuclei, and to a lesser degree the ventrolateral and pulvinar nuclei.

Cortical sites projecting to and receiving projections from the FEF are numerous and diverse [see (Huerta et al., 1987; Schall et al., 1995; Stanton et al., 1988; Stanton et al., 1995) or (Schall, 1997) for an overview], potentially reflecting its relatively high hierarchical location in common cortical parcellation schemes (Felleman and Van Essen, 1991). Reciprocally connected sites in frontal cortex include the contralateral FEF, the supplementary eye fields (SEF), Broadmann areas 46, 12 and 24, and several pre-motor areas posterior to the arcuate sulcus. Moving caudally, the lateral bank of the intraparietal sulcus (area LIP specificially) is heavily connected in both directions with all parts of the FEF. Other extrastriate areas, however, and particularly those areas with a well recognized retinotopic map show a more segregated

relationship. Foveal regions in areas V4 and MT project mostly to ventrolateral FEF, which represents small visual eccentricities, whereas more peripheral parts of theses areas project dorsomedially; both types of connections are reciprocated. Sites along the superior temporal sulcus (STS) such as MST and FST, and temporal areas TEO and TE project reciprocally to both medial and lateral FEF. Projections to and from FEF have been found as early as V2 and V3, but no connectivity with primary visual cortex itself has been found. In general terms, ventral cortical areas and the lower bank of the STS are more reliably interconnected with ventrolateral FEF, and dorsal / parietal areas and the upper bank of the STS with mediodorsal FEF.

At the cellular level, the FEF is distinguished from regions more anterior by its thinner granular layer 4 (Schall, 1997). Ventrolateral FEF features large pyramidal cells in both cortical layers 3 and 5, whereas layer 3 of dorsomedial FEF has fewer pyramidal cells (Preuss and Goldman-Rakic, 1991). The specific cellular recipients in the earlier visual cortices of the connections described above from these cellular layers are not currently known.

1.2.3 Electrical Extracellular Microstimulation

Electrical stimulation of the brain has existed as an experimental tool in humans since the early part of the 20th century (Penfield and Boldrey, 1937) and in animals for 130 years or more (Ferrier, 1874). In more recent years, the technique of microstimulation has risen to prominence, where the suffix micro implies the ability to focally inject current with high spatial and temporal precision to a specific cortical site (Cohen and Newsome, 2004). The goal of applying localized electrical stimulation to the brain is to increase the output from that region of interest, and examine the causal effects of this artificially increased output on overt behavior or neuronal activity at connected sites. This approach has been successfully used to investigate the modulation and thresholds of visual and somatosensory perception (Salzman et al., 1990; Romo

et al., 1998; Afraz et al., 2006; Murphey and Maunsell, 2007; Murphey and Maunsell, 2008), how higher order cognitive areas read and interpret lower level sensory output (Nichols and Newsome, 2002), and the neural origins of spatial attention (Moore and Fallah, 2004). More recently, microstimulation has been used in combination with fMRI in monkeys as a connectography tool to identify brain regions functionally connected to each other [(Tolias et al., 2005; Moeller et al., 2008), in addition to this thesis]. In the clinic, stimulation of the sub-thalamic nucleus and sometimes the pallidum have been used extensively to treat advanced stages of Parkinson's disease that are no longer responsive to other therapies (The Deep-Brain Stimulation For Parkinson's Disease Study Group, 2001; Benabid, 2003). Electrical stimulation of cingulate white matter tracts ventral to the genu of the corpus callosum has been used to treat intractable depression (Mayberg et al., 2005) and stimulation of the thalamus in a patient in a prolonged vegetative state was shown to improve behavioral responsiveness (Schiff et al., 2007). Admittedly, the mechanisms of these treatments are currently not well understood.

Many other techniques used in neuroscience are correlational: electrophysiological recording, fMRI, and PET for example, can demonstrate a correlation between sensory stimulation, a motor response or a cognitive task and observed neural activity, but conclusive statements about causality are more difficult to make (Cohen and Newsome, 2004). Focal lesions of some portion of the brain and the observation of any resulting defect are one method to make stronger statements. Artificially increasing the output from a particular region via microstimulation is another such method, though any further conclusions about direct or indirect effects cannot be made (that is, whether the specific site of stimulation or some other area functionally connected to it is responsible for the observed effects). This qualification is also necessary because microstimulation has been shown to produce both orthodromic and antidromic

neuronal activation distant to the site of stimulation (Segraves and Goldberg, 1987; Sommer and Wurtz, 1998), which further broadens the candidate regions. As a side note, the non-trivial combination of stimulation with the reversible deactivation techniques described above could provide insight into the specific origin of any observed microstimulation effects.

1.2.4 Measuring Anatomical and Functional Connectivity

A key precursor step prior to measuring functional relationships between topographically separated regions in the brain has been the tracing of anatomical connections and determination of their polarity [that is, in which region the connection originates and in which it terminates; see for example (Huerta et al., 1987; Schall et al., 1995)]. The underlying implication of this pursuit is that regions anatomically wired together share at least some functional connections as well, either passing information along in a feedforward manner or potentially modulating each other's activity in a lateral or feedback arrangement. Tract tracing has traditionally been a histological technique of a very invasive nature. In the most common approach [see any of (Huerta et al., 1987; Schall et al., 1995; Morel and Bullier, 1990)], radioactive tracers, such as a tritiated amino acid, fluorescent dyes, such as fluorogold, or enzymatic tracers, such as wheat germ agglutinin-horseradish peroxidase, are surgically injected into the extracellular space surrounding a site of interest. After a recovery period of several days or weeks during which the tracer is first taken up and then transported to the distal end of the labeled axon, the subject is sacrificed. The brain is removed, sectioned into thin slices (~50 μm) and examined in detail by appropriate staining, ultraviolet illumination or autoradiography. Such a procedure is obviously invasive, time-consuming and ill-suited to any further in vivo experiments following tract tracing.

Diffusion-weighted MRI (DWI) has recently been advanced as a possible non-invasive tool for performing this task. A number of variations of this technique exist, including diffusion

tensor imaging (DTI) (Basser et al., 2000), diffusion spectrum imaging (DSI) (Wedeen et al., 2005) and q-ball imaging (Tuch et al., 2005). All of these approaches capitalize on the ability to sensitize a T2*-weighted image to the local diffusion of water molecules within a tissue, which is thought to be indicative of its microarchitecture [though may also have functional origins, (Khachaturian, 2007)]. DTI measures a voxel-wise tensor form $\hat{D}$ of the diffusion coefficient, and then uses the eigen-structure of that tensor to estimate the most likely tracts using either path extension (Xue et al., 1999) or energy minimization (Poupon et al., 2000) algorithms. DSI was introduced to better distinguish complex crossing patterns and adjacent fibers in axonal tracts by sampling the diffusion signal on a three-dimensional grid and then using a Fourier Transform to recover generalized diffusion probability functions not limited to one principal direction (Wedeen et al., 2005). Q-ball imaging also attempts to resolve these complicated fiber arrangements, but reduces the sampling of the diffusion signal to a single shell or ball to recover an orientation distribution function (direction of diffusion) rather than a full probability function (direction and magnitude of diffusion) (Tuch et al., 2005). While diffusion tractography shows much promise, many questions must still be resolved, such as the underlying mechanisms producing the diffusion signal (Beaulieu, 2002), the resolution of the technique and the exact relationship between diffusion orientation and fiber orientation and a comprehensive validation of all the techniques with known histology (Tuch et al., 2005).

Functional network inferences based on the time series analysis of fMRI data can provide another form of connectivity information. Broadly, this approach involves tracing the propagation of a particular patterned signal throughout out the brain. Some common examples of these techniques include the Bayesian-based Dynamic Causal Modeling (Friston et al., 2003), vector autoregressive modeling using Granger causality (Roebroeck et al., 2005), path analysis

using Structural Equation modeling (McIntosh and Gonazlez-Lima, 1994), non-linear system identification using Volterra series (Friston and Buchel, 2000) and functional correlation analysis in the resting state brain (Biswal et al., 1995). By nature, these techniques are all correlational, and therefore somewhat limited. Further, the exact relationship between these functional measurements and any underlying anatomical wiring has not been systemically explored.

1.2.5 Sources of Spatial Attention

A typical visual scene contains far more information than can be simultaneously processed by the bandwidth-limited primate visual system (Desimone and Duncan, 1995). In other words, not all the information reaching the retina can be equally well processed, perceived and acted upon. Spatial attention is one mechanism used to selectively filter this stream of data, to identify and emphasize behaviorally relevant objects for further examination and action while synchronously suppressing unimportant ones (Moore et al., 2003). Attention can be deployed in both a covert manner dissociated from gaze (that is, the attended object falls in the visual periphery), and a more intuitive overt form, when the attended object falls upon the fovea (Sperling and Melchner, 1978). Ample evidence exists that these two forms do employ similar mechanisms and cortical areas (Corbetta et al., 1998); conceptually however, the covert form is certainly more intriguing. A common analogy used for covert attention is the idea of a mental spotlight that can be moved across the visual scene (Posner et al., 1980); the spotlight may be spatially split but the resources of it appear limited, as attending to one object can reduce the attention that can be directed to a second object (Desimone and Duncan, 1995). In the visual cortices, or at least the extrastriate areas, the effects of this spotlight are a specific enhancement of the neural representation of the visual object attended – in other words, increased visually driven activity at the attended location [(Connor et al., 1997); for review see (Kastner and

Ungerleider, 2000) and (Reynolds and Chelazzi, 2004)]. In addition to physiological effects, linked psychological effects have been demonstrated, such as an increased perceptual ability at the attended location (Carrasco et al., 2004) or an ability to detect stimuli that are below the sensitivity threshold in the unattended condition (Reynolds et al., 2000). The boost in neural activity appears to be responsible for the perceptive enhancements that make attention a plausible filter for behavioral relevancy.

While many theories exist, the neural mechanisms and origins of covert spatial attention have not yet been convincingly elucidated. One line of investigation proposes that a fronto-parietal network of areas that largely overlaps the oculomotor control circuitry is the top-down source for the modulation of sensory information during the attentional deployment. This hypothesis started with the pre-motor theory of attention (Rizzolatti et al., 1987), and has since been expanded and generalized (Kastner and Ungerleider, 2000; Corbetta and Shulman, 2002; Moore et al., 2003; Hamker, 2005), partly on the strength of evidence that saccade preparation and production is not required to covertly orient attention (Juan et al., 2004). Identifying which nodes in the oculomotor network [for an overview see Box 1 of Munoz and Everling, (2004)] are most likely to contribute has not been done systematically, but much recent interest has focused on the FEF. Conceptually, if the goal of a purposeful saccade is to foveate a target of interest and spatial attention is used to identify and enhance an interesting target, then a common role for the FEF in both saccade planning and spatial attention seems quite plausible. Evidence in favor of this function for the FEF include studies showing activation of the FEF during covert spatial attention tasks (Corbetta et al., 1998), the presence of a defined retinotopic map of visual space in the FEF (Bruce et al., 1985), reciprocal anatomical connections from the FEF to extrastriate visual areas known to be modulated by spatial attention (Huerta et al., 1987; Schall et al., 1995;

Stanton et al., 1995) and the role of the FEF in selecting relevant visual targets (Tehovnik et al., 2000; Schall, 2002). While the above examples are exclusively visual, evidence also exists of the involvement of FEF and its homologues in the deployment of auditory attention (Winkowski and Knudsen, 2006), suggesting it may play a more generalized role in the modulation of incoming sensory information.

The most suggestive evidence supporting the FEF's role in visual spatial attention has come from a series of recent microstimulation experiments targeting this region. In one study, microstimulation of macaque FEF below the threshold needed to evoke a saccade was shown to cause perceptive enhancement of visual stimuli during a contrast detection attention task, when the stimulus was positioned in the MF of the FEF site (Moore and Fallah, 2004). In another study, the FEF were again stimulated at a sub-threshold level while electrophysiologically recording the visual response of neurons in area V4 (Moore and Armstrong, 2003). Retinotopically specific modulation of visually driven activity was observed – neural activity in V4 from stimuli in the MF was enhanced while responses from stimuli outside the MF were suppressed. A key feature of attention at the neuronal level occurs when multiple competing stimuli are presented in a neuron's receptive field. Spatial attention has been shown to bias the neuronal response towards the attended stimulus (Reynolds et al., 1999), and sub-threshold stimulation of the FEF has been shown to produce the same effect in V4 neurons (Armstrong et al., 2006). Further, both attention (McAdams and Maunsell, 1999a; McAdams and Maunsell, 1999b) and sub-threshold FEF stimulation (Armstrong and Moore, 2007) have been shown to alter the effective discriminability of two stimuli from V4 neuronal responses in a similar manner. In both cases, the magnitude of the response was increased but no change in the ratio of the response magnitude to variance of the signal, which is a measure of its reliability, was found.

The simultaneous combination of a behavioral attention task with one of these electro-physiological measures during FEF stimulation would provide the most substantive evidence yet of the FEF's role in deploying spatial attention.

In addition to the above body of work, support for the FEF's modulatory influence over visual information comes from studies using trans-cranial magnetic stimulation (TMS) of the human homologue of FEF. Grosbras and Paus, (2002) have shown that applying TMS to the probabilistic location of human FEF facilitated the detection of visual stimuli in the contralateral visual field during an attention task. TMS stimulation of the FEF has been further shown to reduce the threshold of simultaneous TMS stimulation of area V5 (the human homologue of monkey MT) needed to produce phosphenes (Silvanto et al., 2006). This increase in cortical sensitivity appears similar to the changes in V4 neuronal sensitivity thresholds observed in monkeys during an attention task (Reynolds et al., 2000). Examining neuronal activity, the modulatory effects of FEF-TMS on visual event-related potentials seem to temporally resemble the modulatory effects of endogenous covert attention (Taylor et al., 2007). As well, the combination of simultaneous FEF-TMS and fMRI has shown the FEF output can exert a topographic pattern of enhancement and suppression in retinotopically organized cortical areas (Ruff et al., 2006). Ruff et al., (2006) also showed in their study that this change in representation strength translates into a perceived change in stimulus contrast, just as Carrasco et al., (2004) have shown for covert spatial attention.

Prior to this thesis, however, no published reports exist of simultaneous fMRI and the much more precise microstimulation technique in the FEF.

Chapter 2

2 Microstimulation and fMRI

This chapter is based upon:

Leeland B. Ekstrom, Pieter R. Roelfsema, John T. Arsenault, Giorgio Bonmassar, Wim

Vanduffel

The idea of combining EM and fMRI to create a tool for tracing tracts in the brain and investigating functional connections was first suggested by the Tubingen group (Logothetis et al., 2001b; Logothetis and Pfeuffer, 2004), and later demonstrated by them in a limited fashion ([i.e.] connections between V1, V2 and MT) in anesthetized animals (Tolias et al., 2005). One of the principal advantages of fMRI though, is the ability to survey the activity of the entire brain quickly, so expanding this combination to a whole brain scale would seem only logical. Further, the use of anesthetics complicates the study of functional connections, may produce an interaction with the electrical stimulation ([i.e.] shift the stimulation level needed to produce an observable effect away from physiologically relevant values), and precludes the transfer of this

technique to alert animals performing a behavioral task. For these reasons, we pursued the combination of EM and fMRI in awake monkeys, using imaging hardware and parameters that allowed us to capture whole brain volumes.

The site we selected for stimulation, the FEF, carried several inherent advantages for this initial validation of the technique. Proximity of the FEF to the cortical surface simplifies the introduction of stimulating electrodes, be it an acute or chronic preparation. The anatomical connections of the FEF are widespread throughout cortical and sub-cortical structures and are well documented by traditional tract-tracing techniques (Huerta et al., 1986; Huerta et al., 1987; Schall et al., 1995; Stanton et al., 1988; Stanton et al., 1995). Stimulating the FEF produces a readily measured behavioral response – induced saccadic eye movements – that allows a functional confirmation of the intended stimulation site and calibration of the stimulation amplitude used. Finally, as discussed above, oculomotor control circuitry and in particular the FEF has been advanced as once possible source region (Rizzolatti et al., 1987; Hamker, 2005; Moore et al., 2003) for signals involved in the deployment of spatial attention. Further, several elegant models have been proposed requiring initial bottom-up activation to enable these signal in early visual areas (Fukushima, 1988; Grossberg, 1999; Roelfsema, 2006). A causal, gated modulation of visual activity in primate V4 following FEF-EM has previously been shown with electrophysiological recording (Moore and Armstrong, 2003). Given the ample evidence of FEF projections to other retinotopically organized areas in occipital cortex, this area should provide access to a rich network of functional connections for exploration with this new tool set.

The initial aims of this portion of the thesis were to establish the technical platform upon which the remaining objectives would be built and to demonstrate functionally defined tract tracing within a widely distributed but well known network. The working hypothesis was that

network nodes identified by simultaneous microstimulation and fMRI would substantially agree with the known anatomical connections of the FEF. The latter aims of this section were to use this combination of tools to identify, map and modulate a neuronal network implicated in spatial attention. The working hypothesis was that electrical stimulation of the FEF would modulate visually driven activity in multiple areas in extrastriate cortex in a retinotopically specific manner and, particularly in early areas, only in the presence of bottom-up visually driven activity.

2.1 Abstract

The frontal eye field (FEF) is one of several cortical regions thought to modulate sensory inputs. Moreover, several hypotheses suggest that FEF can only modulate early visual areas in the presence of a visual stimulus. To test for bottom-up gating of frontal signals, we microstimulated subregions in the FEF of two monkeys and measured the effects throughout the brain with functional magnetic resonance imaging. The activity of higher-order visual areas was strongly modulated by FEF stimulation, independent of visual stimulation. In contrast, FEF stimulation induced a topographically specific pattern of enhancement and suppression in early visual areas, but only in the presence of a visual stimulus. Modulation strength depended upon stimulus contrast and on the presence of distractors. We conclude that bottom-up activation is needed to enable top-down modulation of early visual cortex and that stimulus saliency determines the strength of this modulation.

2.2 Introduction

Contemporary hypotheses propose that feedback signals from areas in frontal and parietal cortex exert control over the processing of incoming visual information (Rizzolatti et al., 1987; Kastner and Ungerleider, 2000; Corbetta and Shulman, 2002; Moore et al., 2003; Hamker,

2005).   Several models suggest that these signals are gated by bottom-up stimulation

(Fukushima, 1988; Grossberg, 1999; Roelfsema, 2006). In these models, feedback signals only

influence neurons activated by visual input, just as has been observed for attentional effects,

which are known to be strongest for neurons well driven by a visual stimulus (Treue and

Martinez-Trujillo, 1999; McAdams and Maunsell, 1999a; Martinez-Trujillo and Treue, 2004).

No causal evidence exists, however, to support these theories, with the exception of area V4,

where feedback effects evoked by stimulation of the FEF are most pronounced for neurons

strongly activated by a visual stimulus (Moore and Armstrong, 2003). To (i) test these models of

bottom-up dependent gating of frontal signals on a whole brain scale, (ii) investigate the impact

of increased FEF activity on visually driven responses throughout occipito-temporal cortex, (iii)

examine the spatial organization of any observed modulations, and (iv) investigate the effects of

visual saliency on such modulations, we developed a combination of functional magnetic

resonance imaging (fMRI) and chronic electrical microstimulation (EM) in awake, behaving

monkeys.

2.3 Methods

All procedures were approved by MGH's Subcommittee on Research Animal Care

(Protocol #2003N000338) and MIT's Committee on Animal Care, and are in accordance with

NIH guidelines for the care and use of laboratory animals.

2.3.1 Subjects

Two male rhesus monkeys (*Macaca mulatta*; MM1 and MM2, 4-6 kg, 4-5 years old) were prepared for fMRI as previously described and trained for a passive fixation task (Vanduffel et al., 2001). After the monkeys mastered the task (i.e. they achieved accurate fixation performance within a 2 degree by 2 degree fixation window), 26 intracortical microelectrodes were chronically implanted for electrical microstimulation (EM). Based on anatomical MR images, a craniotomy was performed over the right arcuate sulcus, and the dura mater opened. 26 Teflon-coated microwires (25 μm diameter, 90% platinum, 10% iridium) were manually inserted normal to the cortical surface (Mioche and Singer, 1988) along the rostral bank of the arcuate sulcus (~2-6 mm deep). Wire tips were beveled and stripped of ~40 μm of Teflon prior to insertion. The dura was then closed and the bone flap replaced. The microwires were soldered to a magnet-compatible connector, which was then encased in dental acrylic (Fig.
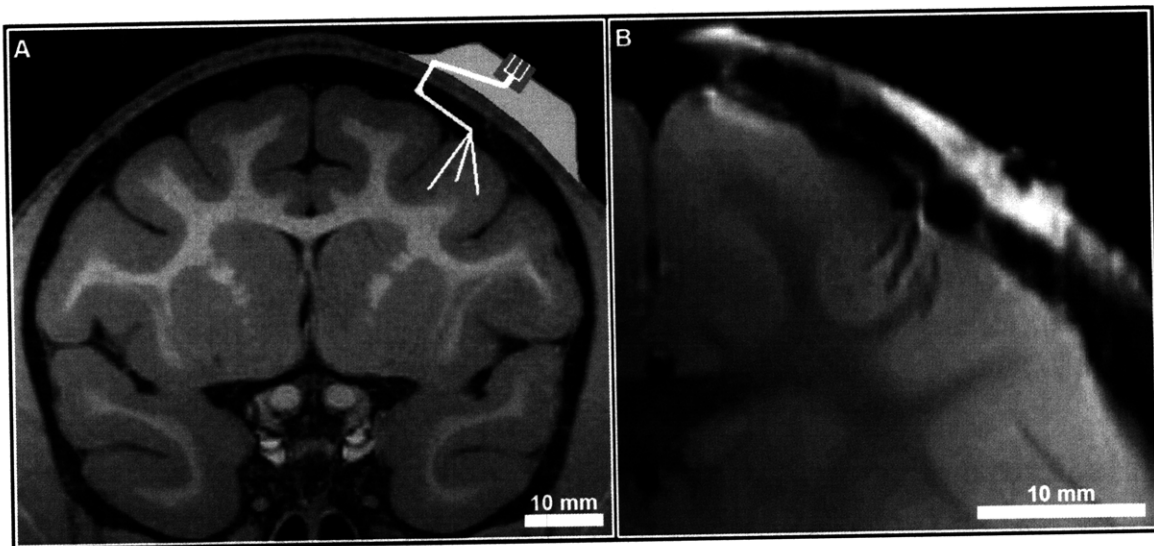
Fig. 2-1: Anatomical location of electrodes. **(A)** Schematic illustration of the approximate location of the chronically implanted electrode wires along with a multi-pin connector superimposed on a T1-weighted image (350 μm isotropic voxels). **(B)** T2-weighted image at 7.0T (0.3 mm by 0.3 mm by 1 mm voxels) showing 3 electrodes in the anterior bank of the superior branch of the arcuate sulcus.

2-1A). A ground electrode was implanted between the skull and muscle and attached to the connector. After surgery, T2-weighted images were collected at 7.0 T (details below) to localize the electrode tips (Fig. 2-1B). Each electrode was also stimulated outside the scanner during a fixation task to identify the movement fields (MFs) and stimulation threshold of the neurons surrounding the individual electrodes (Fig. 2-2).
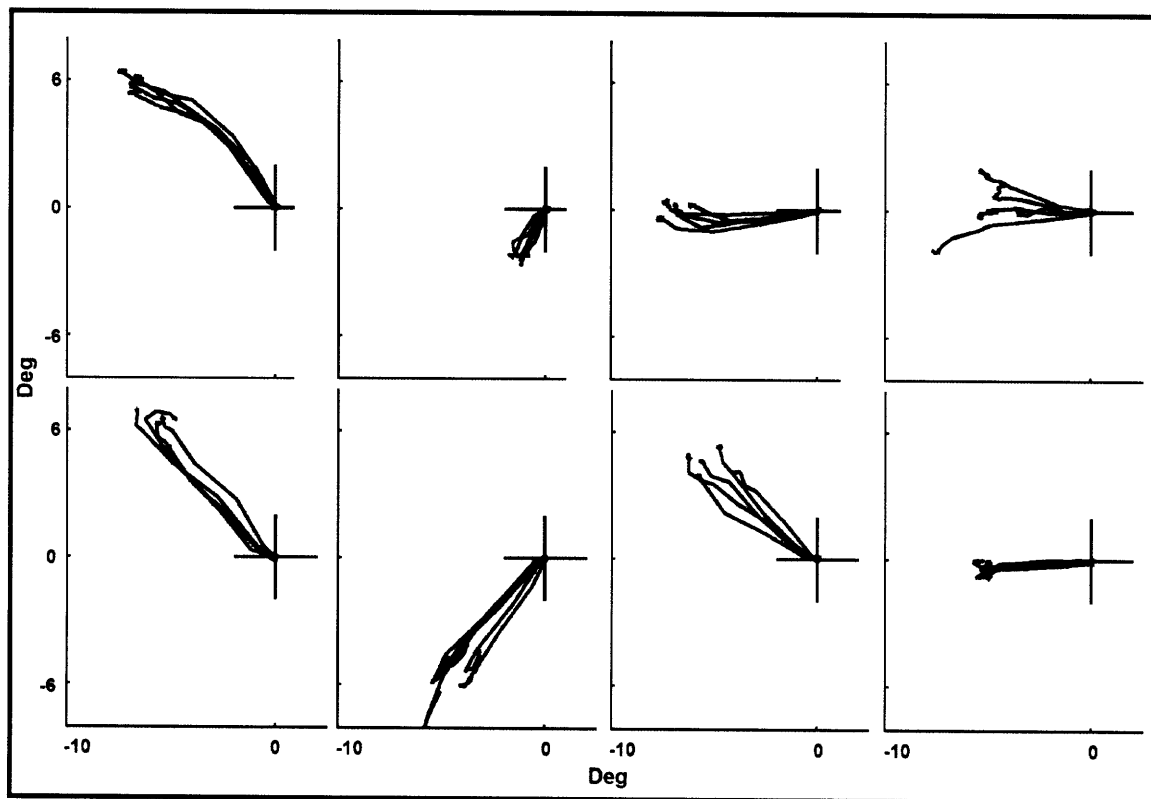
Fig. 2-2: Movement field locations. Example traces of the saccades evoked by supra-threshold stimulation for each of the four electrodes used in MM1 (top) and MM2 (bottom), identifying the movement field of the respective FEF sites and hence the locations of the visual stimuli used.

2.3.2 Microstimulation

The EM signal was produced by an eight-channel Digital Stimulator (DS8000, World Precision Instruments), controlled by custom software that also generated visual stimulation. Stimulation trains lasted 250 ms and were composed of biphasic square-wave pulses with a

repetition rate of 335 Hz, delivered in a monopolar configuration. Each pulse consisted of 190 µs of positive and 190 µs of negative voltage, separated by 100 µs of zero voltage. The sum of the cables' stray capacitance and the monolithic capacitor array EMI filters in the scanner penetration panel ranged from 5.1 to 5.3 nF.

Before each fMRI experiment, the threshold to elicit a saccade was determined inside the scanner for each electrode used by varying the EM amplitude until ~70% of stimulation trains induced a saccade from central fixation. Saccade vectors were calculated to determine the MF of each stimulated FEF site; stimulation was set at ~50% of this behaviorally-defined threshold (Moore and Armstrong, 2003). Also, prior to and after each fMRI session, the impedance of each stimulated channel was measured with a 1V, 100 Hz reference signal to estimate the injected current. For MM1, impedance was 32 ± 4 kΩ, 42 ± 5 kΩ, 54 ± 12 kΩ, and 52 ± 22 kΩ for the 4 electrodes used; for MM2, impedance was 31 ± 16 kΩ, 35 ± 14 kΩ, 48 ± 18 kΩ, and 51 ± 16 kΩ for the 4 electrodes used (mean $\pm$ standard deviation across all sessions). Estimated currents for the four FEF electrodes used in MM1 were 38 ± 11 µA, 38 ± 13 µA, 105 ± 32 µA and 178 ± 43 µA and in MM2 28 ± 11 µA, 29 ± 8 µA, 46 ± 14 µA and 88 ± 29 µA (mean $\pm$ standard deviation across all sessions). It is noted that the currents needed to evoke saccades with chronic electrodes may be larger than those with higher-impedance acute electrodes, most likely because of growth of a fibrous barrier between the electrodes and neural tissue (Bartlett et al., 2005). Finite element simulation showed that gradient switching during MRI scanning barely induced additional currents (Fig. 2-3).
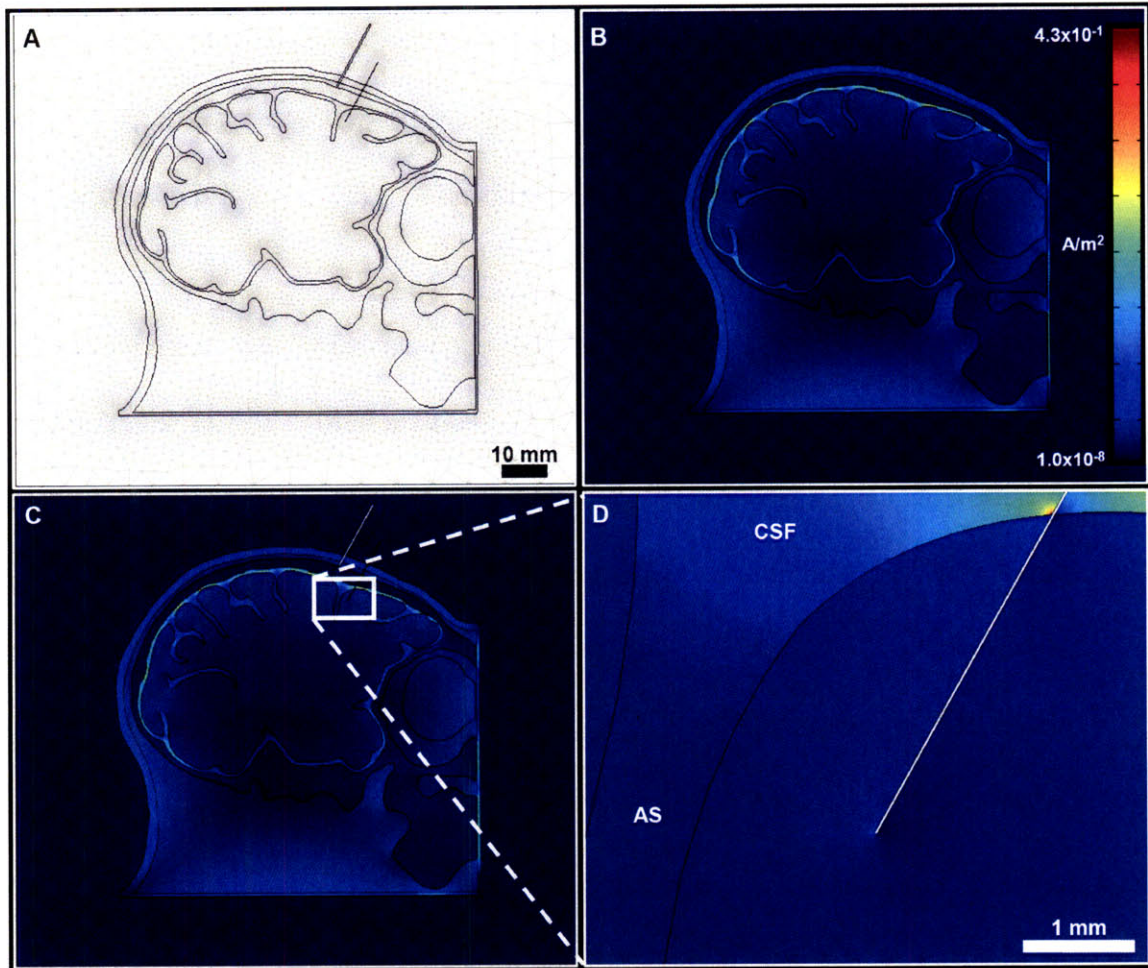
Fig. 2-3: Finite-element model of current induced in electrodes due to switching of the MRI gradient fields. (A) 2-D finite element mesh of sagittal slice of the monkey head, with subcutaneous ground electrode and stimulating electrode positioned in grey matter adjacent to the arcuate sulcus (AS). (B) A finite-element solution showing total current density without electrodes. (C) A finite-element solution showing total current density in the presence of electrodes. (D) Inset [white box in (C)] shows the total current density at stimulating electrode tip (CSF = cerebral spinal fluid).

2.3.3 Functional MRI Acquisition

Functional images were acquired on a 3.0 T head-only scanner with a gradient-echo T2*-weighted echo-planar sequence (55 coronal slices, 64 x 64 matrix, TR = 4 s, TE = 24 ms, 1.25 x 1.25 x 1.25 mm^3 isotropic voxels). Prior to each session, a bolus of Microcrystalline Iron Oxide Nanoparticles (MION; 6-10 mg/kg) in isotonic sodium citrate was injected into the femoral or saphenous vein to increase the contrast-to-noise ratio compared to blood oxygen level dependent

imaging (BOLD) (Vanduffel et al., 2001; Mandeville et al., 2001; Leite et al., 2002). A saddle-shaped, radial transmit-receive surface coil (12 cm diameter) was employed.

Functional images for the luminance contrast variation experiment (experiment five) were acquired on a 3.0 T full-body scanner with a gradient coil insert, using a gradient-echo T2*-weighted echo-planar sequence (50 horizontal slices, 84 x 96 matrix, TR = 2 s, TE = 19 ms, 1 x 1 x 1 mm^3 isotropic voxels). A four-channel phased array coil (individual coils 6 cm diameter), with GRAPPA reconstruction (Griswold et al., 2002) and image acceleration factor of 2, and a saddle-shaped, radial transmit-only surface coil (17 cm diameter) were employed. MION contrast agent was again used.

2.3.4 Anatomical MRI Acquisition

High resolution, T1-weighted anatomical images were collected on a whole-body 3.0 T scanner for the overlay of functional analyses. Under ketamine-xylazine anesthesia (Vanduffel et al., 2001), an MP-RAGE sequence (178 sagittal slices, 256 x 256 in-plane matrix, TR = 2.5 s, TE = 4.35 ms, TI = 1100 ms, 0.35 mm^3 isotropic voxels, flip angle = 8°) was used to obtain 9 whole-brain volumes, which were averaged together to improve the signal-to-noise ratio. A single radial transmit-receive surface coil (12.5 cm diameter) was employed.

T2-weighted images were collected from MM1 on a 7.0 T MRI scanner to assess the location of the chronically implanted electrodes in prefrontal cortex. Under ketamine-xylazine anesthesia (Vanduffel et al., 2001), a turbo spin-echo sequence (22 coronal slices, 256 x 224 in-plane matrix, TR = 3.0 s, TE = 7.7 ms, 0.31 x 0.31 x 1.1 mm^3 voxels, flip angle = 90°) was used to obtain partial brain volumes centered around the arcuate sulcus with a single radial transmit-receive surface coil (4 cm diameter).

2.3.5 EM Paradigm

A block design was used with 32 s long epochs and 8-12 epochs per run (or time series) to measure fMRI activations from FEF-EM only (experiment one), from the interaction of FEF-EM and visual stimuli placed inside and outside the MFs of the stimulated FEF sites (experiments two and three), and from the interaction of FEF-EM and visual stimuli inside the stimulated MFs in the presence of distracter stimuli (experiment four). A block design with 24 s long epochs and 20 epochs per run was used in the contrast variation experiment (experiment five). In total, 102 420 functional volumes were collected from MM1 (49 sessions) and 68 128 functional volumes from MM2 (33 sessions), of which 36 400 and 27 760 volumes (15 sessions in MM1, 11 sessions in MM2) respectively, were used to generate the data shown here. The other sessions were used to optimize the EM paradigm.

In experiments one, two and three, 4 electrodes were stimulated sequentially within a TR (Fig. 2-4 and Fig. 2-5; inter-stimulation interval between consecutive electrodes, ISI = 1 s; ISI for the same electrode = 4 s), with stimulation held constant throughout a session. For experiment four, 2 electrodes were stimulated twice sequentially within a TR (Fig. 2-6; ISI = 1 s between consecutive electrodes; ISI = 2 s for the same electrode). For experiment five, one electrode was stimulated twice within a TR (Fig. 2-4; ISI = 1 s). In experiments two through five, a pseudo-randomized design with multiple stimulus orders was used. Visual stimulation was presented for 133 ms, followed by 250 ms of combined visual stimulation and FEF-EM and then 617 ms with neither (Fig. 2-4 and Fig. 2-6). A central fixation point was continuously present and the monkeys performed a passive fixation task throughout each run. Eye positions were monitored at 120 Hz using an infrared pupil/corneal reflection tracking system. Summary statistics of the quality of fixation (% fixation, saccades / min, mean standard deviation of eye position along the x and y eye axes) for each experiment are given in Table 2-1.
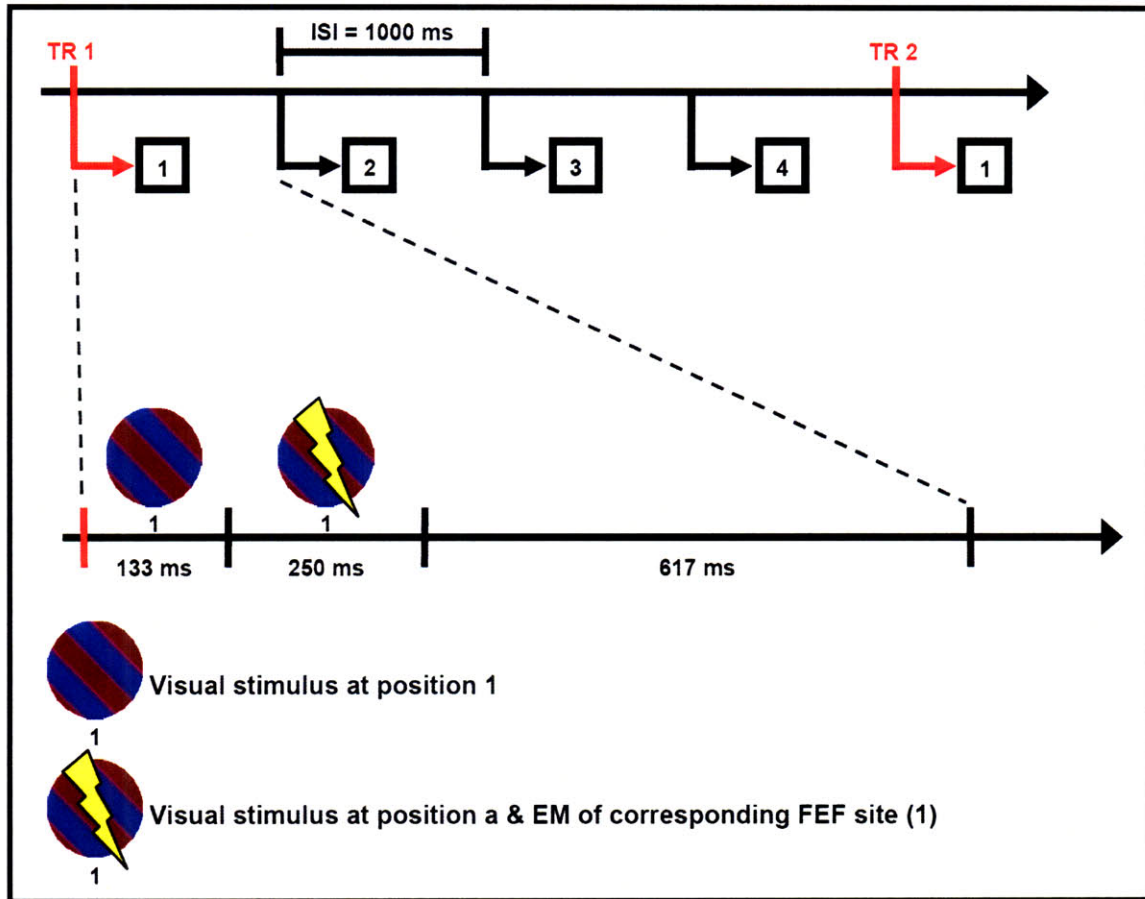
Fig. 2-4: Visual and microstimulation paradigms. In experiment two, 4 stimulation events were used sequentially within a given TR. In epochs of combined visual and EM stimulation (VEM), a visual stimulus was shown for 133 ms, followed by 250 ms of matched visual and FEF-EM and then 617 ms of no stimulation. Note that the lower time line has an expanded time scale and shows one EM and one visual stimulation event. The same timing paradigm was used in visual-only (V) and EM-only epochs, with either the EM or visual stimulation disabled, respectively. In experiment five, only 1 stimulation event was used, and repeated twice, within a given TR (2 s for experiment five).

Visual stimuli were projected at 1024 x 768 resolution and 60 Hz refresh rate from a LCD projector onto a translucent screen 52 cm from the animals' eyes. Stimuli for experiments two through four were 3 deg diameter, red-blue sine-wave gratings with a spatial frequency of 0.5 cycles/deg (mean luminance of red = 105.8 cd/m^2 and of blue = 55.8 cd/m^2) moving at 2 deg/s along one of 4 axes (0, 45, 90 and 135 deg). The background was uniformly gray. In experiment four, 3 distractor stimuli identical to the stimulus presented in the FEF-MF were
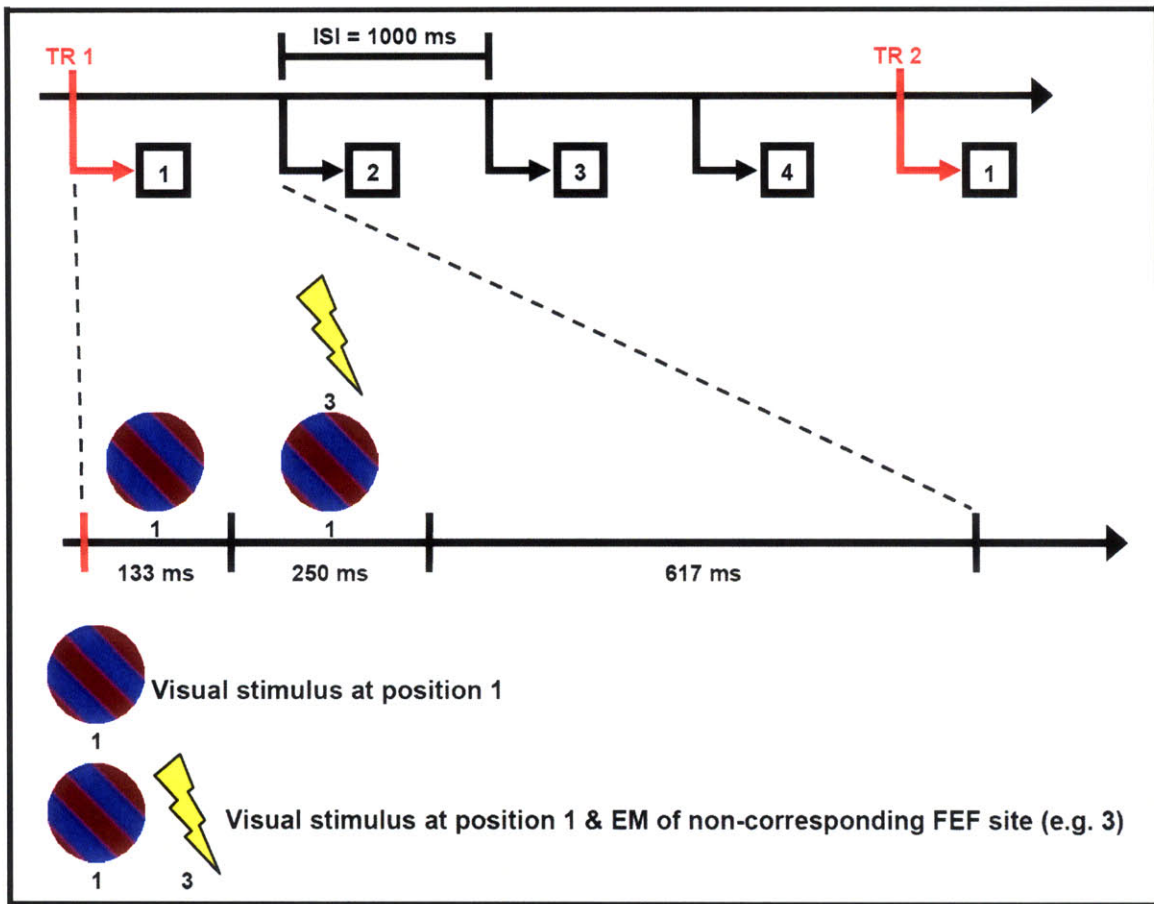
Fig. 2-5: Visual and microstimulation paradigms. In experiment three, 4 stimulation events were again used sequentially within a given TR. Congruent VEM epochs exactly matched that shown in Fig. 2-4. Incongruent (VEM-I) epochs followed the same timing paradigm, except that the visual stimulus was placed in a non-corresponding FEF movement field.

presented for the same 383 ms duration in the contralateral visual field (two at 9 deg eccentricity and at angles of +/- 49 deg from the horizontal meridian, one at 12 deg eccentricity along the horizontal meridian; Fig. 2-6B). For experiment five, stimuli were 6 deg diameter, monochromatic, contrast-varied, sine-wave gratings (3, 6 12 and 50% contrast) with mean luminance matched to the background (76.9 cd/m^2); spatial frequency, speed and direction of motion were as above.
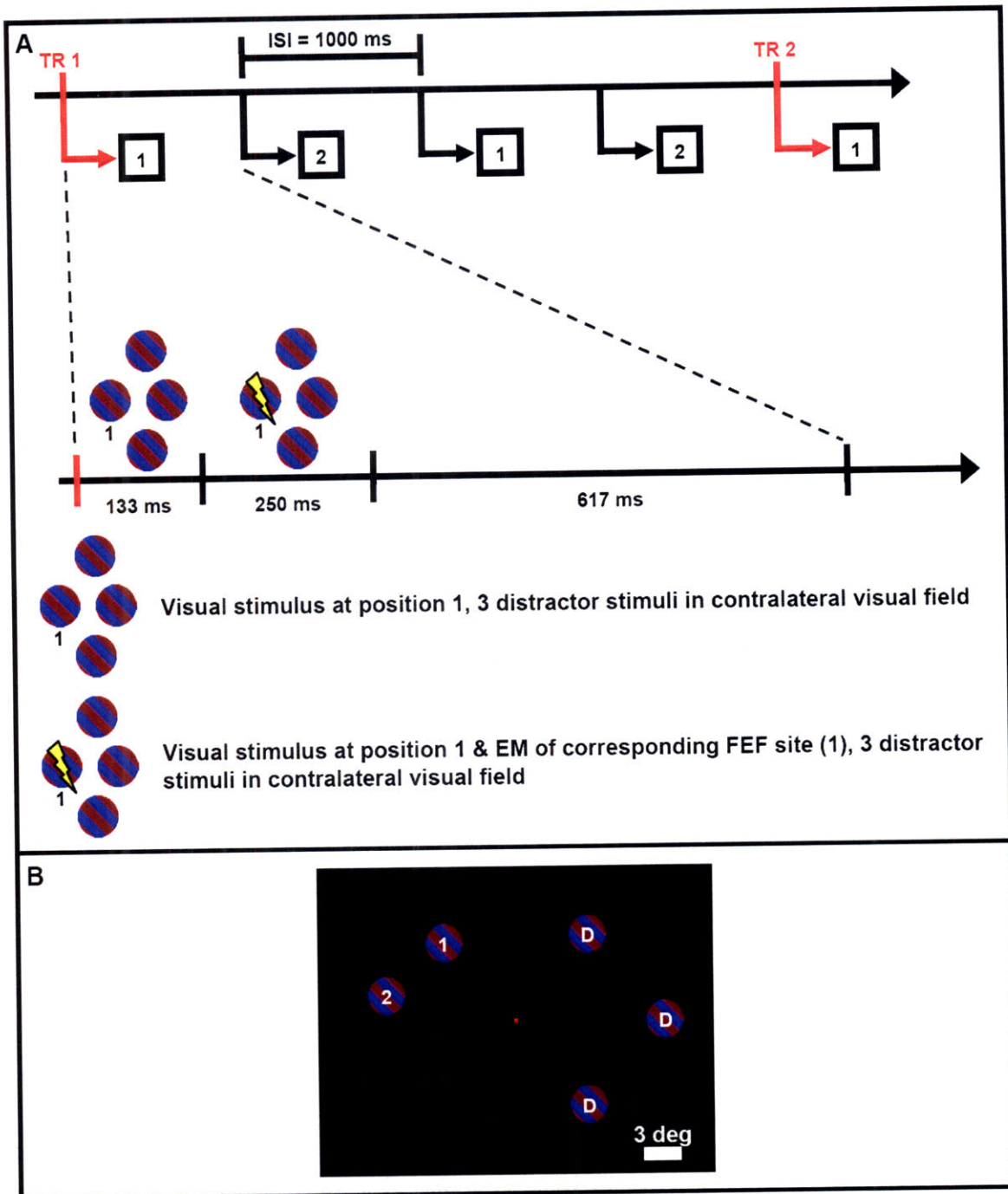
Fig. 2-6: Visual and microstimulation paradigm with distractor stimuli. **(A)** In experiment four, 2 stimulation events were used sequentially within a given TR and repeated (that is, 1-2-1-2); otherwise the V and VEM epochs matched those in experiment two (Fig. 2-4). During epochs with distractors (VD, VDEM, D), 3 contralateral stimuli were presented for the same duration as the single stimulus in the FEF MF. Note that the lower time line has an expanded time scale and shows one EM and one visual stimulation event. **(B)** Location and sequence of visual stimuli presented.

Table 2-1: Fixation behavior during fMRI runs. n is the number of independent fMRI runs collected for each figure. Percentage fixation was calculated using a 2 degree by 2 degree window; σ_x & σ_y are the mean standard deviation of eye position along the x & y eye axes, across all repetitions of a condition within a given run. A one-way ANOVA on each condition pair found no significance differences ($P > 0.05$) in any of the distributions.

Figure	n	Conditions	% Fixation		Saccades / min		σ_x (deg)		σ_y (deg)	
			Median	p	Median	p	Median	P	Median	p
2-14C, D, 17: MM1	65	VEM + F	94.7	0.51	9.8	0.29	0.13	0.80	0.22	0.83
		V + EM	94.6		9.8		0.13		0.22	
2-14D, 16, 17: MM2	65	VEM + F	96.0	0.63	7.5	0.32	0.15	0.58	0.22	0.85
		V + EM	96.6		7.5		0.15		0.22	
2-18, 19	59	VEM	88.8	0.07	13.1	0.81	0.17	0.05	0.28	0.11
		VEM-I	90.9		13.1		0.16		0.27	
2-20A	53	VDEM + V	93.4	0.48	9.4	0.33	0.15	0.49	0.26	0.47
		VEM + VD	93.3		9.8		0.14		0.27	
2-20B: MM1	73	VEM	87.5	0.55	9.8	0.44	0.20	0.19	0.34	0.82
		V	86.3		10.3		0.19		0.34	
2-20B: MM2	88	VEM	87.5	0.33	10.9	0.96	0.25	0.81	0.39	0.69
		V	86.4		11.3		0.25		0.39	

2.3.6 Statistical Analysis

A voxel-based analysis was performed using SPM99, following previously described procedures to fit a general linear model (GLM) (Vanduffel et al., 2001; Leite et al., 2002; Friston et al., 1995; Vanduffel et al., 2002). Images were motion-corrected within session and non-rigidly co-registered to each subject's own anatomical template using Match software (Chef d'hotel et al., 2002). After sub-sampling to 1 mm^3 isotropic voxels, images were smoothed (Gaussian kernel, $\sigma = 0.67$ mm) and registered using Match to MM1's T1-weighted anatomical images. Global scaling, and high- and low-pass filtering were employed prior to fitting the GLM (Vanduffel et al., 2001; Vanduffel et al., 2002).

To account for head and eye movement-related activity, covariates of no-interest from the motion realignment parameters and eye traces were used. Eye traces were thresholded, convolved with the MION hemodynamic response function, and sub-sampled to the TR. To assess the potential effects of eye movements on fMRI activation, we performed a one-way ANOVA on the eye traces to test for any significant differences in fixation percentage, saccade rate, and eye position along the x and y axes between the pairs of conditions shown in Table 2-1. We also plotted the mean eye position aligned to EM onset in these same condition pairs (Fig. 2-7 and Fig. 2-8).

In experiment two, conjunction analysis (Nichols et al., 2005) was used to identify regions that displayed visually driven activity and a significant interaction between visually- and EM-driven activity ($P < 0.05$, conjunction). To increase statistical power, we used the main visual effect (that is, VEM + V versus EM + F; see Fig. 2-14C and Fig. 2-16)) in our conjunction analyses. In experiment three, conjunction analysis (Nichols et al., 2005) was used to identify regions that displayed visually driven activity and a difference in response between congruent (VEM) and incongruent (VEM-I) epochs ($P < 0.05$, conjunction). t-score maps from both monkeys were thresholded [see figure legends for the thresholds used; correction for multiple comparisons was done where noted, using the Family-Wise Error procedures in SPM99 (Worsley et al., 1996)] and overlaid on MM1's T1-weighed anatomical images, which were reconstructed with FreeSurfer (Dale et al., 1999). Flattened cortical representations were created with Caret using the F99 atlas (http://brainmap.wustl.edu/caret, http://brainmap.wustl.edu:8081/ sums/directory.do?id=636032) (Van Essen et al., 2001). Retinotopic mapping data previously collected in three animals was warped to MM1's T1 anatomical space to label borders between early visual areas (Fize et al., 2003).
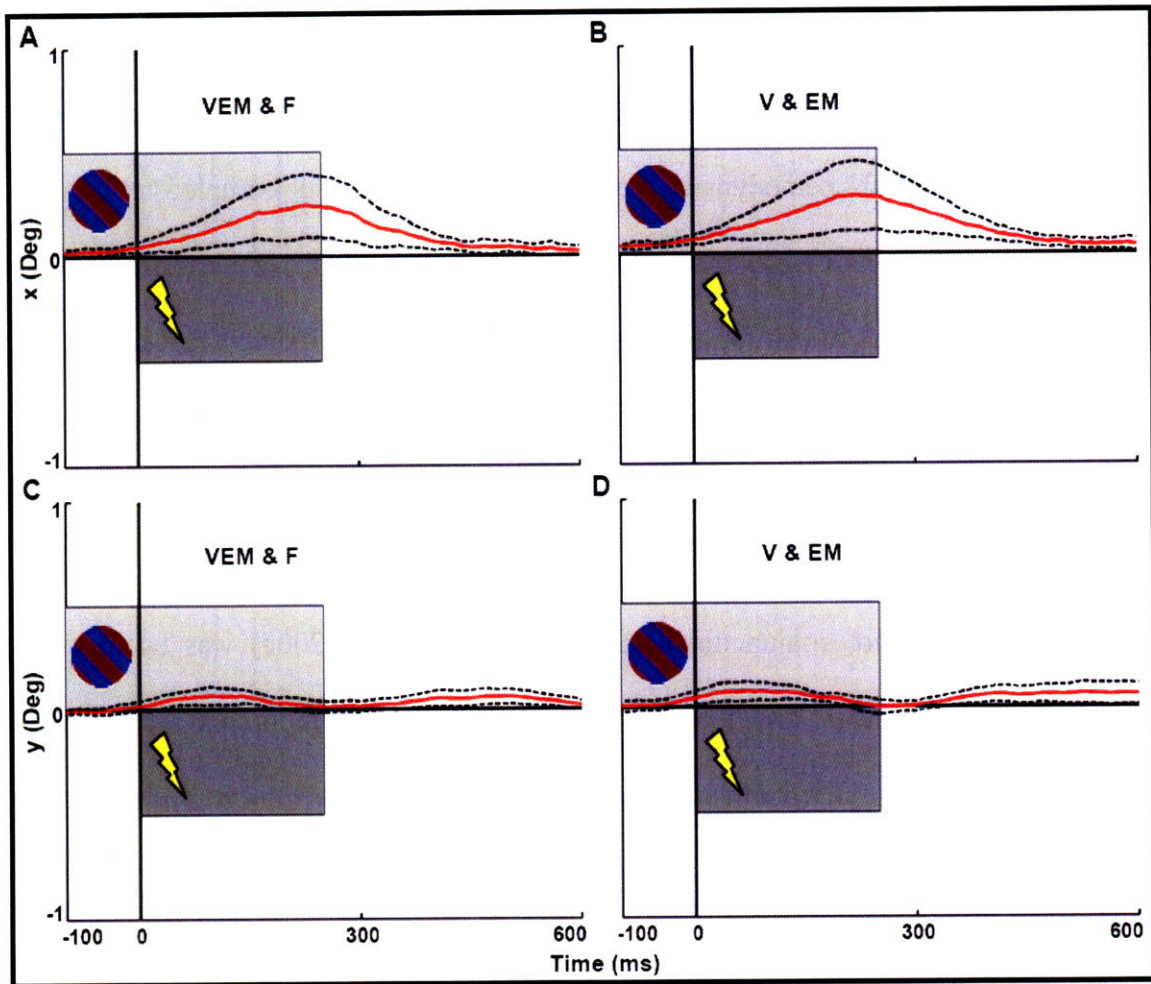
Fig. 2-7: Average horizontal eye position (MM1) during VEM and F epochs **(A),** and during V and EM epochs **(B)**, which represent the condition pairings in the interaction analysis (Fig. 2-14C); **(C)** and **(D)** show the average vertical component during these same epochs. The solid red trace plots mean position and the dashed black lines show +/- SEM across the four electrodes stimulated during the 4 s TR (see Fig. 2-4). Traces have been aligned to EM onset (VEM, EM), or the matching time in epochs without stimulation (V, F); total duration of stimulation is indicated by the lower, dark grey bar (250 ms). The upper, light grey bar indicates the period of visual stimulation (VEM, V); visual onset, at -133 ms, is not shown. No significant difference was found between the mean VEM and F trace and the mean V and EM trace at any time point ($p > 0.05$, corrected for multiple comparisons across time points; two sample, two-tailed t-test across all acquired trials).

2.3.7 Activity Time Courses, Scatter Plots and Activity Profiles

Time courses of percentage change in MR signal (Fig. 2-9C) were calculated with SPM99 by taking a mean over the local t-score maximum and all supra-threshold voxels

bordering the maxima (3-7 voxels total). The borders of 12 visual areas were identified on the flattened cortical representation of MM1 using previous retinotopic mapping data (Fize et al., 2003) and a Caret Atlas based on previous studies (Felleman and Van Essen, 1991; Ungerleider and Desimone, 1986b). Voxels of interest inside these areas were identified and the percentage change in MR signal sampled with SPM99 to generate scatter plots (Fig. 2-14, Fig. 2-17, Fig. 2-18 and Fig. 2-19) and mean signal change values (Fig. 2-13 and Fig. 2-20). To again increase statistical power, in experiment five we used the main visual effect at 50% contrast (that is, 50% VEM + 50% V versus 0% VEM + 0% V) as a localizer to identify voxels for analysis at all contrast levels. In experiments one through four, the first 2 TR in each epoch were excluded to account for the hemodynamic delay of the fMRI signal; for experiment five, the first 3 TR in each epoch were excluded and an additional TR was appended at the end. Standard error of the mean was calculated over the condition epochs.

2.3.8 Finite Element Simulations

Two-dimensional finite element modeling using FEMLAB was used to simulate the effects of switching the magnetic field gradients and estimate what current could be induced in the electrodes during scanning. A manually-segmented head model was generated from T1-weighted anatomical images and filled in using the conductivity and permittivity of ten materials (muscle, eye, bone, brain, CSF, skin, air, platinum, iridium and copper) (Gabriel et al., 1996; CRC Handbook, 2006). One simulation was completed without electrodes, and a second simulation with an electrode in the arcuate sulcus and a sub-cutaneous ground electrode. Current density was calculated by solving Maxwell's equations for a magnetic field of 0.08 T varying sinusoidally at 2.5 kHz along an axis perpendicular to the sagittal plane, simulating a frequency or phase-encoding gradient.
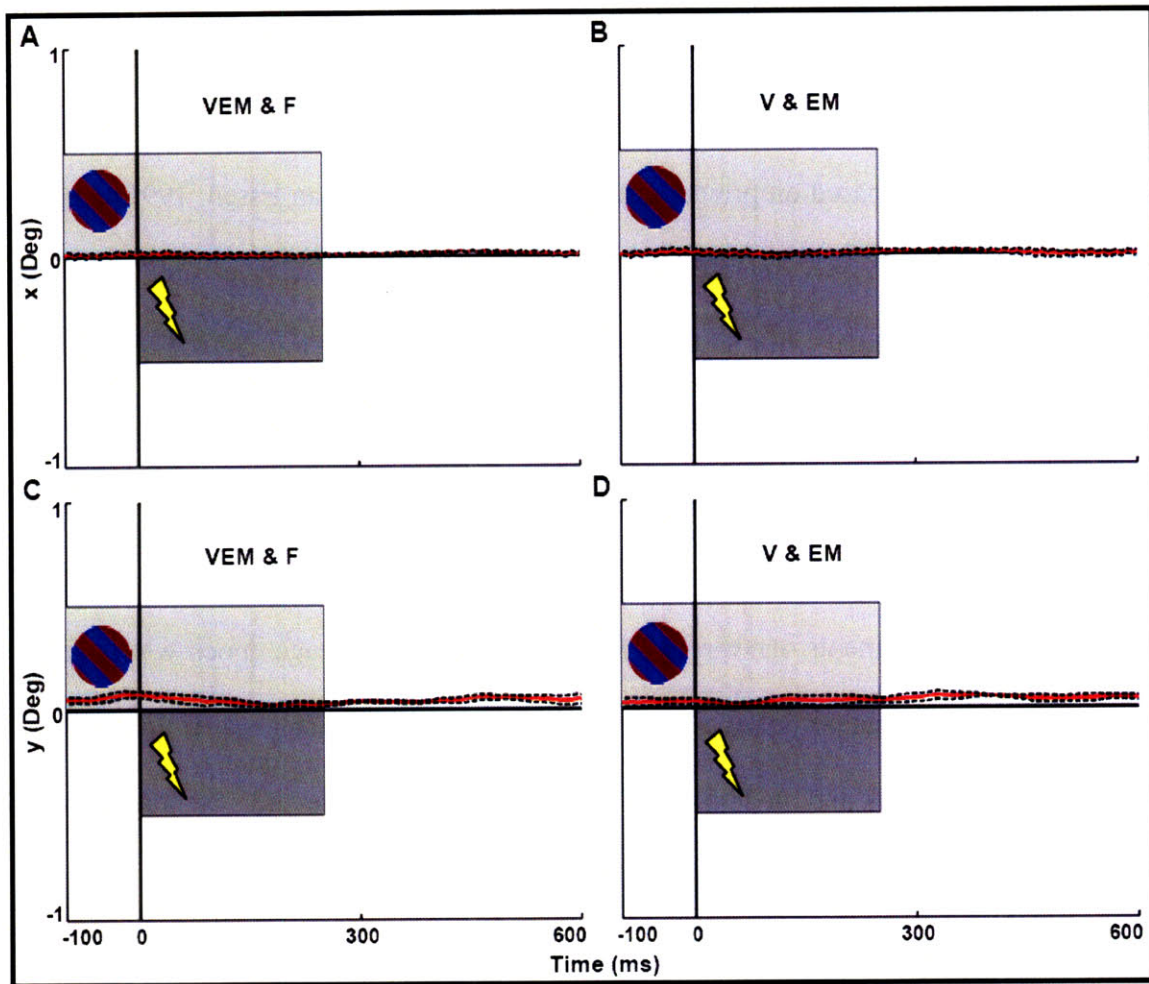
Fig. 2-8: Average horizontal eye position (MM2) during VEM and F epochs **(A),** and during V and EM epochs **(B)**, which represent the condition pairings in the interaction analysis (Fig. 2-14C); **(C)** and **(D)** show the average vertical component during these same epochs. The solid red trace plots mean position and the dashed black lines show +/- SEM across the four electrodes stimulated during the 4 s TR (see Fig. 2-4). Traces have been aligned to EM onset (VEM, EM), or the matching time in epochs without stimulation (V, F); total duration of stimulation is indicated by the lower, dark grey bar (250 ms). The upper, light grey bar indicates the period of visual stimulation (VEM, V); visual onset, at -133 ms, is not shown. No significant difference was found between the mean VEM and F trace and the mean V and EM trace at any time point ($p > 0.05$, corrected for multiple comparisons across time points; two sample, two-tailed t-test across all acquired trials).

2.4 Results

2.4.1 Experiment One – Effects of FEF-EM Alone

In our first experiment, the goal was to detect the functional consequences of EM of the FEF in the absence of a visual stimulus, using stimulation levels below those needed to evoke saccades. We first obtained anatomical (Fig. 2-1B) and behavioral evidence (Fig. 2-2 and Fig. 2-9A) in two monkeys that several chronically implanted microelectrodes were positioned in the FEF. Before each fMRI experiment, we stimulated these electrodes inside the MR-scanner to determine the threshold needed to evoke saccades and to identify the saccade end point, or movement field (MF), of each FEF stimulation site (Fig. 2-2 and Fig. 2-9A). During the actual fMRI experiment, the monkeys carried out a passive fixation task while we alternated between
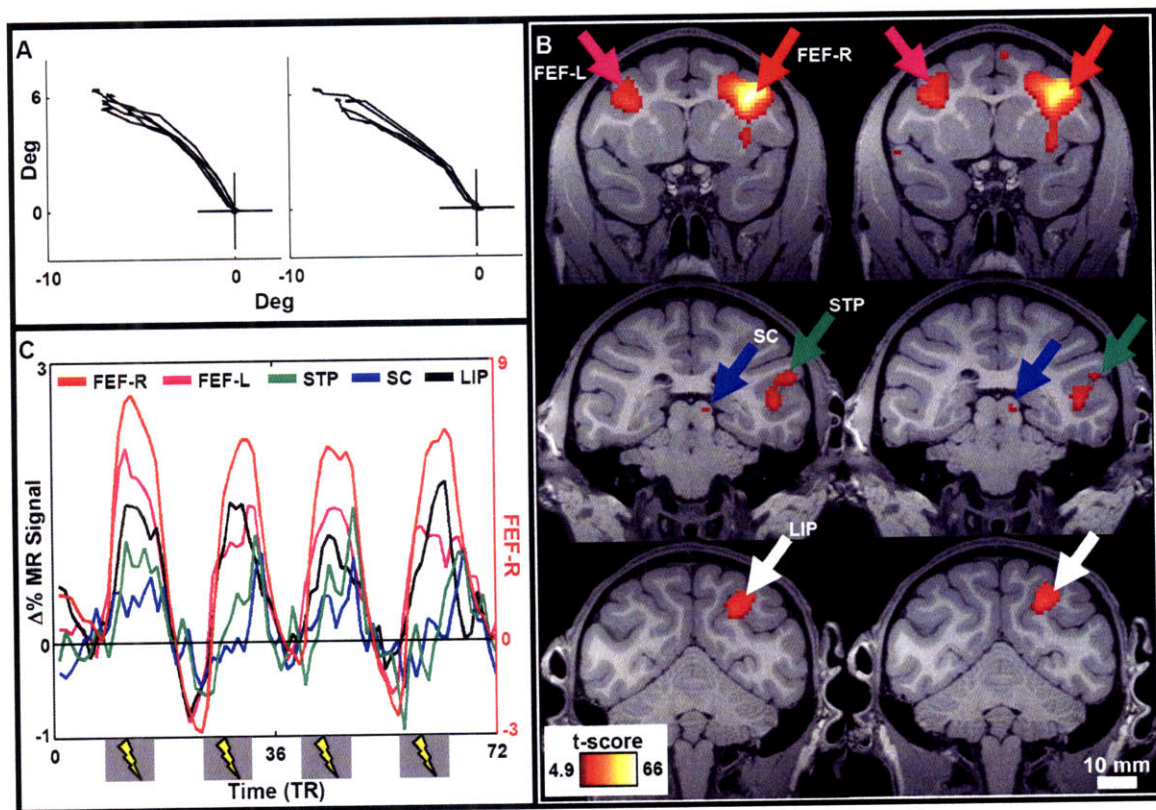
Fig. 2-9: fMRI activity induced by right FEF-EM. **(A)** Eye traces separated by 1 year showing saccades evoked by suprathreshold stimulation of one electrode. **(B)** Coronal slices showing activity (*t*-score maps) from the contrast EM versus no-EM (MM1, $P < 0.05$, corrected; R/L = right / left, see Table 2-2 for anatomical abbreviations). Columns represent test-retest separated by one month. **(C)** Time courses of percentage change in MR signal in areas in **(B)**. Note the secondary y-axis for the FEF-R data. Grey bars (*x* axis) indicate stimulation epochs.

epochs of no-EM and epochs of EM, at a stimulation level of 50% of the saccade-inducing amplitude. The use of this method in awake animals allowed us to titrate the stimulation to functionally relevant levels (see Section 2.6.1), an advantage compared to a previous study in anesthetized animals (Tolias et al., 2005).

The left column of Fig. 2-9B shows *t*-score maps of regions with increased fMRI activity caused by FEF-EM overlaid on coronal, T1-weighted sections. Focal increases in fMRI activity were observed at the site of stimulation and across the brain, in regions known to be connected to the FEF (Huerta et al., 1986; Huerta et al., 1987; Schall et al., 1995; Stanton et al., 1988; Stanton et al., 1995) [Fig. 2-10, Fig. 2-11 and Fig. 2-12; see Section 2.6.2 for a full list of areas]. To illustrate the amplitude of EM-induced fMRI effects in five representative regions, we plotted percentage change in MR signal relative to the no-EM condition (Fig. 2-9C). In comparison with classical tracer studies (Huerta et al., 1987; Schall et al., 1995), we obtained virtually identical results with EM-fMRI (Fig. 2-10, Fig. 2-11 and Fig. 2-12). This close correspondence demonstrates the precision of the technique and suggests that we primarily activated regions mono-synaptically connected to the stimulation site. At the statistical threshold used ($P < 0.05$, corrected), we observed no negative EM-induced activations in visual cortex. The right column of Fig. 2-9B represents a replication of the experiment after one month, showing the reproducibility of the results even for small foci, such as seen in the superior colliculus (Section 2.6.3).

Table 2-2: Anatomical abbreviations used.

Abbreviation	Meaning	Used in
Calc	Calcarine sulcus	Figs. 2-14C, 2-15, 2-16C
FST	Fundus of superior temporal sulcus	Figs. 2-13, 2-17, 2-18C
IOS	Inferior occipital sulcus	Figs. 2-16, 2-18
IPS	Intraparietal sulcus	Figs. 2-14C, 2-15, 2-16C
LIP	Lateral intraparietal area	Figs. 2-9, 2-13, 2-17, 2-19
MT	Middle temporal	Figs. 2-13, 2-17, 2-19
MST	Medial superior temporal area	Figs. 2-13, 2-17, 2-18C
OTS	Occipitotemporal sulcus	Figs. 2-16C, 2-18B
SC	Superior colliculus	Fig. 2-9
STP	Superior temporal polysensory area	Figs. 2-9, 2-13, 2-17, 2-19
STS	Superior temporal sulcus	Figs. 2-14C, 2-15, 2-16C
TE	Temporal area	Figs. 2-13, 2-17, 2-19
TEO	Temporo-occipital area	Figs. 2-13, 2-17, 2-19
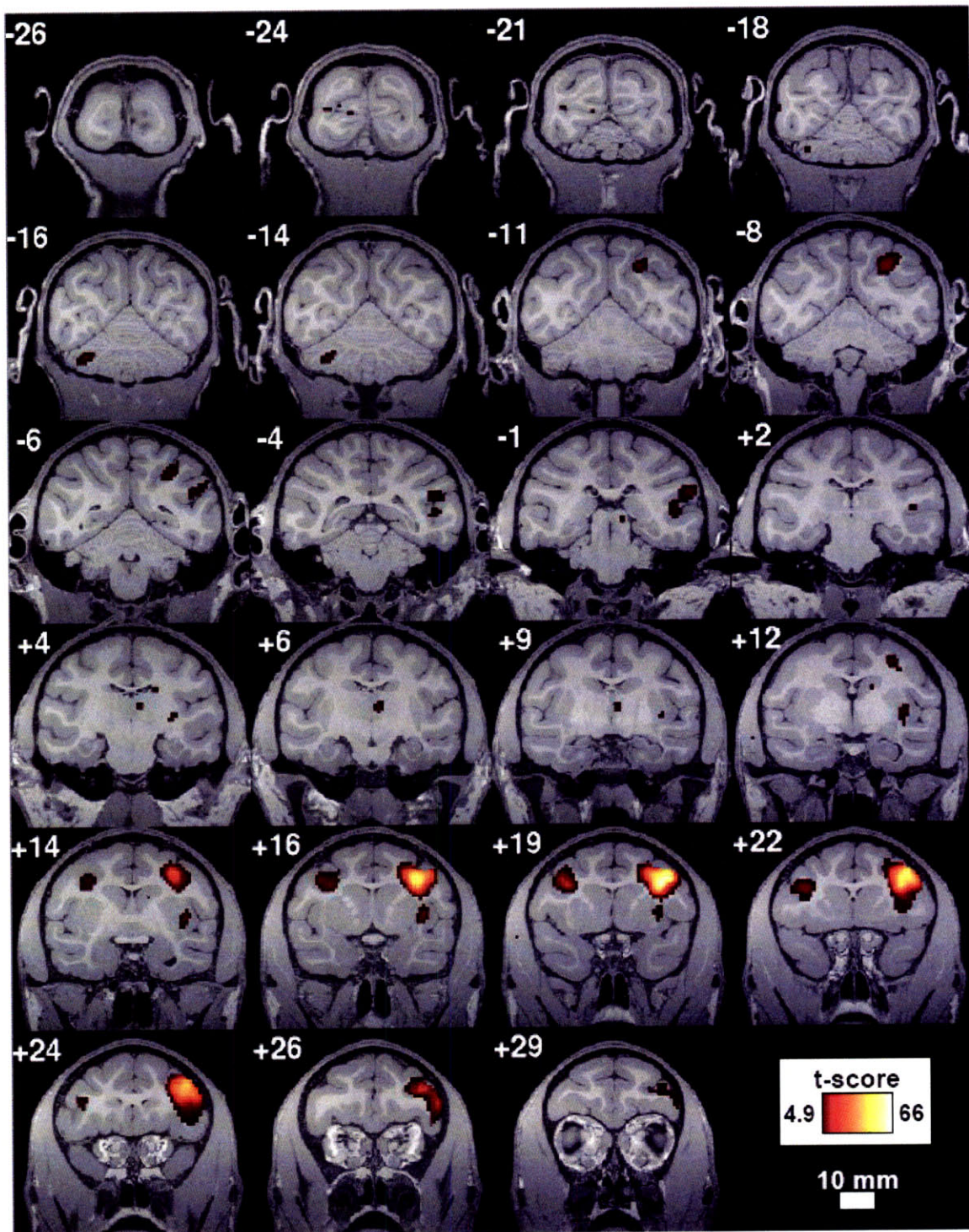
Fig. 2-10: FEF-EM in MM1. Foci of fMRI activation induced by EM of right FEF in MM1 ($P < 0.05$, corrected). White numbers in the top left corner of each slice indicate the antero-posterior distance in mm relative to the interaural line.
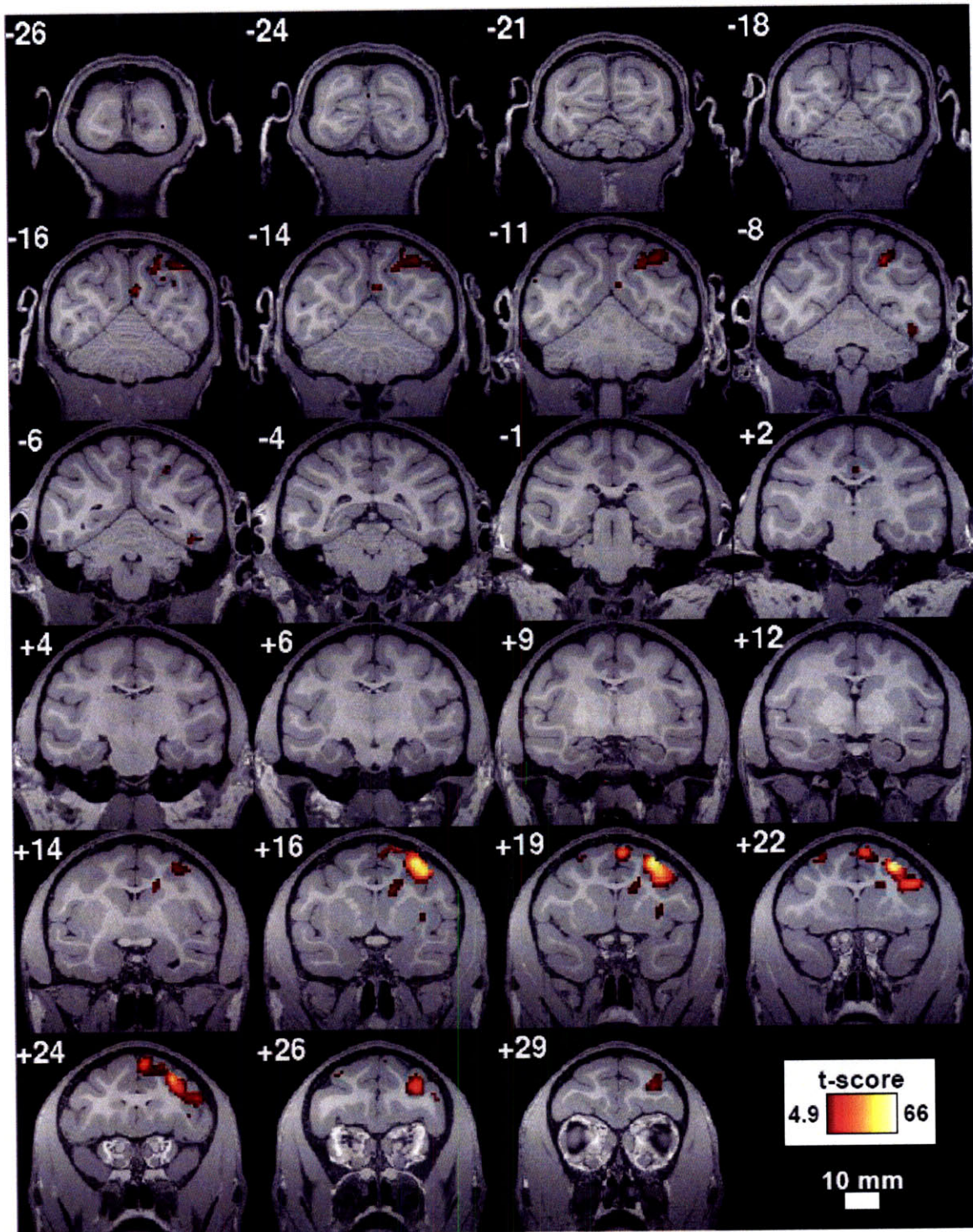
Fig. 2-11: FEF-EM in MM2. Foci of fMRI activation induced by EM of right FEF in MM2 ($P < 0.05$, corrected). White numbers in the top left corner of each slice indicate the antero-posterior distance in mm relative to the interaural line.
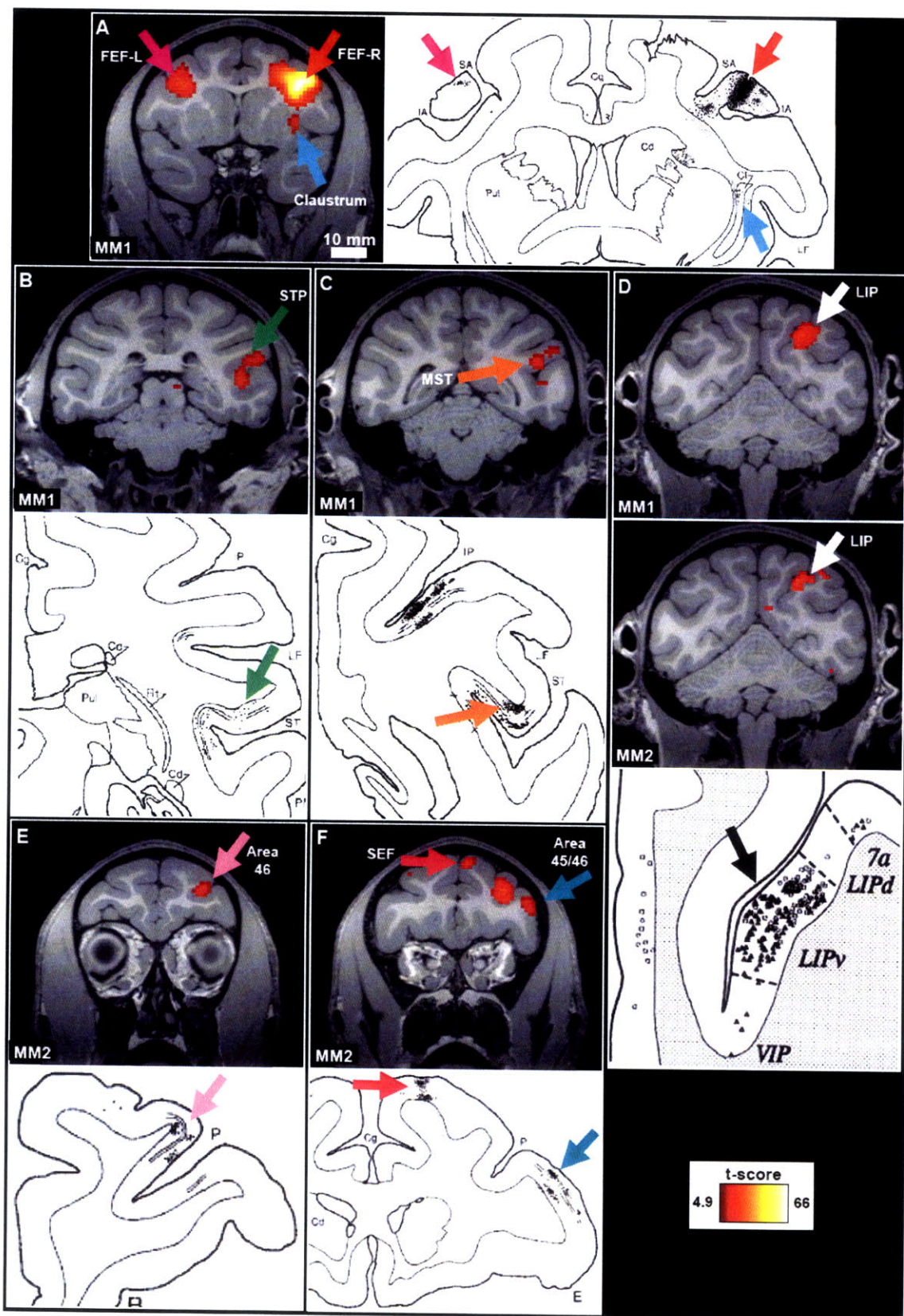
Fig. 2-12 (Previous page): Anatomical EM-fMRI tractography. Comparison of EM-induced fMRI activity ($P < 0.05$, corrected) with previous anatomical tract-tracing data (arrows as in **Fig. 2-9**, cyan = claustrum, orange = middle temporal (MST)). **(A)** Coronal slice (19 mm anterior to the interaural line; MM1), showing ipsilateral FEF, contralateral FEF and claustrum activation. **(B)** Slice at -2 mm (MM1), showing STP activation. **(C)** Slice at -4 mm (MM1), showing MST activation. **(D)** Slice at -9 mm (MM1 & MM2), showing LIP activation. **(E)** Slice at 30 mm (MM2), showing Area 46 activation. **(F)** Slice at 26 mm (MM2), showing SEF and Area 45/46 activation. Tract-tracing slides in **(A – C, E, F)** are from Huerta et al., (1987). Copyright © 1987 Alan R. Liss, Inc. Reprinted with permission of Wiley-Liss, Inc. a subsidiary of John Wiley & Sons Inc. **(D)** is from Schall et al., (1995). Reprinted with permission of the Society for Neuroscience.

2.4.2 Experiment Two – Interaction Between FEF-EM & Visual Stimulation

Our first experiment indicated that FEF-EM increased fMRI activity in higher-order visual areas known to be directly connected to the FEF. If feedback effects are gated by visual stimulation, however, one also predicts FEF-EM effects in visual areas separated from the FEF by multiple synapses, in the presence of a visual stimulus. In a second experiment, we therefore placed high-contrast colored, moving gratings in the MFs of the FEF stimulation sites under passive viewing conditions (Fig. 2-4, Section 2.3), and measured the fMRI response to EM-only, visual-only (V), and combined visual-EM (VEM) stimulation, relative to a fixation-only (F) condition ([i.e.] a 2 × 2 factorial design with factors EM and visual stimulation). To investigate the net influence of visual stimulation on FEF-EM effects, we compared EM minus fixation (Fig. 2-13A) to VEM minus V (Fig. 2-13C) in all visually driven voxels for a number of cortical areas; visually driven activity without EM is shown in Fig. 2-13B. Visually driven voxels in areas directly connected to the FEF (Huerta et al., 1986; Huerta et al., 1987; Schall et al., 1995; Stanton et al., 1988; Stanton et al., 1995), such as the lateral intraparietal area (LIP) and several areas within the superior temporal sulcus, showed an EM-driven increase in fMRI activity that was relatively independent of the presence of a visual stimulus (compare Fig. 2-13A and C). In
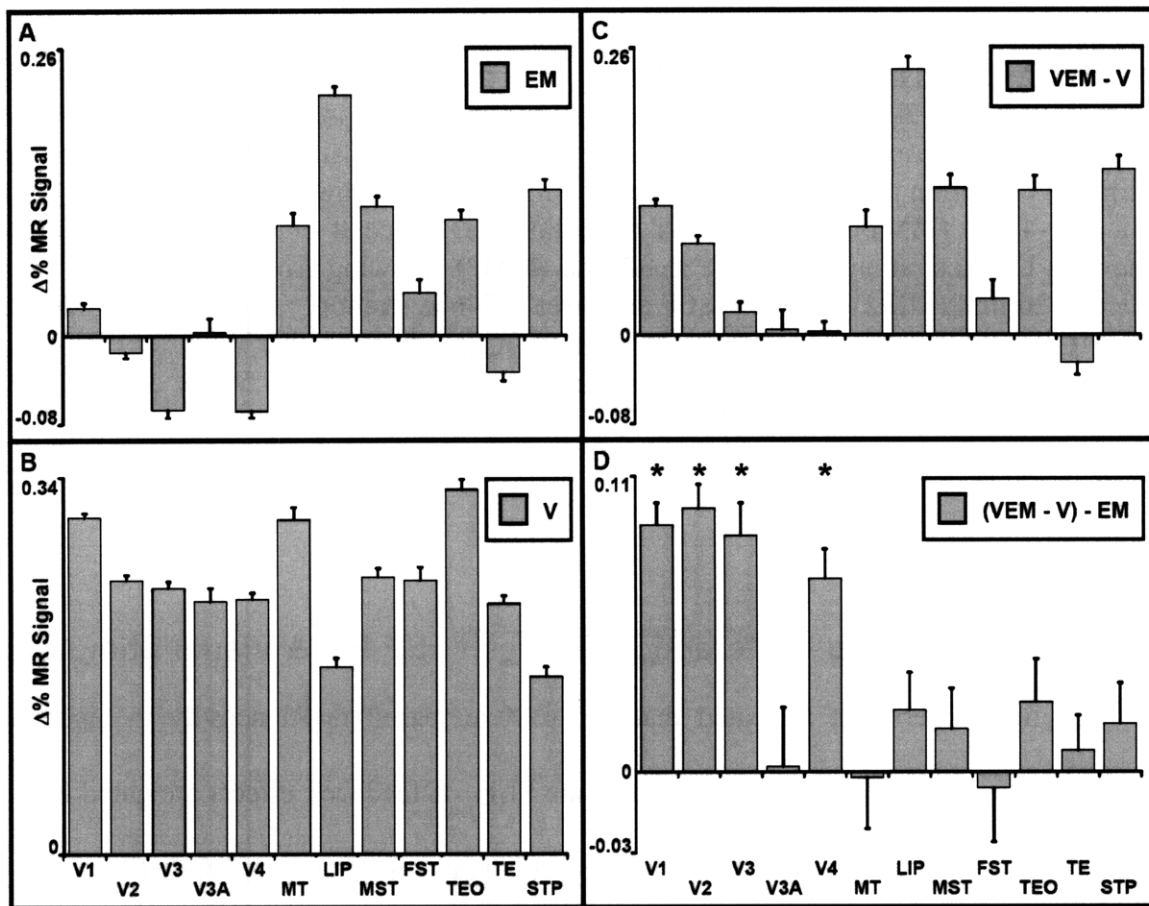
Fig. 2-13: Gating of FEF-EM effects by a visual stimulus. Mean percentage change in MR signal relative to fixation-only (MM1 and MM2) for all visually driven voxels ($P <$ 0.05, uncorrected) in 12 visual areas for **(A)** EM and **(B)** V epochs, **(C)** the difference between VEM and V epochs, and **(D)** the interaction (VEM-V-EM). Error bars denote SEM; * indicates a significant difference between the VEM-V and EM distributions ($P <$ 10^{-17}, two-sample, two-tailed t-test), revealing that on average voxels in early visual areas show a larger EM response in the presence of visual stimuli than in the absence. Higher order visual areas show an EM response both with and without visual stimulation.

contrast, visual stimulation unveiled a significant influence of FEF-EM on the activity of early visual areas (V1, V2, V3 and V4; see Section 2.6.4). Fig. 2-13D isolates the effect of the visual stimulus on FEF-EM, by subtracting the activity evoked by EM in the absence of a visual stimulus (Fig. 2-13A) from the activity evoked in the presence of a visual stimulus (Fig. 2-13C). Visual stimulation enabled the effects of FEF microstimulation to reach early visual areas, including V1, which is not mono-synaptically connected to the FEF.

We next investigated the spatial patterns of increased or suppressed fMRI activity in each of the areas, as the absence of an overall net effect might nevertheless be associated with a pattern of balanced inhibitory and excitatory effects. Fig. 2-14C shows the cortical regions where we observed positive and negative interactions between visual stimulation and FEF-EM in our 2 × 2 factorial design (Fig. 2-14A; see Fig. 2-14B for the stimulus positions used). Voxels shown in yellow-orange are visually driven; visually driven voxels with a positive or negative interaction are shaded green or blue, respectively (see Fig. 2-15; see Fig. 2-16 for MM2). The spatial pattern of these interactions was heterogeneous in most visual areas, as FEF-EM mostly amplified visual activity in subsets of voxels (green) adjacent to those maximally driven by the visual stimuli alone (yellow-orange), while it tended to have little influence or even suppressed the response (blue) in voxels strongly driven by the visual stimuli.

We further quantified these interactions between the visual stimuli and FEF-EM at the level of individual visually driven voxels by comparing the percentage change in MR signal in V epochs with the difference between VEM and EM epochs (Fig. 2-14D and Fig. 2-17). The visual voxels boosted by FEF-EM were weakly driven by the visual stimuli alone, while the voxels that were strongly driven by the visual stimuli were unaffected (both subjects) or even suppressed (mostly MM1) by FEF-EM. We carried out several analyses to exclude the possibility that the modulation of visually driven activity by FEF-EM was due to differences in eye position or saccade rate (see Section 2.6.5, Table 2-1, Fig. 2-7 and Fig. 2-8).
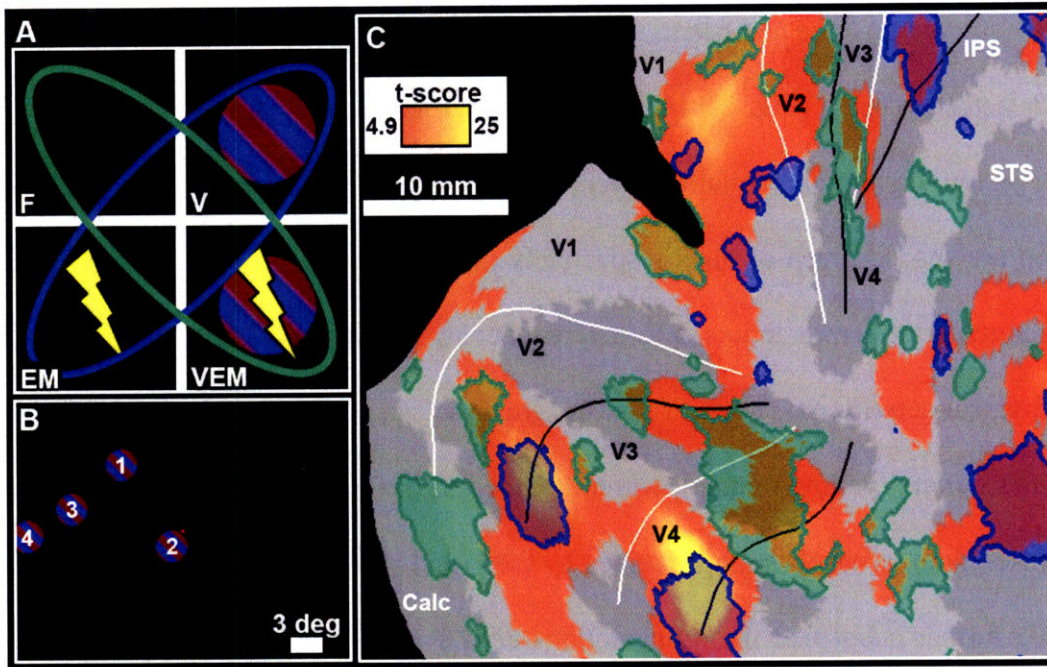
Fig. 2-14: Interaction between FEF-EM and visually driven activity. **(A)** A 2 × 2 factorial design. A positive interaction, indicative of EM-induced enhancement of visually driven activity, occurs when voxels are more active in the green conditions than in the blue ones. **(B)** Location and sequence of visual stimuli presented (see also Fig. 2-4). The red dot close to stimulus 2 is the fixation point. **(C)** Flattened, right occipital cortex (MM1) showing voxels that are visually driven by the four gratings (yellow-orange; $P < 0.05$, corrected), and visually driven voxels with a positive (green) or negative (blue) interaction between visually and EM-driven activity ($P < 0.05$, conjunction). Sulci are dark grey (see Table 2-2) and white and black lines indicate representations of the vertical and horizontal meridians, respectively. **(D) (Next page)** Scatter plots (MM1 and MM2) of voxels in areas V1, V2, V3 and V4 (see also Fig. 2-17) showing percentage change in MR signal for V epochs relative to fixation-only epochs (x axis) and the difference between VEM and EM epochs (y axis). Color code matches (C) (yellow now at $P < 0.05$, uncorrected). Points close to the y axis are weakly visually driven; voxels enhanced by FEF-EM (green) are mainly clustered near the y axis, while strongly visually driven voxels are either unaffected or suppressed (blue).
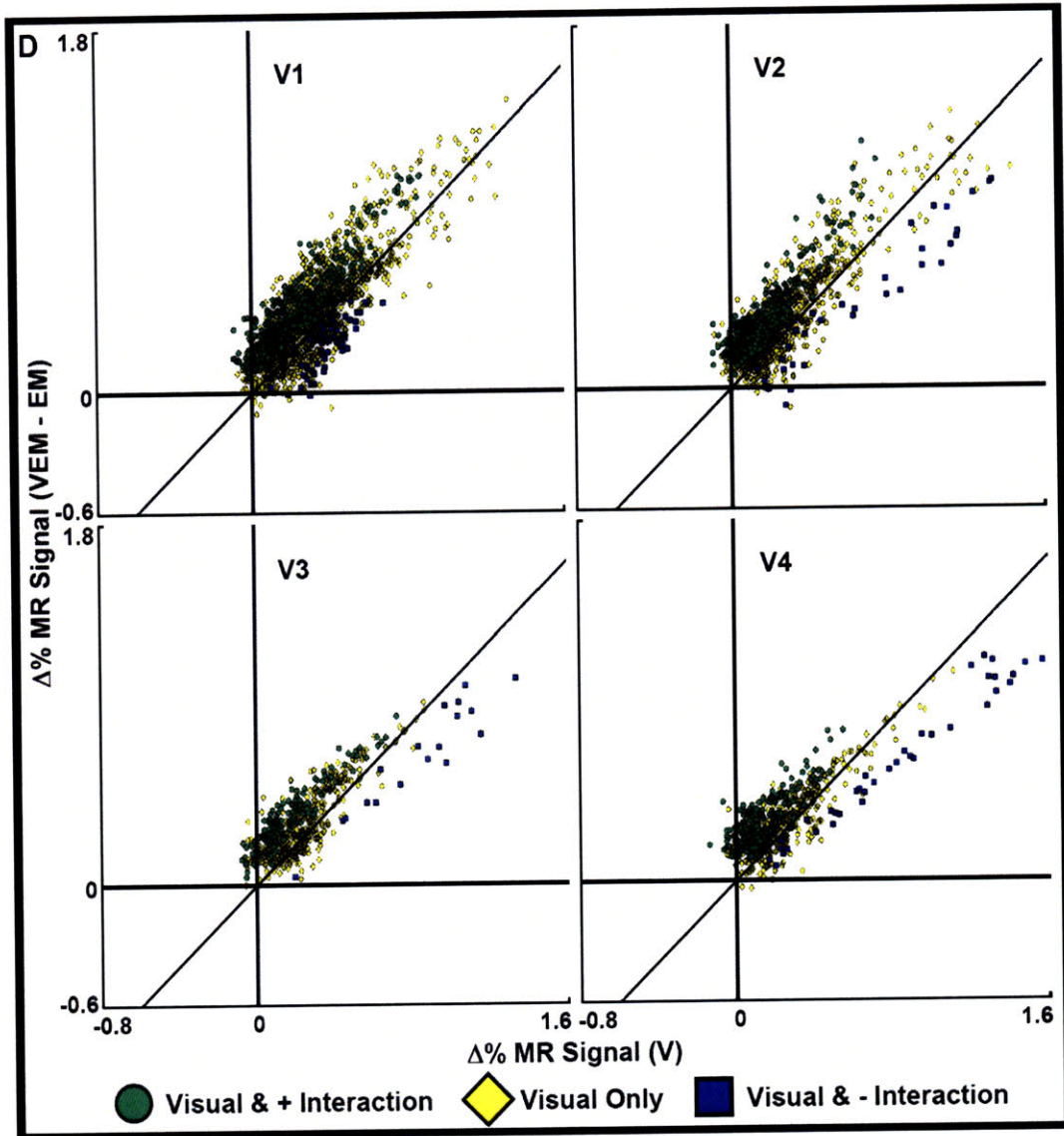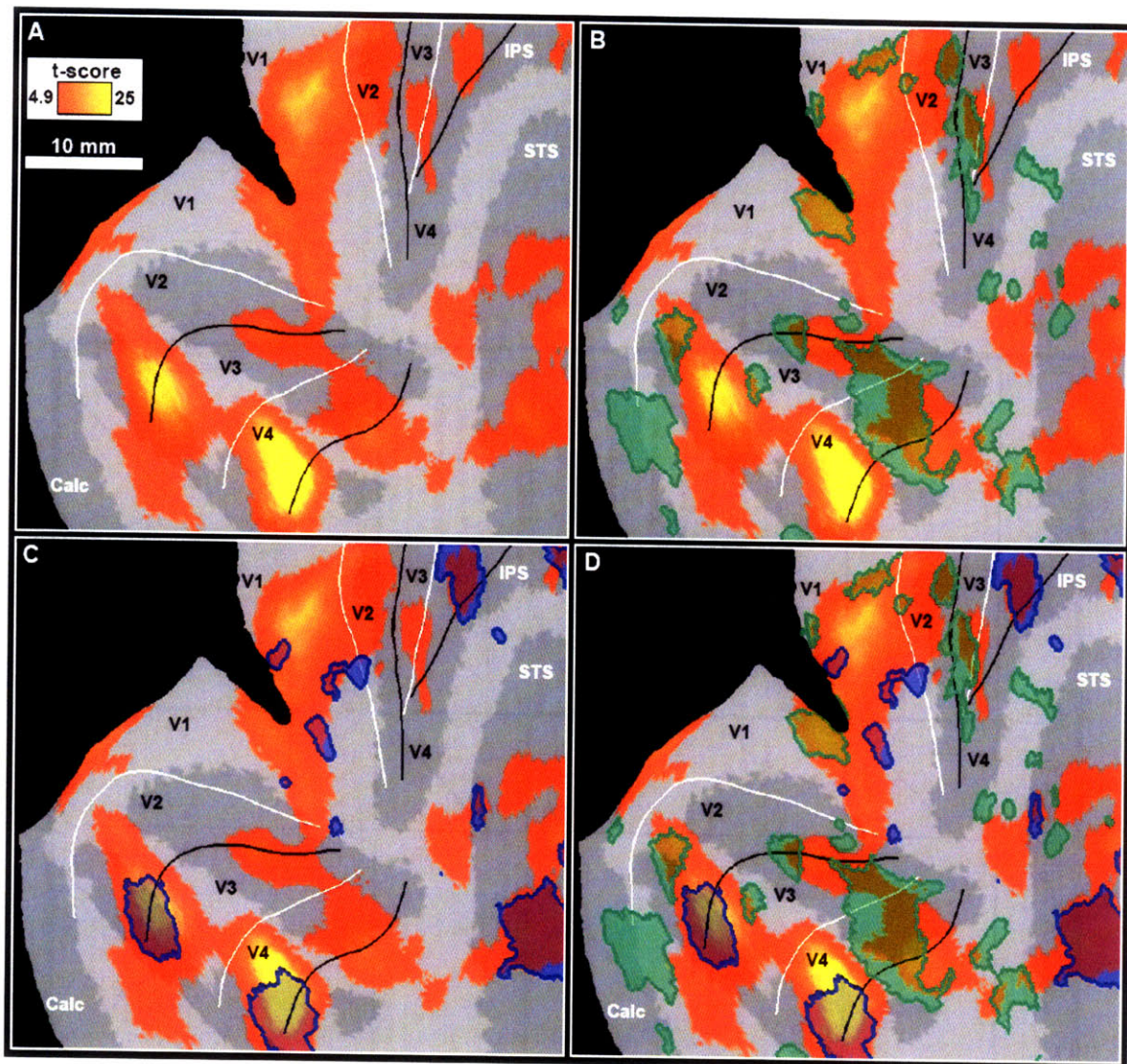
Fig. 2-15: Piecewise assembly of the interaction between FEF-EM and visually driven activity figure. **(A)** Flattened, right occipital cortex (MM1) showing visually driven voxels only ($P < 0.05$, corrected). Sulci are dark grey (see Table 2-2 for abbreviations) and white and black solid lines indicate the representation of the vertical and horizontal meridians, respectively. **(B)** Visually driven voxels with a positive interaction between visual activity and FEF-EM ($P < 0.05$, conjunction). **(C)** Visually driven voxels with a negative interaction between visual activity and FEF-EM ($P < 0.05$, conjunction). **(D)** The combination of all three types of voxels, as in Fig. 2-14C, with green shading indicating the positive and blue the negative interaction subpopulation. Some of the green and blue subpopulations appear separate from the yellow-orange visual representations; these regions are still visually driven, but at a lower significance threshold ($P < 0.05$, uncorrected) through the conjunction.
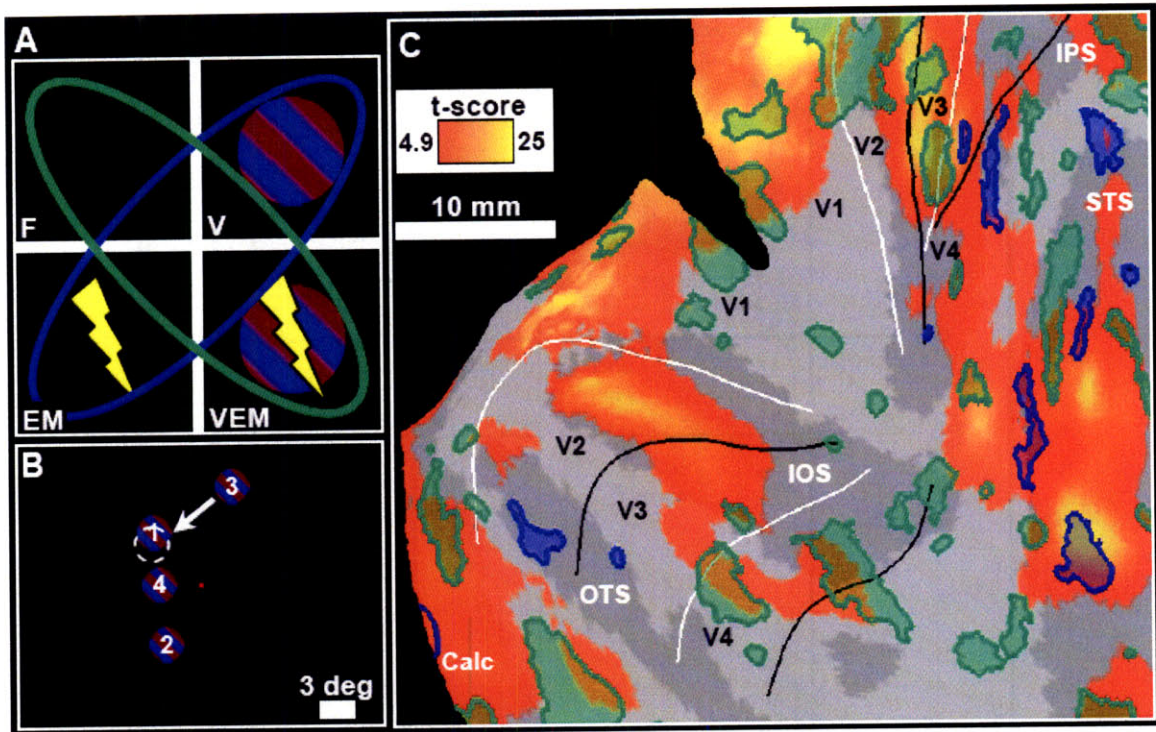
Fig. 2-16: Interaction between FEF-EM and visually driven activity in MM2. **(A)** A 2 by 2 factorial design. **(B)** Location and sequence of visual stimuli presented (see also Fig. 2-4). The red dot close to stimulus 4 is the fixation point. The white dashed line indicates the actual location of stimulus 3, partially overlapping stimulus 1. **(C)** Flattened, right occipital cortex showing voxels that are visually driven (yellow-orange; $P < 0.05$, corrected), and visually driven voxels with a positive (green) or negative (blue) interaction between visually and EM-driven activity ($P < 0.05$, conjunction). Sulci are dark grey (see Table 2-2 for abbreviations) and white and black lines indicate representations of the vertical and horizontal meridians, respectively.

Fig. 2-17 (Next page): MR signal changes across visual regions. Scatter plots (MM1 and MM2) of voxels in areas V3A, MT, LIP, MST, FST, TEO, TE and STP showing percentage change in MR signal for V epochs relative to the fixation-only condition (x axis) and the difference between VEM and EM epochs (y axis). Color code is as in Fig. 2-14C (yellow now at $P < 0.05$, uncorrected).
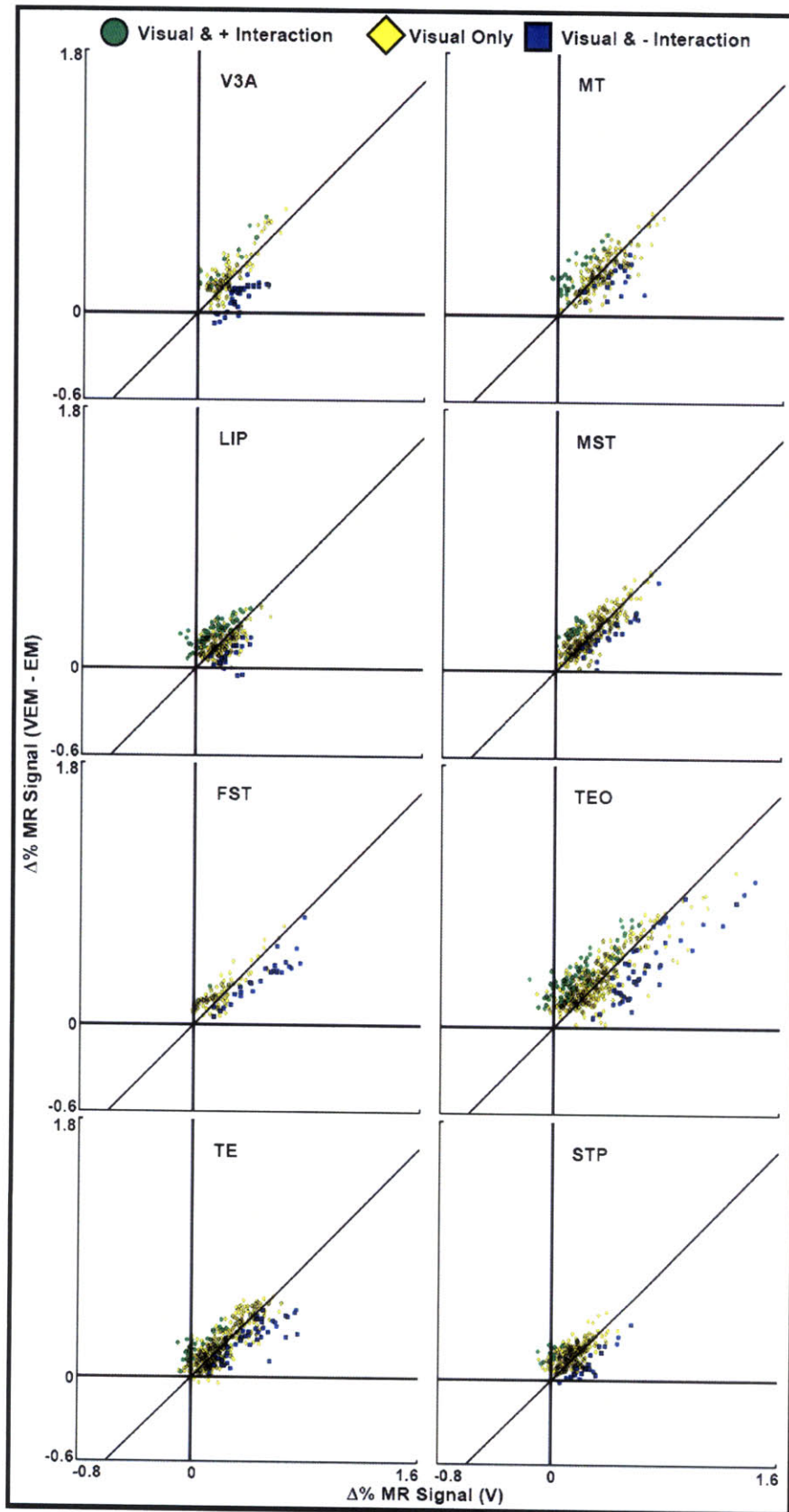
2.4.3 Experiment Three – Specificity of FEF-EM

Modulatory effects from the FEF in visual cortex could be either spatially nonspecific, or require the precise alignment of a visual stimulus with the FEF MF (Moore and Armstrong, 2003). Our third experiment compared the effects of incongruent epochs (VEM-I), in which EM was applied to a particular FEF MF while a visual stimulus was presented in another, non-stimulated MF (separated by 6.5 to 13.7 degrees), to congruent epochs that were identical to the VEM condition of experiment two (Fig. 2-18A and Fig. 2-5). Net EM and visual stimulation were exactly matched between congruent and incongruent epochs. In Fig. 2-18B, we show a portion of flattened right occipital cortex overlaid with a t-score map of visually driven fMRI activity. The spatial pattern supports that seen in experiment two – in general, voxels adjacent to
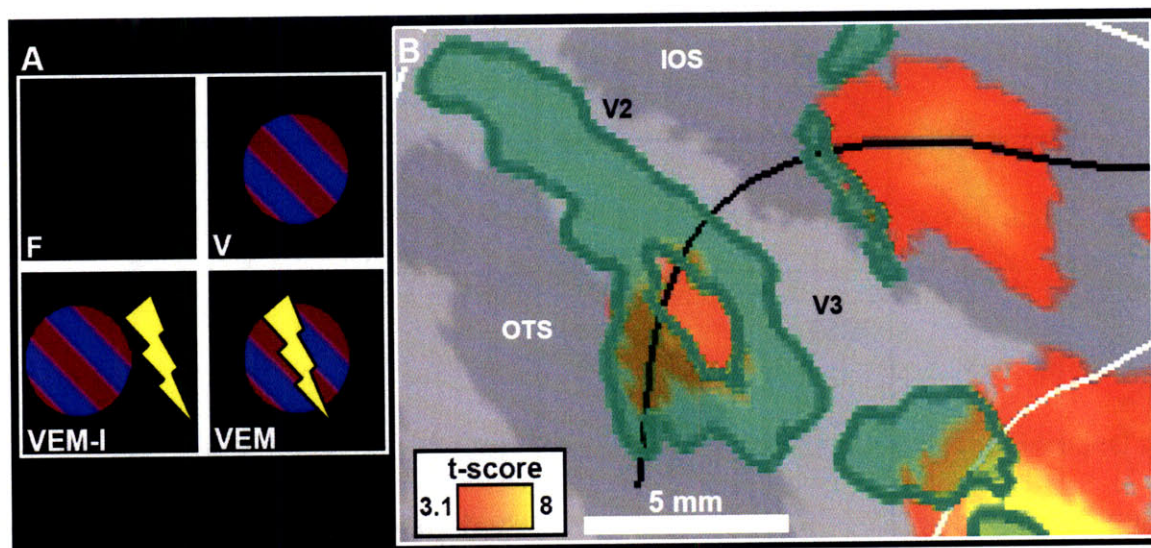
Fig. 2-18: Retinotopic specificity of FEF-EM induced modulations. **(A)** The design used to test for retinotopic specificity of the interaction between EM and visual stimulation (VEM-I, incongruent visual stimulation and FEF-EM). **(B)** Flattened, right occipital cortex (MM1). Yellow-orange voxels show a visual-only response ($P < 0.001$, uncorrected); green voxels are visually driven and exhibit more activity during congruent than during incongruent visual stimulation ($P < 0.05$, conjunction). Sulci and white and black lines are as in Fig. 2-14C. **(C) (Next page)** Responses of voxels (percentage MR signal change; MM1) in areas V2, V3, MST and FST (see also Fig. 2-19) during the VEM-I (x axis) and VEM (y axis) epochs relative to the fixation epoch. Color code matches (A) (yellow now at $P < 0.05$, uncorrected; blue at $P < 0.05$, conjunction).

those maximally driven by the visual stimulus alone showed more fMRI activity during congruent than during incongruent FEF-EM (green). An analysis at the level of individual voxels confirmed that most voxels were better activated during VEM than during VEM-I, especially in motion sensitive areas such as MT, MST and FST (Fig. 2-18C, Fig. 2-19 and Section 2.6.6) (Vanduffel et al., 2001).
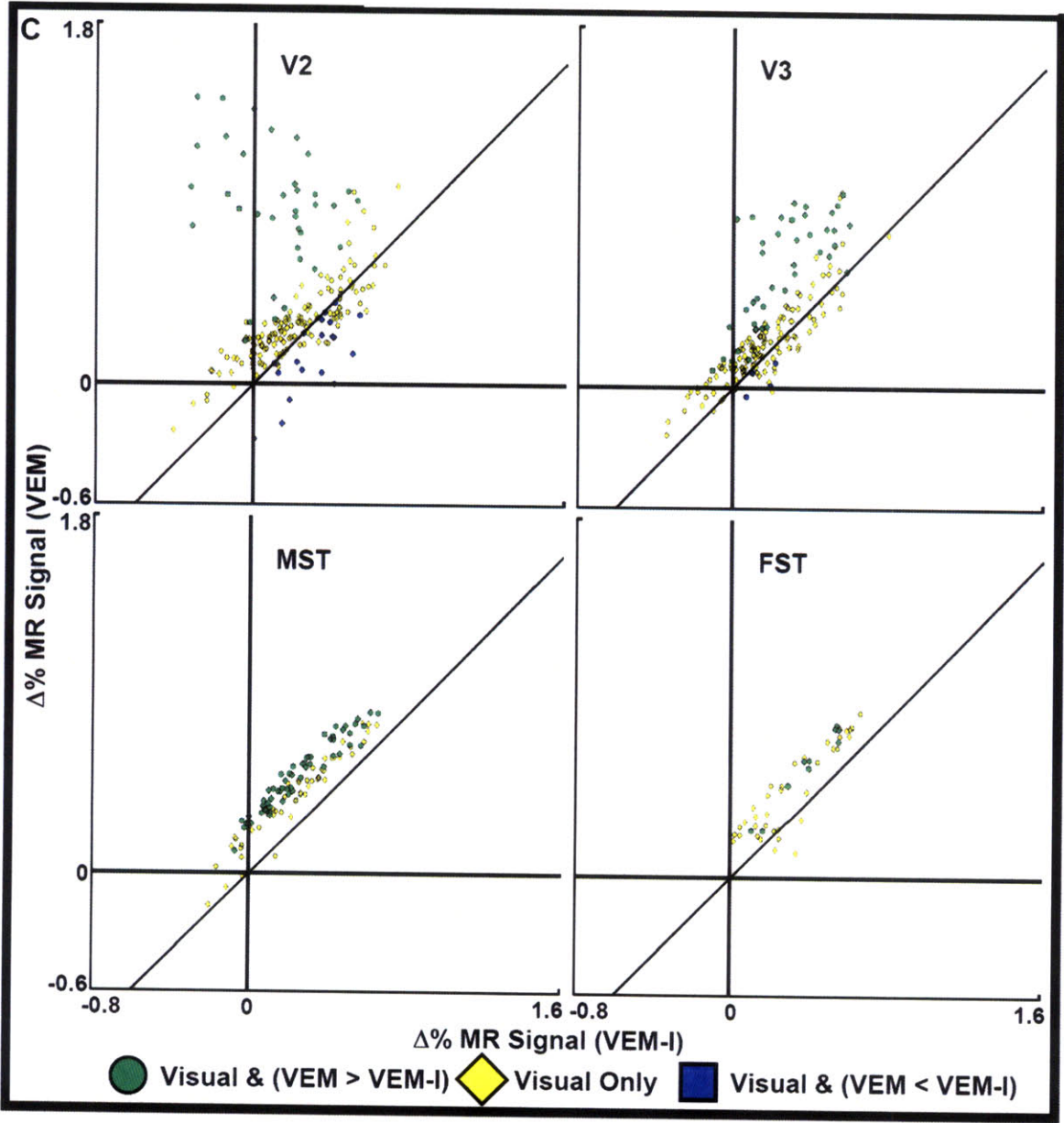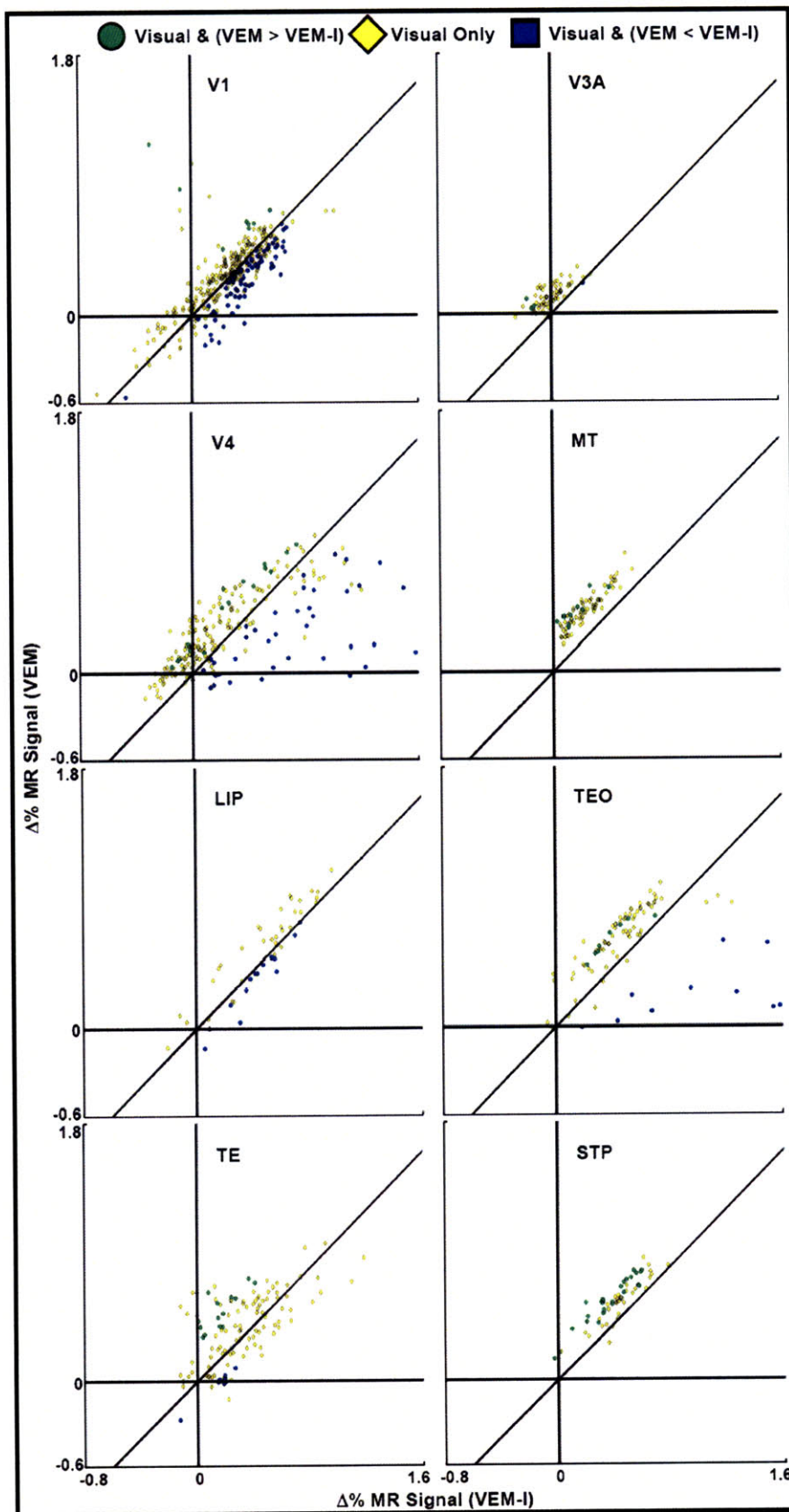
Fig. 2-19 (Previous page): Specificity of FEF-EM induced modulations. Responses of voxels (percentage MR signal change) in areas V1, V3A, V4, MT, LIP, TEO, TE and STP in the VEM-I epoch (x axis) and VEM epoch (y axis) relative to the fixation epoch. Color code is as in Fig. 2-18B (yellow now at $P < 0.05$, uncorrected; blue at $P < 0.05$, conjunction).

2.4.4 Experiments Four & Five – Visual Saliency Effects on FEF-EM Modulation

To assess more directly whether FEF-EM mainly influences the activity of non-optimally driven voxels, our next two experiments manipulated the saliency or strength of the visual response. In experiment four, we placed one stimulus in the FEF-MF and added three distractors (D) in the opposite hemifield (Fig. 2-6). For comparative purposes (Moore and Armstrong, 2003), we focus here on visually driven regions in V4 only. As expected, the distractors did not evoke a response in V4 representing the opposite visual field (Fig. 2-20A). Microstimulation of the FEF in the presence of distractors, however, produced the largest response for the stimulus in the FEF MF, in agreement with a previous study (Moore and Armstrong, 2003). The interaction between distractors and FEF-EM was significant ($P < 1.4 \times 10^{-5}$). In a fifth experiment, we varied the luminance contrast of a single stimulus placed in the FEF MFs, and observed significant enhancement effects of FEF-EM for low-contrast stimuli only (Fig. 2-20B; this sequence of experiments will be explored in more detail in Chapter 3). These results are in accordance with experiment two where we obtained the strongest modulation in voxels with a weaker visual response.
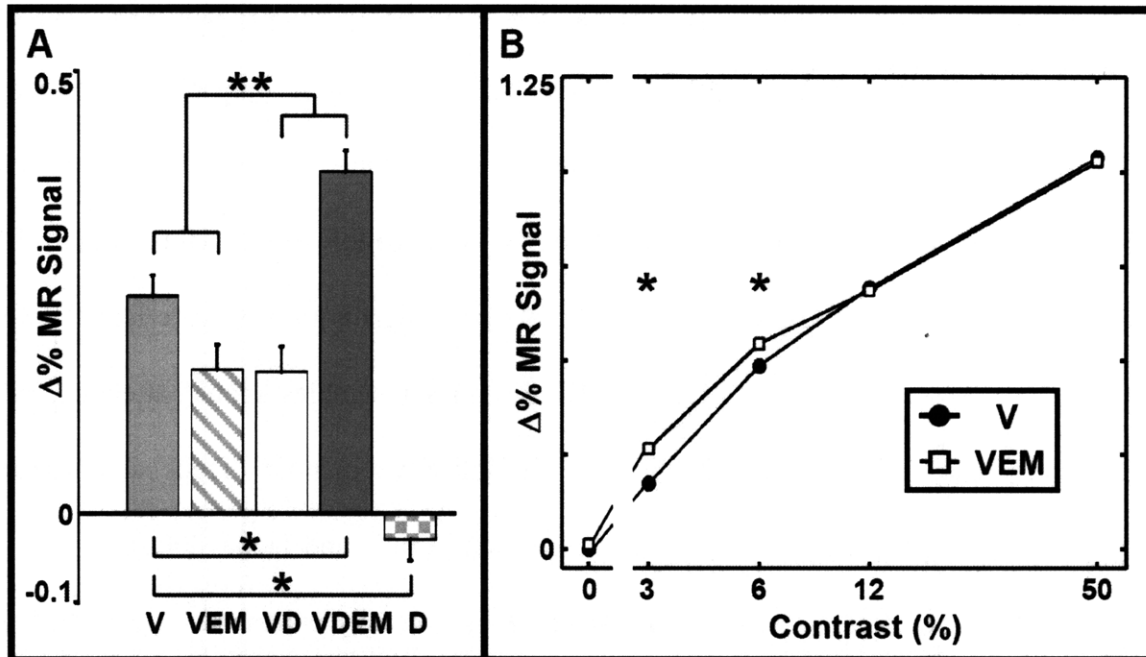
Fig. 2-20: Effects of distractor stimuli and stimulus contrast. **(A)** Mean percentage change in MR signal relative to fixation-only in visually driven voxels in V4 (MM1; $P < 0.05$, uncorrected) during V, VEM, visual + distractor (VD), visual + distractor + EM (VDEM) and distractor-only (D) epochs. Two FEF MFs were stimulated (Fig. 2-6). Error bars denote SEM. * denotes a significant difference between the pair of conditions indicated ($P < 0.05$, two sample, two-tailed t-test); ** indicates that the interaction between distractors and EM is significant ($P < 1.4 \times 10^{-5}$). **(B)** Mean percentage change in MR signal relative to the fixation epoch in visually driven voxels in V4 (MM1 and MM2) as a function of stimulus luminance contrast. Only one visual stimulus was used per session (Fig. 2-4), with the data combined across all four MF locations from each subject. The highest contrast stimulus was used as a localizer ($P < 0.05$, uncorrected). Error bars denote SEM. * denotes a significant difference between the VEM and V conditions at a given contrast ($P < 0.05$, two sample, two-tailed t-test).

2.5 Discussion

We have demonstrated spatially specific, causal interactions between activity in area FEF and many areas of the visual cortex. Signals from frontal cortex activated higher-order areas directly connected to the FEF irrespective of visual stimulation, mimicking attention-driven baseline shifts in activity (Section 2.6.7) (Colby et al., 1996). In the presence of visual stimulation, modulations were observed at even the earliest levels of visual cortex, including area V1, which may account for previous findings that the effects of FEF-EM are retinotopically

highly specific (Armstrong et al., 2006). These effects are likely trans-synaptic, because these early areas do not receive direct connections from the FEF and were only observed when the neurons were congruently activated by a visual stimulus. One interpretation is that visual stimulation opens feedback pathways closed in the absence of stimuli (Fukushima, 1988; Grossberg, 1999; Roelfsema, 2006), allowing these frontal signals to propagate from higher to earlier visual cortical areas. The effect of FEF-EM thus resembles spatial attention, which interacts with visual stimuli in a comparable, multiplicative manner (Treue and Martinez-Trujillo, 1999; McAdams and Maunsell, 1999a; Martinez-Trujillo and Treue, 2004).

An unexpected finding was that the voxels most strongly enhanced by FEF-EM were adjacent to the voxels with the strongest visual response, which were themselves unaffected or even suppressed by FEF-EM. These results support a recent model for the effects of feedback connections proposing that feedback and horizontal connections mediate a contrast-dependent inhibition of a central zone in the next lower area, while exciting the near surround (Schwabe et al., 2006). Strong effects of FEF-EM in weakly driven voxels also dovetails with previous findings that attentional effects and the effects of FEF microstimulation on neuronal activity in area V4 are most pronounced in the presence of competitive distractors that reduce the strength of neuronal responses (Moore and Armstrong, 2003; Reynolds et al., 1999). As another means to reduce the activity of V4 neurons, we lowered the luminance contrast of the visual stimulus. We observed that FEF-EM evoked stronger effects in low-contrast rather than high-contrast stimuli. This result is reminiscent of a non-proportional scaling of the contrast response function in area V4, with stronger positive modulations for low contrast stimuli, as seen in previous spatial attention studies [(Reynolds et al., 2000), but see (Williford and Maunsell, 2006)]. All these results, taken together make it tempting to speculate that FEF-EM engages similar neuronal

circuits as spatial attention. Speculation aside, the present results clearly strengthen past observations that structures involved in generating eye-movements (Rizzolatti et al., 1987; Moore and Armstrong, 2003; Corbetta et al., 1998; Cavanaugh and Wurtz, 2004; Ruff et al., 2006) are well-suited to modulate sensory-driven activity in a topographically specific manner.

2.6 Additional Notes

2.6.1 Why Target the FEF?

The FEF is an ideal initial target for this combination of techniques because: (i) EM of the FEF evokes an easy-to-measure behavioral correlate (saccadic eye-movements), which (ii) allows the determination of exactly what level of stimulation is needed to increase FEF output in a behaviorally relevant manner. (iii) The anatomical connections of the FEF are well characterized; hence, the accuracy of the EM-fMRI results without visual stimulation can easily be validated.

2.6.2 *In vivo* Tractography: Areas Showing Increased fMRI Activity in the Absence of Visual Stimulation

EM of specific sub-regions of the FEF increased fMRI activity in several functionally connected regions (Huerta et al., 1986; Huerta et al., 1987; Schall et al., 1995; Stanton et al., 1988; Stanton et al., 1995). These sites included (i) ipsilateral areas within the superior temporal sulcus including MST, MT, and STP, LIP, V4, supplementary eye fields (SEF), area 45, area 46, superior colliculus, claustrum, putamen, caudate nucleus and medio-dorsal thalamus, and (ii) contralateral FEF and cerebellum (Fig. 2-10, Fig. 2-11 and Fig. 2-12; see Table 2-2 for abbreviations). Slightly different patterns of functional activation were observed in the two animals (compare Fig. 2-10 and Fig. 2-11). This apparent discrepancy is not unexpected though,

given that the remote activations are induced by clusters of neurons surrounding the individual electrodes (Tehovnik, 1996) and not the entire FEF, and also that the exact position of electrode implantation within the FEF varied between animals. In addition to this demonstration of accurate and precise *in vivo* tractography, further potential uses of this novel combination of techniques include: (i) tracing connections *in vivo* from a virtually unlimited number of neighboring regions within a single individual, (ii) guiding simultaneous electrophysiological recordings in multiple functionally connected sites, (iii) guiding (ir-)reversible deactivation experiments, and (iv) validating other effective connectivity techniques, such as with diffusion-tensor imaging (Conturo et al., 1999) and dynamic causal modeling (Friston et al., 2003).

2.6.3 Stability of the Chronic EM-fMRI Method

Chronically implanted electrodes allowed for repeated stimulation of the same FEF sites and were remarkably stable over time. We were able to elicit virtually identical saccades using similar current thresholds during sessions spanning more than 47 and 35 months in monkeys MM1 and MM2 respectively (see e.g. Fig. 2-9A). Furthermore, we quantified the overall repeatability of the fMRI activations by calculating three-dimensional spatial correlation coefficients, which ranged from 0.71 to 0.83 for pairs of thresholded full-brain t-score maps ($P <$ 0.05, corrected) derived from runs in different sessions or within the same session, respectively. Importantly, we did not observe large aspecific activations in regions not known to be connected to the FEF. The specificity, repeatability and accuracy of EM-fMRI through chronically implanted electrodes show the great potential of this tractography technique, which can be used without the need to sacrifice the subjects.

2.6.4 Interactions Driven by Negative EM Effects

In those voxels in areas V3 and V4 that showed a visually driven response, FEF-EM in the absence of a visual stimulus caused a reduction of fMRI activity. This reduction was not observed in the presence of a visual stimulus (Fig. 2-13A and C), so that the interaction between FEF-EM and visual stimulation was positive in these areas as well (Fig. 2-13D).

2.6.5 Effects of Eye-movements and Induction of Phosphenes

We considered the possibility that subthreshold FEF-EM induces eye-movements, which could lead to either a blurred representation or an enhanced representation of the stimuli in retinotopically organized cortex. We performed a one-way ANOVA on eye position (x and y), saccade rate and percentage fixation during each experiment (Table 2-1). None of these measures were significantly different ($P > 0.05$) between epochs in the interaction comparison (VEM and F versus V and EM, experiment two; VDEM and V versus VEM and VD, experiment four), specificity comparison (VEM versus VEM-I, experiment three) or the luminance contrast comparison (VEM versus V, experiment five). For the interaction contrast in experiment two, we also plotted mean eye traces in both the x and y directions, aligned to the onset of FEF-EM (Fig. 2-7 and Fig. 2-8). While some deviation was seen (mostly for MM1), the amplitude of this deviation was small (< 0.25 degrees) and there were no time points where a significant difference ($P > 0.05$, corrected for multiple comparisons across time points) was found between the pairs of conditions forming the interaction. Thus, differences in eye-movements between conditions cannot explain the observed modulation of visually driven activity. A second concern is that FEF-EM may induce a non-specific phosphene or cue that could lead to enhanced visually driven activity. Recent work (Cavanaugh et al., 2006), however, showed that EM of the SC in monkeys

did not produce a phosphene but rather an apparent shift in attention. This conclusion is supported by the failure to generate phosphenes during TMS of human FEF (Ruff et al., 2006).

2.6.6 Feature Specific Gating

In motion sensitive areas, such as MT, MST and FST, most voxels were significantly more active in the VEM condition than in the VEM-I condition (Fig. 2-18C and Fig. 2-19). In object-sensitive regions, such as V4 and TEO, we unexpectedly observed a few voxels that were more active during the incongruent epochs (Fig. 2-19). One speculative possibility is that FEF stimulation in the presence of a moving stimulus tends to have stronger excitatory effects in motion sensitive areas than in more shape selective regions. Future research might investigate the feature preference of the neurons in the voxels with increased activity in the incongruent conditions and compare it to the feature preference in voxels responding more in the congruent condition.

2.6.7 Ventral Area Shifts in Baseline Activation due to FEF-EM

An increase in baseline activation in ventral extrastriate areas due to FEF-EM was observed in MM2 (Fig. 2-11) but not in MM1 (Fig. 2-10). That baseline shifts were not consistently observed in these areas (Heinze et al., 1994; Luck et al., 1997; Kastner et al., 1998) may be partly due to the distribution of MFs we obtained, which favored large amplitude saccades. FEF neurons generating large amplitude saccades are more robustly interconnected with dorsal stream areas than ventral ones (Schall et al., 1995). This observation therefore suggests that other parts of area FEF or multiple fronto-parietal control areas are also recruited during the deployment of spatial attention.

2.6.8 MR Gradient-induced Currents

Another concern is that switching of the gradient fields during MRI scanning could induce additional current in the electrodes. First, we simulated the effects of gradient switching using a finite-element model (Fig. 2-3). Both with and without electrodes present, we found that the induced current density did not surpass the 1.23 A/m^2 threshold needed for axonal activation (20 µm diameter fibers) (Reilly, 1998). In the vicinity of the electrode tips, the induced current densities were two to three orders of magnitude below the stimulation threshold. Moreover, we never induced saccadic eye-movements during EPI acquisition while stimulating at 50% of the amplitude needed to generate a saccade (Table 2-1). This observation shows that any induced currents due to gradient switching must have been less than 50% of the actual injected current.

Chapter 3

3 Effects of FEF Stimulation on Contrast Response

This chapter is based upon:

Modulation of the Contrast Response Function by Electrical Microstimulation of the

Macaque Frontal Eye Field

(In preparation)

Leeland B. Ekstrom, Pieter R. Roelfsema, John T. Arsenault, Hauke Kolster, Wim Vanduffel

One of the most obvious questions to emerge from our initial work on the effects of FEF stimulation on a visual stimulus was how the salience or strength of the visual stimulus affected the modulations observed. From the spatial pattern of modulations we saw (Fig. 2-14 and Fig. 2-16), we initially noted that any enhancements of visual activity tended to occur away from the most active visually driven voxels on the cortical surface, in voxels that comprised the periphery or margin of the stimulus representation. In turn, the most active voxels at the center of the stimulus representation showed little effect, or in some cases a slight suppression of fMRI activity. This spatial variation of the modulations, presumably due to the underlying strength of activation, thus led us to the above question.

To more definitively test this presumption, we set out to actively manipulate the strength of the visual stimulus placed in the FEF movement field (MF). A common technique for varying stimulus strength is to systematically alter its luminance contrast and generate a contrast response function (CRF) [see any of (Albrecht and Hamilton, 1982; Sclar et al., 1990; Reynolds et al., 2000; Williford and Maunsell, 2006; Buracas and Boynton, 2007; Li et al., 2008)]. Equipped with enhanced new imaging tools that substantially boosted image SNR and the amount of data we could collect (Kolster et al., Submitted), we undertook a series of experiments to measure CRFs in the primate visual cortex and how they were altered by simultaneous stimulation of the FEF. Without this new equipment, we would have been unable to perform these experiments, given the number of experimental conditions required. To simplify the definition of a contrast varying stimulus, we switched to mono-chromatic sine-wave gratings and also doubled their size to reduce the possibility of a mismatch between stimulus location and FEF MF. Of course, a systematic evaluation of how color and stimulus size affect modulations caused by FEF microstimulation (FEF-EM) would be interesting in its own right and remains an open question not addressed here. As well, we sought to simplify one of the aspects that made the interpretation of our initial results more challenging by using only a single stimulus location and FEF site in a given experiment, rather than the sequential use of multiple stimuli that we first employed.

This work was initially a standalone study, but we later included the CRF result from area V4 in our first publication (see Fig. 2-20) at the request of a reviewer. This chapter thus elaborates upon the results introduced in the preceding chapter. The aims of this portion of the thesis were to understand how stimulus strength affects the modulation of visual activity caused by FEF-EM. The working hypothesis was that low contrast stimuli, which produce little visual

drive, would be primarily enhanced by FEF stimulation while high contrast stimuli would show little change in the response they produce.

3.1 Abstract

Spatial attention strongly influences representations in visual cortical areas as well as perception. Some models of this effect predict a contrast gain, while others a response or activity gain when attention is directed to a contrast varying stimulus. Recent evidence has indicated that microstimulating the FEF can produce modulations of V4 neuronal firing rates that resemble spatial attention-like effects, and we have shown similar modulations of fMRI activity throughout the visual system. Here, we used functional magnetic resonance imaging (fMRI) in awake, fixating monkeys to first measure the response in twelve visual cortical areas to stimuli of varying luminance contrast. We compared these fMRI-derived contrast response functions (CRFs) to several previous electrophysiological studies in monkeys and fMRI studies in humans and, at least in early visual areas, found a better match with human fMRI than electrophysiological data. Then, we simultaneously microstimulated sub-regions of the Frontal Eye Field (FEF) with movement fields that overlapped the stimulus locations and measured how this artificially increased FEF output modulated CRFs throughout visual cortex. In general, we found evidence for a non-proportional scaling of the CRF (resembling a contrast gain effect) under these conditions. Representations of low contrast stimuli were enhanced by stimulation of the FEF below the threshold needed to evoke saccades, while those of high contrast stimuli were unaffected or in some areas even suppressed. Further, we measured a characteristic spatial pattern of enhancement and suppression across the cortical surface, and here propose a simple schematic of this contrast-dependent fMRI response.

3.2 Introduction

Luminance contrast is one of several cues that define objects in visual space, along with other features such as motion, texture, spatial frequency, disparity and color. In the primate visual system, cortical sensitivity to these visual features has been shown to vary with the locus of spatial attention [for review see (Kastner and Ungerleider, 2000; Reynolds and Chelazzi, 2004)]. Specifically, attending to a stimulus in isolation has been shown to alter the effective luminance contrast detected by a neuron, causing a modulation of the neuron's contrast response function (CRF). Further, the exact form of this modulation is not constant but varies with the underlying contrast presented. Different models have been proposed to describe these attention-dependent contrast response modulations, and are still under debate: (i) One model suggested that attention causes a non-proportional scaling across varying contrasts, which manifests as a leftward shift of the CRF or effective contrast gain (Reynolds et al., 2000; Martinez-Trujillo and Treue, 2002b; Reynolds and Chelazzi, 2004). (ii) Another model proposed a proportional scaling of neuronal response with attention, which would produce either a response or activity gain effect (Williford and Maunsell, 2006). Further, this second model may be a closer match to attentional effects seen with orientation (McAdams and Maunsell, 1999a) and direction tuning curves (Treue and Martinez-Trujillo, 1999). Very recent work has suggested these two models may not be competitive but rather derived from a common model circuit (Reynolds and Sundberg, 2007), though neither model offers insight into the origin of the signals causing these modulations.

Several lines of evidence suggest that the top-down sources for the presumptive feedback signals that mediate spatial attention are tightly linked with the oculomotor system (Rizzolatti et al., 1987; Corbetta and Shulman, 2002; Hamker, 2005). In particular, the Frontal Eye Field

(FEF), on the anterior bank of the arcuate sulcus, is thought to be involved in modulating incoming sensory input in an attention-dependent manner. The FEF would be an excellent candidate for sending top-down signals to visual cortex in part because of its role in visual target selection (Tehovnik et al., 2000), its defined retinotopic map of visual space (Bruce et al., 1985) and its reciprocal connections to many cortical visual areas (Huerta et al., 1987; Schall et al., 1995; Stanton et al., 1995). Experiments that artificially increase the output of the FEF using electrical microstimulation (FEF-EM) have shown i) decreased contrast detection thresholds during a spatial attention task (Moore and Fallah, 2004), and changes in ii) neuronal firing rates in area V4 (Moore and Armstrong, 2003) and iii) fMRI activation in multiple visual areas (Ekstrom et al., 2008). Both the type of stimulus used (preferred or non-preferred) in the single unit study (Moore and Armstrong, 2003) and the spatial pattern of modulation observed across the cortical surface in the fMRI study (Ekstrom et al., 2008) suggest that the observed modulations may depend on the underlying strength of neuronal drive produced by the stimuli, similar to attentional effects on the CRF.

To measure the effects of stimulus saliency on FEF-EM induced modulations of activity throughout visual cortex, we collected cerebral blood volume (CBV)-weighted functional magnetic resonance imaging (fMRI) data from two awake monkeys (Vanduffel et al., 2001) while simultaneously stimulating the FEF (Ekstrom et al., 2008). We first measured the visually driven fMRI response to stimuli of varying luminance contrast in a number of cortical visual areas (Ungerleider and Desimone, 1986b; Felleman and Van Essen, 1991), and compared that response to previously derived CRFs from several primate single cell (Albrecht and Hamilton, 1982; Sclar et al., 1990; Williford and Maunsell, 2006) and human fMRI studies (Tootell et al., 1995; Buracas and Boynton, 2007; Li et al., 2008). With the stimuli positioned in the movement

fields (MFs) corresponding to the locations of chronically implanted electrodes in the FEF (Moore and Armstrong, 2003; Ekstrom et al., 2008), we also measured the fMRI response to combined visual and FEF electrical (FEF-EM) stimulation. By computing the difference in these responses, we characterized how the CRF is altered by increased FEF output. We found evidence for a non-proportional scaling of the CRF, though particularly at high contrast levels this did not follow the appropriate model prediction. In general, the largest enhancement of fMRI activity was observed at the lowest contrasts, while high contrast stimuli were unaffected or in some cases even suppressed by this artificially increased output of the FEF.

3.3 Materials and Methods

Many of the details of the primate imaging and stimulation techniques used have been described previously (Vanduffel et al., 2001; Ekstrom et al., 2008), and will only be summarized here briefly. All procedures were approved by MGH's Subcommittee on Research Animal Care (Protocol #2003N000338) and MIT's Committee on Animal Care, and are in accordance with NIH guidelines for the care and use of laboratory animals.

3.3.1 Subject Preparation

In short, we prepared two male rhesus monkeys (*Macaca mulatta*; MM1 and MM2, 5-7 kg, 4-5 years old) for fMRI with surgical implantation of a MR compatible head post, and then trained them for a passive fixation task. Once the subjects achieved accurate fixation performance, we chronically implanted 26 intracortical microelectrodes in the right FEF. Guided by anatomical MR images, we made a craniotomy over the right arcuate sulcus and opened the dura mater. Twenty six Teflon-coated microwires (25 μm diameter, 10% platinum / 90 % iridium; California Fine Wire Company; Grover, CA) were inserted by hand normal to the cortical surface (Mioche and Singer, 1988) along the rostral bank of the arcuate sulcus (~2-6 mm

deep). Wire tips were beveled and ~40 μm of insulation stripped prior to insertion. The dural

and bone flaps were then replaced. We soldered the microwires to a magnet-compatible

connector (Omnetics Connector Corporation; Minneapolis, MN), which was then encased in

dental acrylic as a part of the subject's head set. A ground electrode was implanted between the

skull and muscle and attached to the connector. After surgery, we verified the correct anatomical

placement of the electrode tips in the FEF using T2-weighted images collected at 7.0 T. We also

obtained behavioral verification, in the form of successfully induced saccadic eye movements,

during a fixation task outside the scanner. These eye movements defined for the neurons

surrounding each electrode the so-called FEF MF and the stimulation threshold to evoke a

saccade [see also (Ekstrom et al., 2008)].

3.3.2 Anatomical and Functional MRI Acquisition

High resolution, T1-weighted anatomical images were collected on a 3.0 T full-body

scanner (Trio, Siemens Healthcare; Erlangen, Germany) for the overlay of functional analyses.

Under ketamine-xylazine anesthesia, a MP-RAGE sequence (178 sagittal slices, 256 × 256 in-

plane matrix, TR = 2.5 s, TE = 4.35 ms, TI = 1100 ms, $0.35 \times 0.35 \times 0.35$ mm^3 isotropic voxels,

flip angle = 8°) was used to obtain 9 whole-brain volumes, which were averaged together to

improve the signal-to-noise ratio. A single radial transmit-receive surface coil (12.5 cm

diameter) was employed.

Functional images were acquired on a 3.0 T full-body scanner (TIM Trio, Siemens

Healthcare; Erlangen, Germany) with a gradient coil insert (AC88; 80 mT/m maximum gradient

strength, 800 T/m/s maximum slew rate), using a gradient-echo T2*-weighted echo-planar

imaging sequence (50 horizontal slices, 84 × 96 matrix, TR = 2 s, TE = 19 ms, $1 \times 1 \times 1$ mm^3

isotropic voxels). A four-channel phased array receive coil (individual coils 6 cm diameter),

with GRAPPA reconstruction (Griswold et al., 2002) and an image acceleration factor of 2, and a saddle-shaped, radial transmit-only surface coil (17 cm diameter) were employed (H. Kolster et al., unpublished observations).

Prior to each session, we injected a bolus of Microcrystalline Iron Oxide Nanoparticles (MION; 6-10 mg/kg) in isotonic sodium citrate into the femoral or saphenous vein to increase the contrast-to-noise ratio compared to blood oxygen level dependent imaging (BOLD) (Vanduffel et al., 2001; Leite et al., 2002). Accordingly, we have flipped the polarity of all percent signal change values to account for the difference between MION Cerebral Blood Volume (CBV) and BOLD activation maps (increased brain activation produces a decrease in MR signal in MION CBV maps).

In many cases, we were able to generate robust and well-localized fMRI activation maps for a given stimulus location from a single session (for example, see Fig. 3-1D). We obtained a high MR contrast-to-noise ratio (CNR) largely due to the use of: (i) the four-channel phased array receive coil that enabled two-fold image acceleration, which increased the SNR (Griswold et al., 2002) and reduced susceptibility distortions at the air-tissue interfaces around the brain, and (ii) the gradient insert coil, which increased the strength and slew rate of the MR scanner's gradients to permit shorter TR and TE values in our scanning sequence, so that we could collect more data per unit time. A shorter TE value also reduced the overall $T2^*$ decay caused by the MION contrast agent, yielding further increases in image SNR (Mandeville et al., 2004). We limited our design to the five contrast values shown in Fig. 3-1A, chosen to get a general overview of the contrast response function. The instances where multiple sessions were needed for a given stimulus were largely due to monkey behavior because of the long runs required by

this stimulus design – five different luminance contrasts × two electrical stimulation conditions × two repetitions yielded individual runs of twenty epochs.

3.3.3 Visual and Electrical Stimulation

We used a block design with 24 s long epochs (12 TRs) and 20 epochs per run, or time series, to measure fMRI activation during ten different conditions (contrast levels of 0, 3, 6, 12 and 50%, each with and without EM stimulation; Fig. 3-1A). In total, 24 960 functional volumes were collected from MM1 (6 sessions) and 23 280 functional volumes from MM2 (6 sessions), of which 15 360 and 18 600 volumes respectively, were used to generate the data shown.

Visual stimulation was presented to the subjects at 1024 x 768 resolution and 60 Hz refresh rate with a LCD projector (DLA-SX21, JVC; Yokohama, Japan) onto a translucent screen 51 cm from the animals' eyes. Prior to the beginning of our first experiment, we measured the luminance response of the projector's red, green, and blue channels combined and separately with a photometer (CS-100 Chroma Meter; Minolta; Tokyo Japan). From these response curves, we selected an approximately linear operating region, and used the combined curve to calculate luminance values to generate stimuli at the desired contrasts. Compared to the stimuli in our previous study, here we have discarded color information, and increased the size of the stimuli to 6 degrees diameter to reduce the possibility of any mismatch between onscreen stimulus location and the corresponding FEF MF. Stimuli were 6 visual degrees diameter, monochromatic, clipped sine-wave, contrast-varied gratings, where we defined contrast as the ratio between the difference and sum of luminance in the bright and dark regions (Michelson, 1927). The stimuli had a spatial frequency of 0.5 cycles / degree and moved at 2 degrees / s along one of 2 axes (0 and 90 degrees), with mean luminance matched to that of the uniformly gray background (76.9 cd/m^2).
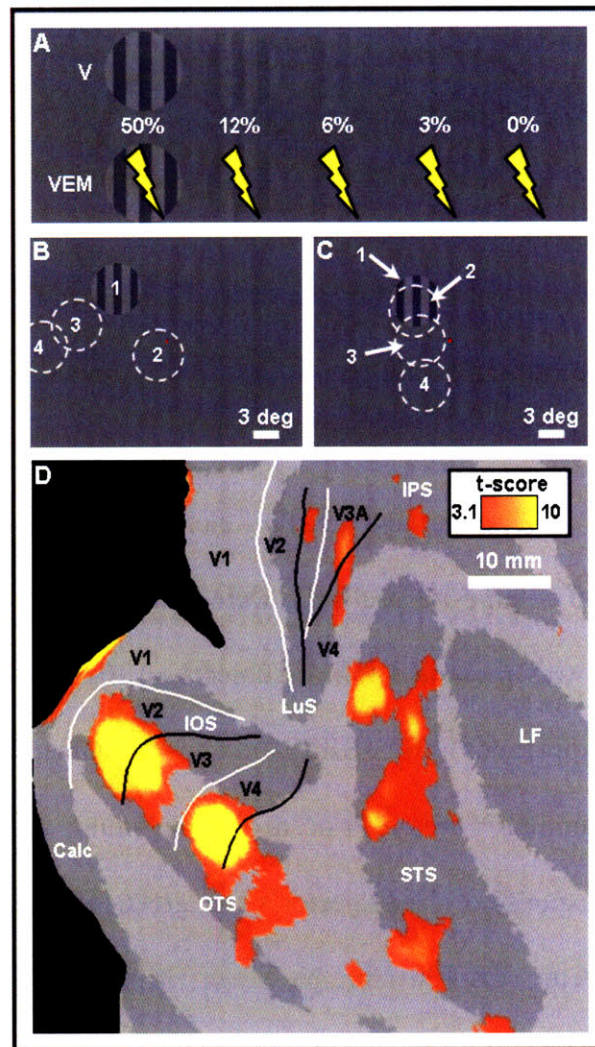
Fig. 3-1: Stimulus conditions, stimulus locations and localizer example. **(A)** The ten stimulus conditions used: stimuli at five different luminance contrast levels, presented without (V) and with (VEM) simultaneous FEF-EM. 0% V was used as the baseline condition. The main visual effect at 50% contrast (See 3.3.4 Statistical Analysis) was used as a localizer to identify a common population of visual voxels for further analysis. **(B, C)** Stimulus locations for MM1 and MM2, respectively. The stimuli were positioned at the endpoint of the saccade vector produced by stimulating each electrode above the threshold needed to elicit a saccade. During a given fMRI session, we stimulated at 50% of this behaviorally-defined saccade threshold, and used only one stimulus and electrode. One stimulus example is shown in each panel, and the dotted white lines indicate the other stimulus positions used for that subject. The red dot in the center represents the fixation spot, which was visible in all conditions. **(D)** A thresholded t-score map (P < 0.001, uncorrected) of the localizer contrast (50% VEM + 50%V versus 0% VEM + 0% V) overlaid on the flattened representation of occipital cortex from MM1. The results shown correspond to representation of stimulus 3 in B. Sulci are dark grey, and white and black solid lines indicate the representations of the vertical and horizontal meridians, respectively. Anatomical labels: Calc, Calcarine sulcus; CS, Central sulcus; IOS, Inferior Occipital sulcus; IPS, Intraparietal sulcus; LF, Lateral fissure; LuS, Lunate sulcus; OTS, Occipitotemporal sulcus; STS, Superior Temporal sulcus.

Stimulus location was matched to the MF of the single electrode stimulated in that particular session (Moore and Armstrong, 2003; Ekstrom et al., 2008). Note that this single stimulus method differs from the multiple sequential stimuli and FEF sites approach used in our previous study, which produced fMRI activation maps averaged across all stimuli presented and electrodes used within a TR. While such sequential presentation is arguably closer to the physiological operating state of the visual system and produces very robust EM-only effects, it complicates the final interpretation of visual results due to averaging across multiple stimuli and the additional possibility of temporal interactions. Here, we used only a single stimulus-FEF electrode pairing in each session and concatenated the data after GLM analysis to calculate CRFs averaged across the stimulus-electrode pairings in both subjects.

We used a pseudo-randomized design with multiple stimulus orders. In the epochs with FEF-EM, we stimulated the selected electrode twice within a TR (ISI = 1 s). The visual stimulus was presented for 133 ms, followed by 250 ms of combined visual stimulation and FEF-EM and then 617 ms with neither; this sequence was repeated twice within the 2 s TR. A central fixation point was continuously visible and the monkeys performed a passive fixation task throughout each run. Eye position was monitored at 120 Hz using an infrared pupil/corneal reflection tracking system (Iscan Inc.; Burlington, MA). The EM signal was generated by an eight-channel Digital Stimulator (DS8000, World Precision Instruments; Sarasota, FL), controlled by custom software that also generated the visual stimulation. Stimulation trains consisted of biphasic square-wave pulses with a frequency of 335 Hz for 250 ms, and were delivered in a monopolar configuration. Each pulse consisted of 190 μs of positive and 190 μs of negative voltage, separated by 100 μs of zero voltage. The sum of the cables' stray capacitance and the monolithic capacitor array EMI filters in the scanner penetration panel ranged from 5.1 to 5.3 nF.

Prior to each fMRI experiment, we determined the threshold to elicit a saccade with each electrode by varying the EM amplitude until ~70% of stimulation trains induced a saccade from central fixation. A saccade vector was determined to identify the MF of the FEF site of interest for that experiment (see Fig. 3-1B for MM1's MFs and Fig. 3-1C for MM2's MFs used in the current study); a stimulation level of ~50% of this behaviorally-defined threshold was then used for the actual imaging experiment (Moore and Armstrong, 2003). At the beginning and end of each fMRI session, we measured the impedance of the stimulated channel, as well as the impedance of the three channels not used, with a 1V, 100 Hz reference signal to estimate the injected current. For MM1, impedance was 32 ± 2 kΩ, 35 ± 1 kΩ, 48 ± 2 kΩ, and 55 ± 3 kΩ for the 4 electrodes used; for MM2, impedance was 24 ± 1 kΩ, 27 ± 1 kΩ, 36 ± 1 kΩ, and 42 ± 11 kΩ for the 4 electrodes used (mean $\pm$ standard deviation across all sessions). Estimated stimulation amplitudes for the four FEF electrodes used in MM1 were 26 µA, 36 µA, 55 µA and 72 µA and in MM2 37 µA, 38 µA, 49 µA and 58 µA. We note that the current necessary to evoke saccades through chronic electrodes may be larger than with higher impedance acute electrodes. One reason for this is the possible growth of a fibrous barrier between the electrodes and neural tissue over the 2-3 years between implantation and collection of the present data set (Bartlett et al., 2005).

3.3.4 Statistical Analysis

We performed a voxel-based analysis with SPM99, following previously described procedures to fit a general linear model (GLM) (Friston et al., 1995; Vanduffel et al., 2001; Leite et al., 2002; Vanduffel et al., 2002). Images were motion-corrected within session and non-rigidly co-registered to each subject's own anatomical template using Match software (Chef d'hotel et al., 2002). Images were then smoothed (Gaussian kernel, $\sigma = 0.67$ mm) and registered

using Match to MM1's T1-weighted anatomical volume. Global scaling, and high- and low-pass filtering were employed prior to fitting the GLM.

We used the main visual effect at 50% contrast (that is, 50% VEM + 50% V versus 0% VEM + 0% V, Fig. 3-1A) as a localizer to identify visually driven voxels (hereafter referred to as *visual voxels*) for analysis across all contrast levels. *t*-score maps of this contrast from each session in each monkey were thresholded [$P < 0.05$, uncorrected; for split population analysis, low *t* voxel distribution is 0.05, uncorrected $> P > 0.05$ corrected, high *t* voxel distribution is $P < 0.05$, corrected; correction for multiple comparisons used the Family-Wise Error procedures in SPM99 (Worsley et al., 1996)] and overlaid on the common anatomical space defined by MM1's T1-weighed anatomical volume as reconstructed by FreeSurfer (Dale et al., 1999). We created flattened cortical representations with Caret using the F99 atlas (http://brainmap.wustl.edu/caret, http://brainmap.wustl.edu:8081/sums/directory.do?id=636032) (Van Essen et al., 2001) (see Fig. 3-1D for an example of one session). The borders of twelve visual areas were identified on this flattened cortical representation using retinotopic mapping data previously collected in three animals (Fize et al., 2003) and a Caret Atlas based on two previous studies (Felleman and Van Essen, 1991; Ungerleider and Desimone, 1986b). We extracted the population of visual voxels inside each area satisfying the above contrast and sampled the percent change in MR signal for each condition with SPM99. The first 3 TRs in each epoch were excluded and an additional TR appended at the end to compensate for hemodynamic delay. Standard error of the mean was calculated over the condition epochs. We concatenated the entire population of voxels in each area to generate CRFs and various derivatives.

To account for any head and eye movement-related fMRI activity, covariates of no-interest from six motion realignment parameters and the *x* and *y* eye trace components were

generated and included in the GLM analysis. Eye traces were thresholded at approximately 2 degrees, convolved with the MION hemodynamic response function, and sub-sampled to the TR. We performed several analyses to assess the potential effects of eye movements on fMRI activation. First, for each run collected, we aligned the stimulation events across all contrast levels to EM onset and the visual-only conditions to the matching time. We then performed a *t*-test at each time point to identify any significant differences in eye position ($P < 0.05$, corrected for multiple comparisons across time points; two sample, two-tailed *t*-test across all trials in that run). Any run with a significant difference at any time point was excluded from further analysis. The mean *x* and *y* eye position aligned to EM onset across all sessions is illustrated in Fig. 3-2. Second, for each subject's aggregate data we utilized a one-way ANOVA on the eye traces to test for any significant differences in percent fixation, saccade rate, and eye position along the *x* and *y* axes between the VEM and V conditions across all contrast levels (Table 3-1).

3.3.5 Model Fitting

To the mean data points calculated in each brain area during the V and VEM conditions, we fit the Naka-Rushton equation (Naka and Rushton, 1966; Li et al., 2008):

$$R = \frac{R_{\max}c^2}{c^2 + c_{50}^2} + b , [1]$$

where *c* is the fractional contrast level, c_{50} the contrast at which the response curve attains half of its maximum, R_{max} the maximum response of the region and *b* the baseline response value. When fitting the V conditions, we omitted the baseline response parameter because the 0% V condition was used as reference. This equation is a simplified form of the more general one used to fit contrast response data from single cell recordings (Albrecht and Hamilton, 1982). We used an *F*-test to assess the goodness-of-fit in each region. To estimate 95% confidence intervals for

all parameters we implemented a non-parametric bootstrap algorithm (Efron and Tibshirani, 1993). In a particular region, the *visual voxel* population was randomly sampled with replacement and the best fitting parameters calculated for that particular sample. We repeated this sampling 1000 times and determined the 2.5% and 97.5% quantile values from the resulting parameter distribution to indicate the confidence interval.

3.3.6 ROC Analysis

To estimate the distinguishability between the distributions of V and VEM percent change in MR signal values at a particular contrast level for the voxels in a given functional brain region, we calculated the area under a receiver-operator-characteristic (ROC) curve (McNicol, 1972). An ROC curve is determined by plotting the percentage of one distribution less than a given criterion value as a function of the percentage of the second distribution less than that same criterion, for all possible criterion values in the distributions. The area under the ROC curve then reflects how separate or distinguishable the two distributions are. An area of 0.5 means the V and VEM distributions could not be discriminated at that contrast level in that region; deviations from 0.5 indicate increasing discriminability, with maximum possible values of 0 or 1. In order to include the 0% contrast level in this analysis, we changed the reference point for the signal change distributions in all conditions on a voxel-by-voxel basis from the

Fig. 3-2 (Next page): Average eye position aligned to EM onset. **(A, B)** Mean horizontal eye trace, and **(C, D)** mean vertical eye trace for MM1. **(E, F)**, Mean horizontal eye trace, and **(G, H)** mean vertical eye trace for MM2. The solid red line plots mean eye position across all sessions and contrasts during VEM and V epochs; the dashed black lines show +/- SEM across the four electrodes stimulated. Traces have been aligned to EM onset (VEM) or the matching time in epochs without stimulation (V); total duration of FEF-EM is indicated by the lower, dark grey bar (250 ms). The upper, light grey bar indicates the period of visual stimulation (VEM, V); visual onset, at -133 ms relative to EM onset, is not shown. Any run showing a significant difference between the two conditions at any time point was removed ($P > 0.05$, corrected for multiple comparisons across time points; two sample, two-tailed t-test across all acquired trials). These mean traces from the included runs show no significant difference at the aggregate level.

baseline 0% V condition to the mean fMRI signal value. To estimate 95% confidence intervals on each of the ROC areas, we again used the non-parametric bootstrap algorithm (Efron and Tibshirani, 1993) described above.
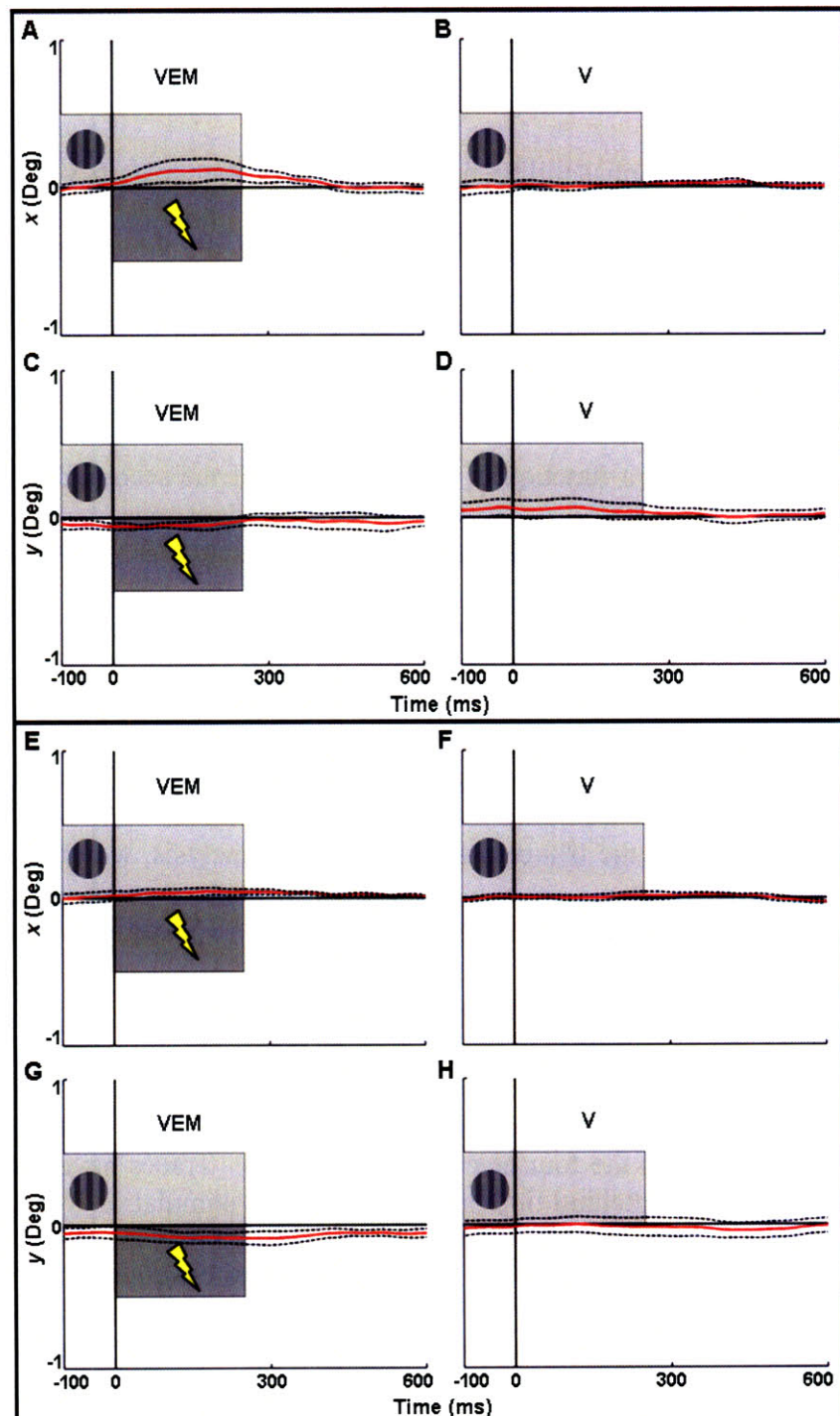
Table 3-1: Fixation behavior during fMRI runs. n is the number of independent fMRI runs collected from each subject. Percent fixation was calculated using a 2 degree × 2 degree window; σ_x & σ_y are the mean standard deviation of eye position along the x and y eye axes, across all repetitions of a condition within a given run. A one-way ANOVA on each condition pair showed no significant differences ($P > 0.05$) in any of the distributions.

Subject	n	Conditions	% Fixation		Saccades / min		σ_x (deg)		σ_y (deg)	
			Median	P	Median	P	Median	P	Median	P
MM1	63	VEM	88.0		9.8		0.20		0.34	
				0.40		0.25		0.51		0.92
		V	86.2		10.3		0.20		0.34	
MM2	78	VEM	87.1		10.9		0.25		0.39	
				0.53		0.90		0.81		0.69
		V	86.2		11.0		0.24		0.40	

3.4 Results

3.4.1 Quality of fMRI data

In both monkeys, we collected data from four stimulus locations (Fig. 3-1B and C), corresponding to four implanted FEF electrodes and associated MFs, over six fMRI sessions. Stimuli were spread across the left visual field, contralateral to the side of the brain in which we implanted the electrodes, with examples in the upper and lower visual field and along the horizontal meridian. Eccentricities ranged from 1.8 visual degrees to 15.0 visual degrees in MM1, and from 3.5 visual degrees to 7.3 visual degrees in MM2. Saccade vectors were for the most part larger in MM1 than in MM2, suggesting that we stimulated slightly different parts of the FEF in the two subjects. This does not reflect a conscious bias in the implantation procedure though, as in both subjects we attempted to distribute the electrode wires throughout the anatomically defined location of the FEF on the anterior bank of the arcuate sulcus. Because of the small number of samples we did not attempt to distinguish between eccentricities and polar angles, and instead included all stimulus locations in one analysis (Fig. 3-1B and C).

For MM1, data from three identical sessions were combined for one target location, and data for the remaining three stimuli were each collected in a single session. For MM2, data for two stimulus locations were collected in individual sessions and the remaining two locations were each collected over two sessions. On average, we collected 17.3 and 16.2 runs per session in MM1 and MM2, of which 10.7 and 12.9 runs per session were included in the analysis presented here. Inclusion criteria were based on a run by run analysis of the eye monitoring data recorded during each run. Runs in which the monkey's eye position at any time point in the stimulation sequence (1 s, sampled at 120 Hz) was significantly different between V and VEM epochs were excluded from further analysis (see Section 3.3 Materials and Methods, Fig. 3-2).

3.4.2 Visual-only Contrast Response Functions

For each stimulus location, we identified a population of *visual voxels* for further analysis from the fMRI contrast defined by the main visual effect at the highest luminance contrast (that is, 50% VEM + 50% V versus 0% VEM + 0% V). Using this population, we extracted the percent change in MR signal with respect to the fixation only or 0% V condition for each voxel at each of the other luminance contrast levels presented to the subjects. For each cortical area of interest, we then pooled the population of *visual voxels* across all sessions from both subjects and computed the mean response as a function of contrast to generate a V CRF.

Fig. 3-3 shows the average CRF for each of the twelve cortical areas identified, grouped according to approximate cortical hierarchy (Felleman and Van Essen, 1991) and plotted on the same scale for comparative purposes. The smooth curves were calculated from the best fitting model to eq. [1] with the baseline parameter *b* omitted (see Section 3.3.5 Model Fitting). Fig. 3-3A shows the response for early visual areas, including areas V1, V2, V3 and V3A. The CRFs for V2 and V3 were relatively similar to each other, as were the CRFs for V1 and V3A. In

general, contrast sensitivity in areas V2 and V3 was higher than that in areas V1 and V3A, perhaps indicating that areas V2 and V3 are more driven by magnocellular-dominated input compared to V1 and V3A with these stimuli. This observation also supports previous studies showing reduced motion sensitivity in monkey area V3A compared to V2 and V3 (Vanduffel et al., 2001). Fig. 3-3B shows the response functions for visual areas in the ventral stream leading into inferotemporal (IT) cortex, including areas V4, TEO and TE. The V4 CRF was qualitatively similar to the response seen for area V3. The two areas located more rostrally in IT cortex showed a decreased response to the contrast stimuli, with area TE showing the lowest contrast response. This low level of fMRI activity was likely because our gratings were non-optimal stimuli for driving these more object sensitive areas (Vogels and Orban, 1994).

Fig. 3-3C shows the response functions for visual areas in the STS more commonly identified with the dorsal stream, such as areas MT and MST, as well as area FST. Area MT showed the highest contrast sensitivity and the largest overall fMRI activation of all the areas sampled (mean response of 0.578 ± 0.011 percent change in MR signal across all contrasts). MST and FST had lower contrast responses, with area FST being the least responsive of this group, though qualitatively quite similar to area MT in terms of change in response between contrasts. Fig. 3-3D shows the response functions for the two highest-order visual areas sampled, area LIP in the lateral bank of the intraparietal sulcus and area STP in the upper bank of the STS. These two areas were the least responsive of all to luminance contrast, perhaps reflecting their role in integrating information from multiple sensory modalities (mostly STP) or their large receptive field sizes compared to the small stimuli size we used. Despite considerable differences in methodology and the stimuli used, we attempted to compare the CRFs obtained here with CRFs collected in previous human (Tootell et al., 1995; Buracas and Boynton, 2007;
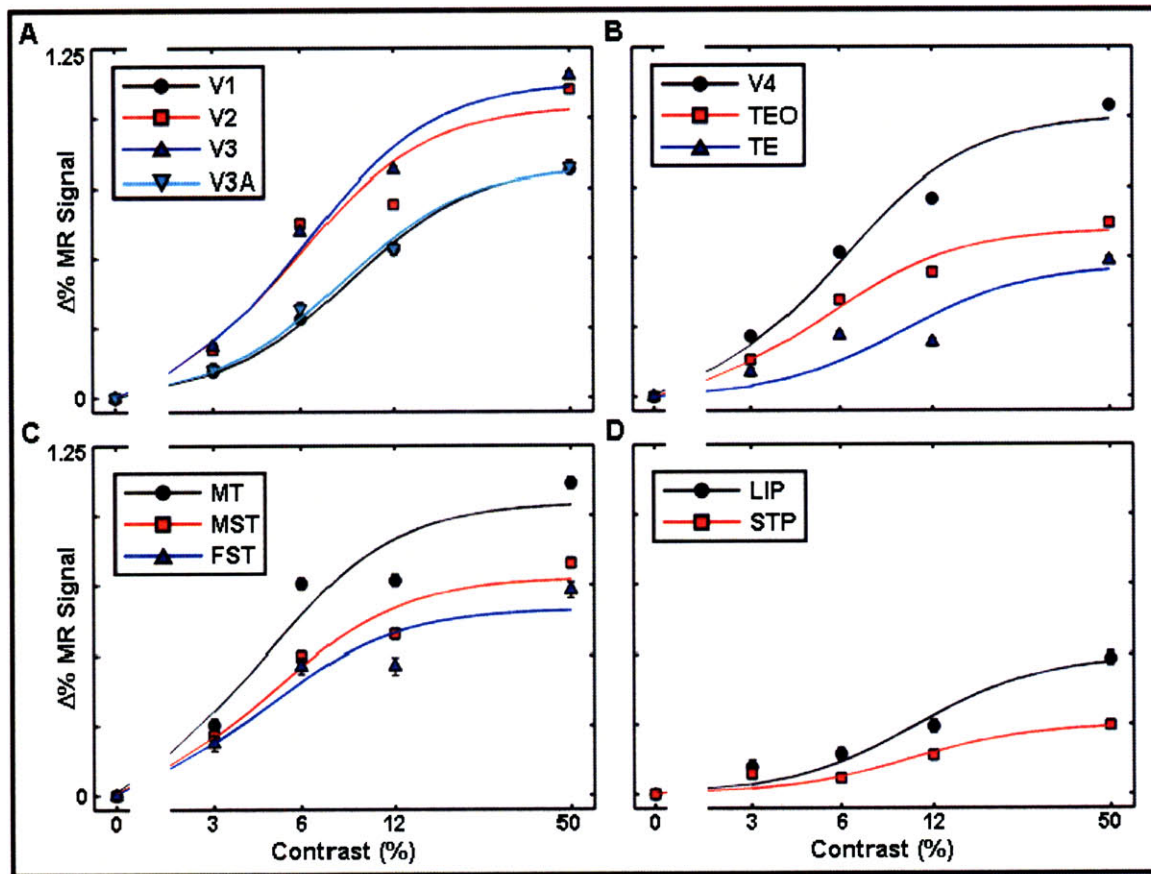
Fig. 3-3: Visual contrast response functions. Percent change in MR signal with respect to the baseline, or 0% contrast, condition as a function of luminance contrast for twelve visual cortical areas, including: **(A)** early visual areas V1, V2, V3 and V3A; **(B)** ventral extrastriate areas V4, TEO (Temporal-occipital area) and TE (Temporal area); **(C)** areas within the STS: MT (Middle Temporal area), MST (Medial Superior Temporal area) and FST (Fundus of Superior Temporal sulcus); and **(D)** higher order areas LIP (Lateral Intraparietal area) and STP (Superior Temporal Polysensory area). See Section 3.3.4 Statistical Analysis for a full description of how areal borders were determined. Each trace plots the mean response for all *visual voxels* localized in a given area, from both subjects across all sessions (only one stimulus location was used in each session). The smooth curves show the best fitting Naka-Rushton model for that area. Error bars indicate 1 SEM across epochs, and some error bars are smaller than the symbol used. Note that the *x* axis is a logarithmic scale, with a break between 0% and 3% contrast, to allow the inclusion of the 0% contrast values.

Li et al., 2008) and non-human primate studies (Albrecht and Hamilton, 1982; Sclar et al., 1990; Williford and Maunsell, 2006) (see Fig. 3-4 and Section 3.5.2). In general, we found good agreement with past human fMRI studies in early visual areas and some divergence in area MT.

Table 3-2 gives a summary of the best fitting parameters for each area from the Naka-Rushton model, with 95% confidence intervals estimated from a non-parameteric bootstrap algorithm (n = 1000). Several of the qualitative trends described above are apparent in these modeling results. Area MT had the sharpest rising CRF, and accordingly the lowest c_{50} value, indicating that this area is the most contrast sensitive of all visual areas measured. Extrastriate areas V2, V3 and V4 all had similar CRFs and thus relatively similar model parameters. Some of the higher order areas that showed the least responsivity to contrast (LIP, TE and STP in particular) had the highest c_{50} and lowest R_{max} values. The goodness of each model fit was assessed and determined to be satisfactory ($P < 0.05$; $F_{1,2}$ -test) in all areas except area TE.

Fig. 3-4 (Next page): Comparisons of human and non-human primate contrast response functions (CRFs) in multiple visual areas. CRFs for areas V1 **(A)**, V2 **(B)**, V4 **(C)** and MT / MT+ **(D)** were extracted where possible from human imaging (Tootell et al., 1995; Buracas and Boynton, 2007; Li et al., 2008) and primate single cell (Albrecht and Hamilton, 1982; Sclar et al., 1990; Williford and Maunsell, 2006) studies for comparison with the primate fMRI results generated in the current study. A consistent color code is used to delineate each study across all areas. All CRFs are normalized to the response level at 50% luminance contrast; for the data from Li et al. (2008), this level was estimated by linear interpolation and for Tootell et al. (1995) the 51% contrast level was used instead.

fMRI data is indicated by a solid trace and plots normalized percent change in MR signal values at the contrast levels reported in each study. CRFs from the current study and Tootell et al. (1995) indicate the response to visual stimuli only compared to a baseline fixation condition. CRFs from Li et al. (2008) represent the response to visual stimuli in the attend-away condition compared to a baseline fixation condition; the non-zero response at 0% contrast was subtracted in each area prior to normalization. CRFs from Buracas and Boynton (2007) represent the response to visual stimuli in the attend-toward condition compared to a baseline fixation condition, but the 0% response level was not presented in this study so no subtraction was made.

Single cell data is indicated by a dashed trace and plots the function generated from parameter values for the hyperbolic ratio fit to CRF data (Albrecht and Hamilton, 1982) at contrast values spanning the range used in the current study. Median values of each parameter were extracted from the Sclar et al. (1990) and Williford and Maunsell (2006) studies; means values were used from Albrecht and Hamilton (1982).

A

B

C

D

Legends:
- Ekstrom et al. (fMRI)
- Buracas-Boynton (fMRI)
- Li et al. (fMRI)
- Tootell et al. (fMRI)
- Sclar et al. (e-phys)
- Albrecht-Hamilton (e-phys)
- Williford-Maunsell (e-phys)

V1, V2, V4, MT

Activity (Norm)

Contrast (%)
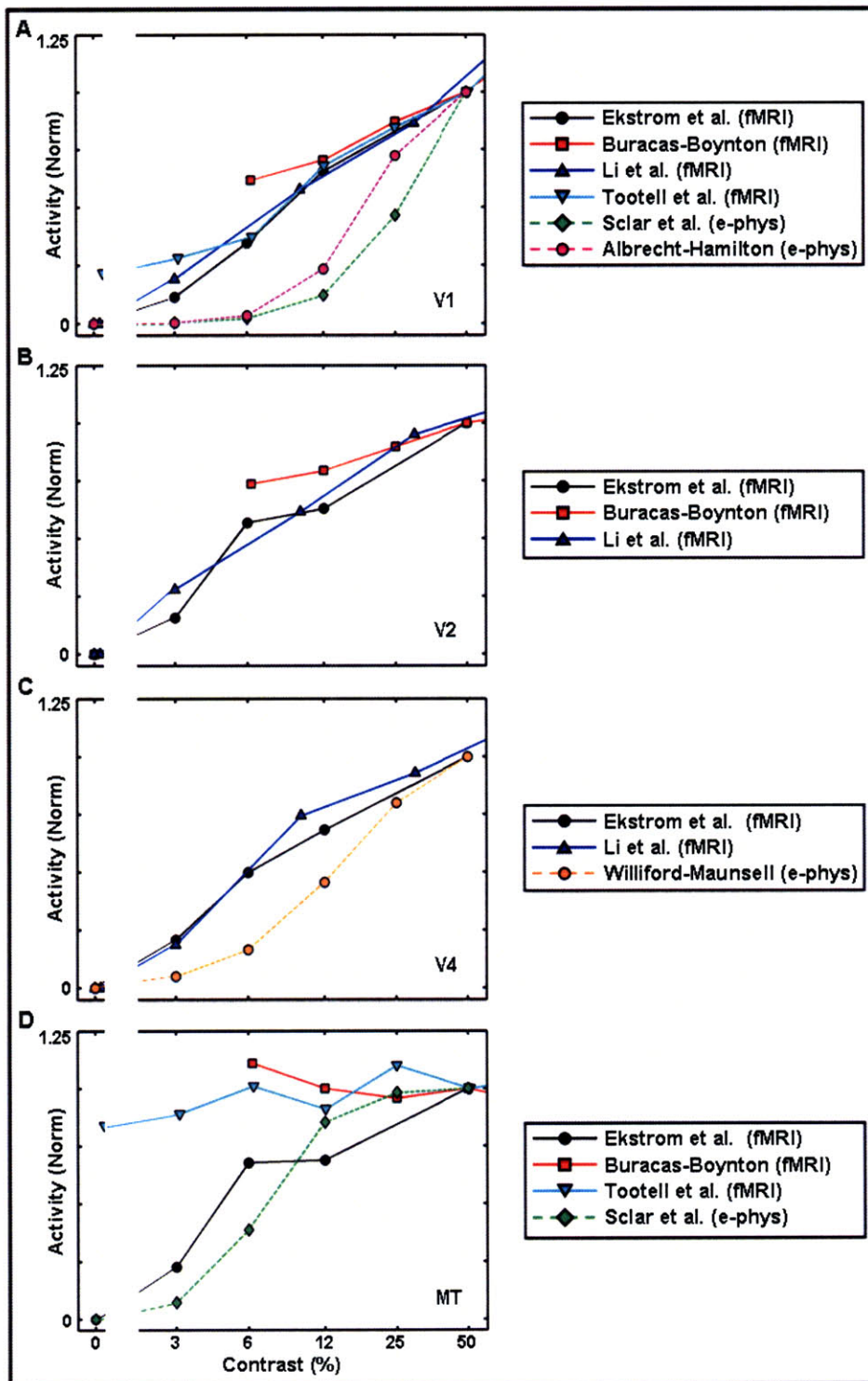
Table 3-2: Naka-Rushton model parameters and *F*-test results of the best fit to the percent change in MR signal values in the V conditions for each visual area. Best fit was determined by minimizing the sum of the squared error. Confidence intervals were estimated using a non-parametric bootstrap algorithm (n = 1000; see 3.3.5 Model Fitting). Shading indicates area did not exceed the critical $F_{1,2}$ value ($P > 0.05$).

Visual Area	(% MR signal)		(% Contrast)			
	R_{max}	95% CI	c_{50}	95% CI	$F_{1,2}$	*P*
V1	0.83	(0.81, 0.86)	8.8	(8.6, 9.1)	943	.001
V2	1.04	(1.00, 1.08)	6.1	(5.8, 6.3)	35	.027
V3	1.13	(1.08, 1.17)	6.4	(6.1, 6.7)	131	.008
V3A	0.83	(0.75, 0.91)	8.3	(7.6, 9.2)	274	.004
V4	1.01	(0.97, 1.04)	6.3	(6.0, 6.6)	100	.010
MT	1.05	(0.99, 1.10)	4.7	(4.5, 5.0)	35	.027
LIP	0.49	(0.46, 0.53)	10.8	(9.1, 12.7)	48	.020
MST	0.78	(0.73, 0.83)	5.0	(4.6, 5.4)	59	.017
FST	0.67	(0.62, 0.71)	4.8	(4.1, 5.6)	27	.035
TEO	0.60	(0.57, 0.63)	5.7	(5.2, 6.2)	111	.009
TE	0.47	(0.44, 0.51)	9.9	(7.6, 12.5)	14	.07
STP	0.25	(0.22, 0.28)	10.3	(7.3, 14.1)	27	.035

3.4.3 Contrast Response Functions with FEF-EM – Area V1

From the same population of *visual voxels*, we also extracted the percent change in MR signal for the epochs that combined a visual stimulus with simultaneous electrical stimulation of the FEF location with a matching movement field. We again calculated a mean response at each contrast level, across all stimulus locations in both subjects, to generate a VEM CRF. Fig. 3-5A shows for area V1 the resulting VEM CRF, along with the V CRF repeated from Fig. 3-3A for comparative purposes. Note that in this and following two figures, we plotted only the measured mean VEM and V responses and their derivatives rather than any fitted functions to give the most accurate indication of how FEF-EM modulates the cortical contrast response. For area V1, the FEF-EM dependent modulation of visually driven activity varied as function of the underlying luminance contrast of the visual stimulus. For the low contrast stimuli, we measured

an increase in mean fMRI activation (from 0.094 ± 0.010 to 0.221 ± 0.011 percent change in MR signal at 3% luminance contrast, without and with FEF-EM, respectively), whereas for the highest contrast stimuli we measured a decrease in mean fMRI activation (from 0.816 ± 0.011 to 0.695 ± 0.010 percent change in MR signal at 50% luminance contrast). The crossover point, when activation in the visual-only condition exceeded activation in the combined visual and FEF-EM condition was somewhere between 6 and 12% luminance contrast.

Next, we computed the difference between these two CRFs, shown by the black trace in Fig. 3-5B, and used a two-way ANOVA to assess whether there was a significant interaction between FEF-EM and visual stimulation, relative to the 0% V and 0% VEM conditions ($P < 0.05$; factors EM and visual stimulation). A positive interaction is indicated by the presence of a black filled square at each contrast level and a negative interaction by an open black symbol. In area V1, we found that there was a significant interaction at the 3% (positive), 12% (negative) and 50% (negative) luminance contrast levels. In agreement with our previous work (Ekstrom et al., 2008), no significant difference was found in V1 at the 0% contrast level, which indicates no EM-only effect or so-called baseline shift in this region ($P > 0.05$; one sample, two tailed t-test).

After comparing the difference between the VEM and V epochs, we also computed the fractional change this difference represents in terms of the underlying visual-only activation. For a particular area, we reasoned that a large change to a small initial activation would convey more information to any region reading out these signals than a change of equal magnitude on top of an already large activation. Fig. 3-5C shows this fractional change as a function of contrast for area V1. The use of the 0% V condition as our reference point precluded us from calculating this value at 0% contrast (though, as shown in Fig. 3-5B, the difference between V and VEM at this contrast is clearly quite small), but for all other contrast levels we calculated a fractional change

response function. Using this measure, we found that the modulations due to FEF-EM at the lowest contrast became even more apparent: the change in activation caused by FEF-EM in V1 represented a 1.4 ± 0.3 fold increase in fMRI activity. Conversely, the arithmetic difference at high contrast represented a much smaller effect, in this case a decrease of 0.15 ± 0.02 times the initial activation.

In addition to modulations of the mean response, another way to characterize how well an ideal observer could read out changes due to FEF-EM is to determine how separate or distinguishable the distributions of V and VEM signal change values are for the population of *visual voxels*. We estimated distinguishability by implementing a ROC (receiver-operator-characteristic) analysis at each contrast level, and then determining the area under the ROC curve (see Section 3.3.6 ROC Analysis). Fig. 3-5D shows a series of ROC curves for each contrast level and Fig. 3-5B (red) the resulting area under each ROC curve as a function of luminance contrast, for area V1. To include the 0% contrast values in this analysis, we recalculated all our signal change values with respect to the mean fMRI signal value rather than the 0% V baseline condition prior to computing ROC curves. This shift has no effect on the difference curve seen in black in Fig. 3-5B, as the reference point is always removed by the subtraction. It does preclude, however, the calculation of a meaningful fractional change response curve (Fig. 3-5C), and slightly alters the results of the ANOVA used to assess significant interactions between the VEM and V conditions. The red filled squares in Fig. 3-5B thus indicate significant interactions generated from a two-way ANOVA on this shifted data ($P < 0.05$). To estimate 95% confidence intervals, we used a non-parametric bootstrap algorithm (n = 1000; see Section 3.3.6 ROC Analysis).
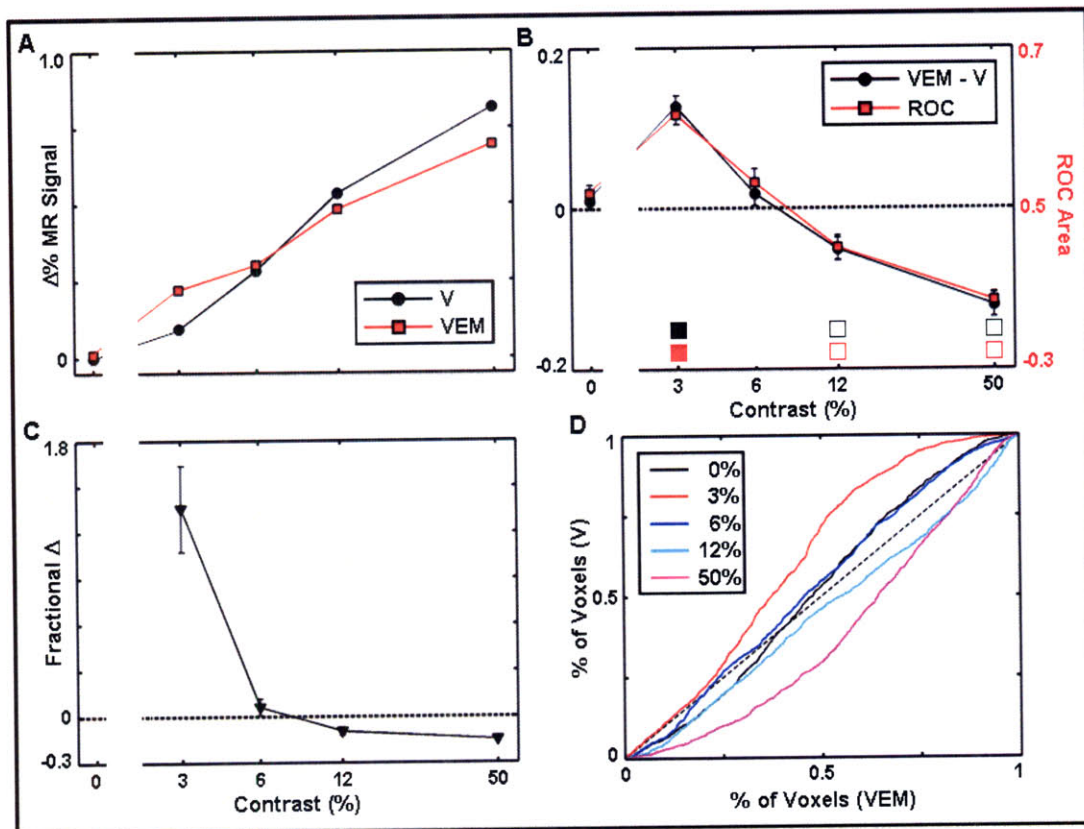
Fig. 3-5: Modulation of visual contrast response by microstimulation of the FEF in area V1. **(A)** Percent change in MR signal with respect to the baseline condition in the visual-only (V) and visual with FEF-EM (VEM) conditions as a function of luminance contrast. Each trace plots the mean response for all *visual voxels* localized in V1, from both subjects across all sessions. **(B)** Black trace plots the difference in fMRI activity between the VEM and V conditions at each contrast level [a subtraction of the two curves in (A)]. Red trace plots the area under an ROC curve [see (D)] between the voxel distributions of VEM and V percent MR signal change values at each contrast level; note the secondary y axis for red. An ROC area of 0.5 means an ideal observer could not distinguish the two distributions; larger deviations reflect greater distinguishability. To generate an ROC value for 0% contrast, all voxel values were shifted about the mean signal value of the voxel (across all conditions) rather than its baseline 0% V signal. Filled / hollow squares below the traces indicate a significant positive / negative interaction between factors EM and V at that contrast with respect to the 0% values, and correspond to the trace of matching color ($P < 0.05$; two-way ANOVA). **(C)** Fractional change in percent MR signal, determined by dividing the difference (black trace) in (B) by the underlying V signal change value. This fraction indicates the effective change in fMRI activity caused by FEF-EM relative to the visual-only activation level. Note that this parameter cannot be calculated for 0% contrast, because the 0% V condition was used as baseline. In all preceding panels, error bars indicate 1 SEM across epochs except for red in (B), which indicate 95% confidence intervals; some error bars are smaller than the symbol used. Note that all preceding x axes use a logarithmic scale. **(D)** ROC curves between the VEM and V MR signal change distributions for each contrast level.

In general, we observed in area V1 with this measure a similar trend as with the arithmetic difference metric. The VEM and V signal change distributions were most distinguishable for the lowest contrast stimuli, with VEM greater than V, and for the highest contrast stimuli, with V greater than VEM. As outlined below, the largest suppressive effect of FEF-EM ([i.e.] V greater than VEM) was observed in area V1.

3.4.4 Contrast Response Functions with FEF-EM – All Visual Areas

We extended the above analysis to all visual cortical areas from which we collected fMRI data. Fig. 3-6 shows difference CRF and fractional change plots for the twelve cortical areas first identified in Fig. 3-3, with the corresponding plots for V1 repeated from Fig. 3-5 for comparative purposes. We have grouped areas together that are close to each other in terms of cortical hierarchy and that show similar qualitative features in their difference CRFs. In all areas except STP, we observed the largest increase in fMRI activity in the VEM epochs at the 3% luminance contrast level, while the highest contrast stimuli showed no or even a negative interaction, which indicates a reduction in fMRI activity due to EM. We think these high contrast observations are not likely attributable to a ceiling effect for our fMRI measurements, given that we found a decrease in activation in some regions and were able to measure much larger percent signal change values in some areas in our previous study (Ekstrom et al., 2008). In several areas, including V3, V4, MT, MST, FST, LIP and STP, we measured a significant baseline shift due to FEF-EM ($P < 0.05$; one sample, two tailed t-test). This group of areas is mono-synaptically connected with the FEF (Huerta et al., 1987; Schall et al., 1995; Stanton et al., 1995) and so a robust, fMRI-detectable, EM-only effect is expected here (Tolias et al., 2005; Ekstrom et al., 2008). In four areas, including V2, MT, MST and FST, we observed a significant negative interaction at the 6% contrast level that does not seem to match the trend established by

the next lower and higher contrasts. Although we have no obvious explanation for this effect, we note that this feature is common to mainly dorsal stream areas which are strongly interconnected anatomically (Ungerleider and Desimone, 1986a; Ungerleider and Desimone, 1986b; Boussaoud et al., 1990).

As we did for the V only conditions, we fit the Naka-Rushton model (eq. [1]) to the mean VEM response in each area (Table 3-3). In this instance we included the baseline parameter b in the model fit. As before, the goodness of each model fit was assessed and this time determined to be satisfactory ($P < 0.05$; $F_{2,2}$-test) in only seven of the areas examined (not areas LIP, FST, TEO, TE and STP). Thus in general, eq. [1] provides a less satisfactory description of the data in the VEM conditions than in the V conditions. This deficiency is indicated by the increase in the number of areas that failed to satisfy the goodness-of-fit test and by directly comparing P values, which are almost uniformly higher in the VEM fit. Fig. 3-5A illustrates well the features of the data responsible for this difference in fit quality. The Naka-Rushton model (Naka and Rushton, 1966) and more general hyperbolic ratio models (Albrecht and Hamilton, 1982) produce a smooth sigmoid function that seems to characterize well the visual only CRF in cortical visual areas. With the addition of FEF-EM, however, the model does not well capture both the pronounced rise in activity that we observed at 3% contrast coupled with the decrease in activity at high contrast. As a result, the best-fitting baseline parameter b in V1 is found to be non-zero, which disagrees with our earlier statistical analysis and our previous findings (Ekstrom et al., 2008). Further, many of the c_{50} values do not reflect the downward shift expected by the increase in activity observed at 3% contrast. Thus, although eq. [1] appears to adequately model the V data, this does not hold not true for the VEM data in all visual areas.
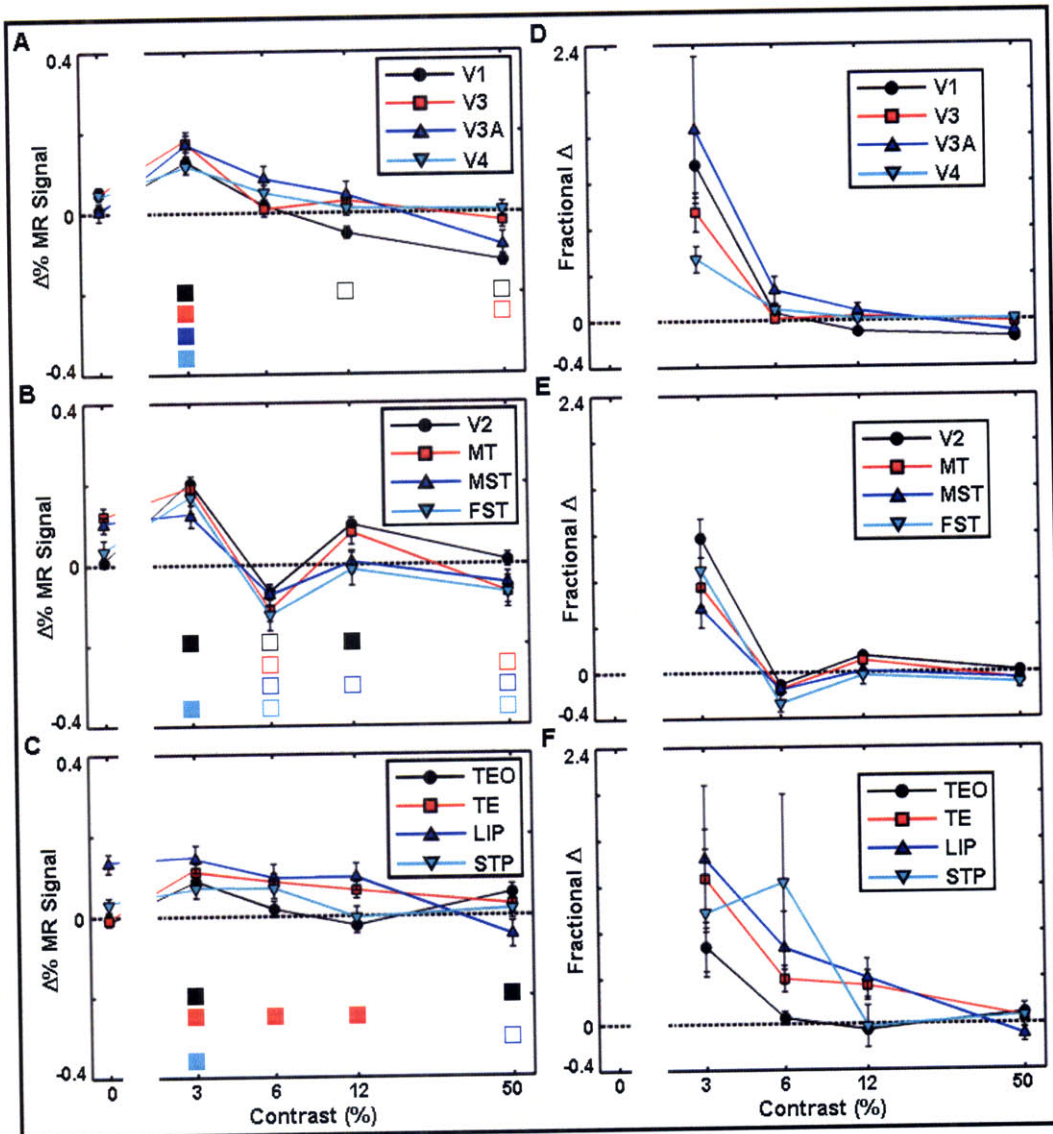
Fig. 3-6: Modulation of visual contrast response by microstimulation of the FEF in multiple visual areas. **(A, B, C)** The difference in fMRI activity between the VEM and V conditions at each contrast level (see Fig. 3-5B; area V1 is repeated here for comparative purposes) for the twelve areas defined in Fig. 3-3. Filled / hollow squares below the traces indicate a significant positive / negative interaction between factors EM and V at that contrast with respect to the 0% values, and correspond to the trace of matching color ($P < 0.05$; two-way ANOVA). **(D, E, F)** Fractional change in percent MR signal, determined by dividing the difference in VEM and V epochs by the underlying V signal change value (see Fig. 3-5C; area V1 is repeated here for comparative purposes), at each contrast level for the twelve areas defined in Fig. 3-3. In all panels, error bars indicate 1 SEM across epochs, and some error bars are smaller than the symbol used. Note that all x axes use a logarithmic scale.

Table 3-3: Naka-Rushton model parameters and F-test results of the best fit to the percent change in MR signal values in the VEM conditions for each visual area. Best fit was determined by minimizing the sum of the squared error. Confidence intervals were estimated using a non-parametric bootstrap algorithm (n = 1000; see 3.3.5 Model Fitting). A shaded row indicates the area did not exceed the critical $F_{2,2}$ value ($P > 0.05$). For areas that did satisfy the goodness of fit test, compared to the V condition model fits (Table 3-2), R_{max} values mostly decreased, except in V2 and V3A, where the confidence intervals remained overlapped. Comparing c_{50} values, only in V1 and V3A did the shift to lower contrasts produce a difference in the confidence intervals. Finally, in this model all areas that satisfied the F-test yielded a non-zero value of the baseline parameter b.

Visual Area	(% MR signal)		(% Contrast)		(% MR signal)			
	R_{max}	95% CI	c_{50}	95% CI	b	95% CI	$F_{2,2}$	P
V1	0.63	(0.60, 0.66)	7.4	(6.9, 7.9)	0.06	(0.04, 0.07)	26	0.037
V2	1.00	(0.95, 1.04)	5.9	(5.5, 6.2)	0.07	(0.04, 0.09)	25	0.038
V3	1.01	(0.96, 1.06)	5.8	(5.6, 6.1)	0.09	(0.07, 0.11)	55	0.018
V3A	0.68	(0.59, 0.76)	4.9	(4.3, 5.6)	0.03	(0.01, 0.05)	38	0.025
V4	0.91	(0.87, 0.94)	5.9	(5.5, 6.4)	0.09	(0.07, 0.11)	26	0.037
MT	0.86	(0.81, 0.92)	4.8	(4.4, 5.3)	0.15	(0.12, 0.17)	56	0.018
LIP	0.27	(0.24, 0.31)	8.8	(5.7, 11.0)	0.16	(0.13, 0.19)	14	0.07
MST	0.61	(0.57, 0.65)	6.2	(5.3, 7.3)	0.15	(0.12, 0.17)	21	0.046
FST	0.51	(0.46, 0.55)	3.8	(2.6, 8.4)	0.06	(0.02, 0.15)	5	0.16
TEO	0.59	(0.56, 0.62)	5.4	(4.7, 6.2)	0.03	(0.01, 0.04)	13	0.07
TE	0.41	(0.39, 0.43)	3.8	(3.1, 5.1)	0.00	(-0.01, 0.03)	4	0.19
STP	0.20	(0.16, 0.71)	17.9	(2.7, 93.2)	0.09	(0.03, 0.11)	3	0.23

As before, we computed the fractional change response functions for all twelve areas, by dividing the difference between VEM and V epochs by the underlying visual-only activation. These response functions are presented in Fig. 3-6D to F, following the same grouping of areas used above. The response function for V1 is repeated from Fig. 3-5C for comparative purposes. These curves further accentuate the pattern seen in the preceding graphs. For most areas, the largest enhancement of fMRI activity by FEF-EM above the underlying visual response was seen for the lowest contrast stimuli used.

Finally, for each area we computed a ROC curve using the VEM and V signal change distributions at each contrast level, and associated areas under the ROC curve. To save space,

we have not included the individual ROC curves for each area (see Fig. 3-5D), but rather plot

only ROC area response curves in Fig. 3-7, with the curve for V1 repeated from Fig. 3-5E for

comparative purposes. We have grouped the areas in the same manner as in Fig. 3-6. Filled

squares indicate a significant positive interaction between factors EM and visual stimulation,

determined at each contrast level using signal change values calculated with respect to the mean

response rather than the baseline ($P < 0.05$; two-way ANOVA). Open symbols indicate

significant negative interactions calculated in the same manner. In general, the VEM and V

distributions were most distinguishable at the 3% luminance contrast level. For areas V3, V4,

MT, MST, LIP and STP we found a significant difference in the baseline or 0% contrast level (P

< 0.05; one sample, two tailed t-test), which was matched by deviations of the ROC area from

the 0.5 value that exceeded the estimated confidence intervals. Using this measure, areas V3A

and TE, in addition to those areas seen in Fig. 3-6, showed a significant interaction at the highest

contrast level, which were matched by confidence intervals that did not include the 0.5 value.
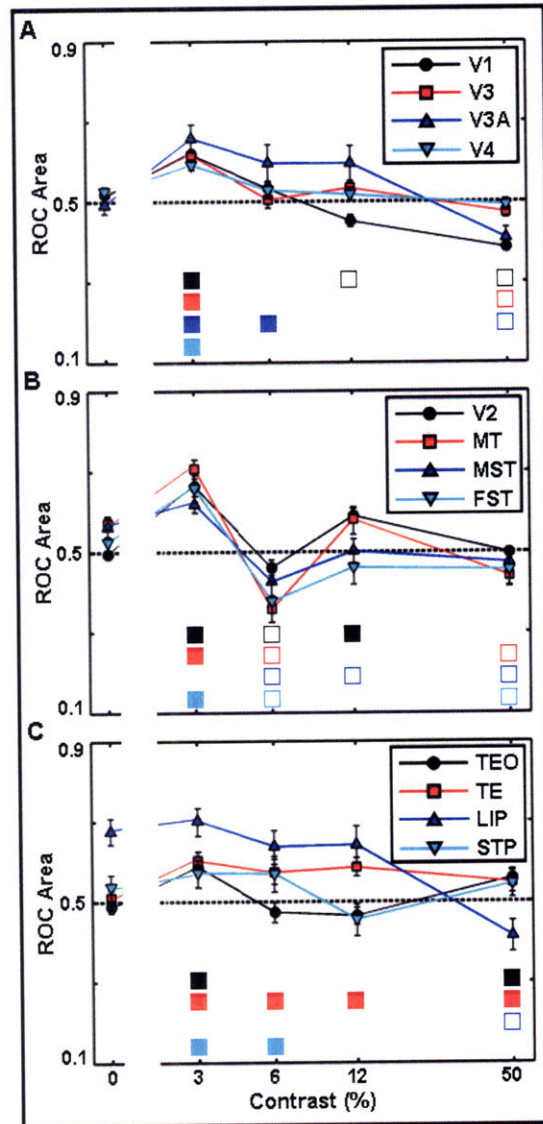
Fig. 3-7: Distinguishability between VEM and V distributions in multiple visual areas. ROC area (see Section 3.3.6 ROC Analysis) at each contrast level for the twelve cortical areas defined in Fig. 3-3: **(A)** areas V1, V3, V3A and V4; **(B)** areas V2, MT, MST and FST; **(C)** areas TEO, TE, LIP and STP. Filled / hollow squares below the traces indicate a significant positive / negative interaction between factors EM and V at that contrast with respect to the 0% values. The color of the square corresponds to the trace of the matching color ($P < 0.05$; two-way ANOVA). Positive deviations away from an ROC area of 0.5 indicate that the VEM distribution of signal change values was shifted towards higher levels of fMRI activity than the V distribution; negative deviations indicate the opposite. Error bars indicate 95% confidence intervals estimated by a non-parametric bootstrap algorithm. Note that all x axes use a logarithmic scale.

3.4.5 Generalized CRF for Visual Cortex

By pooling all voxels from the identified cortical areas, we calculated an overall CRF, difference CRF and fractional change function for all visually driven voxels in the primate occipital cortex. In Fig. 3-8A, we show this overall CRF along with the best fitting model for eq. [1]. In Fig. 3-8B, we plot the overall difference CRF, and indicate at which contrast levels a significant interaction exists between EM and visual response ($P < 0.05$; two-way ANOVA). Fig. 3-8C shows the fractional change response function. We measured a significant overall baseline shift at 0% contrast ($P < 0.05$; one sample, two tailed t-test). While a mean across all voxels biases the measurement towards larger regions, it nonetheless gives a more accurate estimate of the overall response of the visually driven areas in cortex than a mean calculated across the twelve individual areas would. For this overall mean response, we measured a significant positive interaction at 3% luminance contrast and a significant negative interaction at 50% luminance contrast.

In an additional analysis, we split our population of *visual voxels* into two groups, using each voxel's t-score in the localizer contrast (that is, 50% VEM + 50% V versus 0% VEM + 0% V) as a criterion, and by extension a surrogate, for how well the voxel was driven by the visual stimulus. All voxels that exceeded a P value of 0.05 at the corrected level were included in the *high* population (in other words, visually very well driven voxels). The remaining visual voxels (that is: 0.05, corrected $< P < 0.05$, uncorrected) were included in the *low* population (in other words, less well visually driven voxels). In Fig. 3-8A we also present the CRFs for these two subdivisions of our larger population along with the best fitting model for each group. Fig. 3-8B also shows the difference CRFs for these additional populations, and Fig. 3-8C the fractional change functions for each group. Table 3-4 gives the best fitting model parameters to the V only conditions and Table 3-5 the fit parameters for the VEM responses. Not surprisingly, the *high*

population showed a larger average percent change in MR signal at each contrast than the total population, and the *low* population lower average values (Fig. 3-8A). In terms of model parameters, the R_{max} values followed this same trend; the c_{50} values for the high and entire population were relatively similar, while the low population had a much higher one. Examining the difference CRFs, we found that the *low* population displayed a significant baseline shift ($P < 0.05$; one sample, two tailed t-test), a significant positive interaction at 3% and 12%, and a significant negative interaction at 50% ($P < 0.05$; two-way ANOVA). For the *high* population, we also found a significant baseline effect ($P < 0.05$; one sample, two tailed t-test) and positive interaction at 3%; however, we found a negative interaction at all three higher contrast levels ($P < 0.05$; two-way ANOVA).

This split-population analysis allowed us to construct a generalized spatial schematic of the macroscopic cortical response in visual areas to FEF-EM, as shown in Fig. 3-9. The color coded circles (Fig. 3-9A) represent these two populations of voxels on the cortical surface. For simplicity, we projected these populations onto a single spatial dimension to generate summary activity profiles. For the lowest contrast stimuli, all points along the projection are enhanced or amplified (compare solid, V-response curve and dotted, VEM-response curve, Fig. 3-9B). For the highest contrast stimuli (Fig. 3-9D), the macroscopic circuit has switched to a discriminatory mode; all points are slightly suppressed, though peripheral points are suppressed more. For intermediate contrasts (Fig. 3-9C), a hybrid of these two modes occurs; peripheral voxels are still amplified, while central points are slightly suppressed.
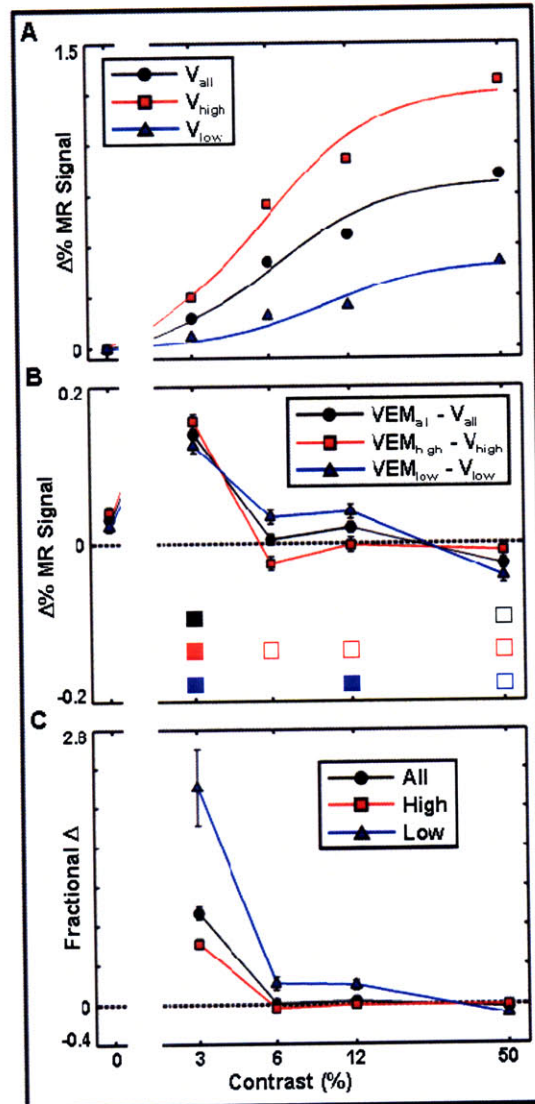
Fig. 3-8: Overall contrast response and modulation of contrast response by FEF microstimulation. **(A)** Mean percent change in MR signal for the V conditions as a function of contrast, across both subjects and all visual voxels in the twelve visual areas defined in Figure 4. The mean was weighted by the number of voxels in each region. Vall represents all visual voxels ($P < 0.05$, uncorrected). V_{high} represents the best visually driven voxels ($P < 0.05$, corrected). V_{low} represents all remaining voxels from the visual voxels pool not included in V_{high} (0.05, corrected $< P < 0.05$, uncorrected); on the cortical surface, these voxels are primarily located in annuli surrounding the best driven population. The smooth curves show the best fitting Naka-Rushton model for that population. **(B)** Mean difference between VEM and V conditions in the twelve regions for the three populations identified above. Filled / hollow squares below the traces indicate a significant positive / negative interaction between factors EM and V at that contrast with respect to the 0% values, and correspond to the trace of matching color ($P < 0.05$; two-way ANOVA). **(C)** Fractional change in percent MR signal, determined by dividing the difference in VEM and V epochs by the underlying V signal change value at each contrast level for the three populations. In all panels, error bars indicate 1 SEM across epochs, and some error bars are smaller than the symbol used. Note that all x axes use a logarithmic scale.

Table 3-4: Naka-Rushton model parameters and *F*-test results of the best fit to percent change in MR signal values in V conditions for the mean response in the *all*, *high* and *low* populations of voxels. Best fit was determined by minimizing the sum of the squared error. Confidence intervals were estimated using a non-parametric bootstrap algorithm (n = 1000; see 3.3.5 Model Fitting).

Visual Area	(% MR signal)		(% Contrast)			
	R_{max}	95% CI	C_{50}	95% CI	$F_{1,2}$	P
All	0.82	(0.81, 0.83)	6.6	(6.5, 6.7)	74	0.013
High	1.27	(1.25, 1.29)	6.0	(5.9, 6.1)	43	0.023
Low	0.42	(0.41, 0.43)	10.1	(9.4, 10.8)	112	0.009

Table 3-5: Naka-Rushton model parameters and *F*-test results of the best fit to percent change in MR signal values in VEM conditions for the in the *all*, *high* and *low* populations of voxels. Best fit was determined by minimizing the sum of the squared error. Confidence intervals were estimated using a non-parametric bootstrap algorithm (n = 1000; see 3.3.5 Model Fitting). A shaded row indicates the voxel population did exceed the critical $F_{2,2}$ value ($P > 0.05$). For the two populations that did satisfy the goodness of fit test, R_{max} and c_{50} values both decreased with the addition of FEF-EM, and the baseline shift parameter b was found to be slightly larger than 0.

Visual Area	(% MR signal)		(% Contrast)		(% MR signal)			
	R_{max}	95% CI	c_{50}	95% CI	b	95% CI	$F_{2,2}$	P
All	0.71	(0.70, 0.72)	6.0	(5.8, 6.2)	0.07	(0.07, 0.08)	22	0.043
High	1.16	(1.14, 1.18)	6.0	(5.9, 6.2)	0.09	(0.08, 0.10)	6	0.14
Low	0.29	(0.28, 0.30)	5.6	(4.3, 7.4)	0.05	(0.04, 0.07)	36	0.027

3.5 Discussion

Using CBV-weighted fMRI, we have measured response functions to visual stimuli at five luminance contrast levels in twelve defined functional areas of the macaque visual cortex and determined the best fit parameters according to the Naka-Rushton model. Further, we observed how this contrast response was modulated by the simultaneous stimulation of FEF sites with movement fields corresponding to the stimuli locations. We observed a significant baseline shift ([i.e.] at 0% contrast) due to FEF-EM in a subset of areas known to be well connected to the FEF, and in general we found the largest increases of fMRI activity for the lowest contrast
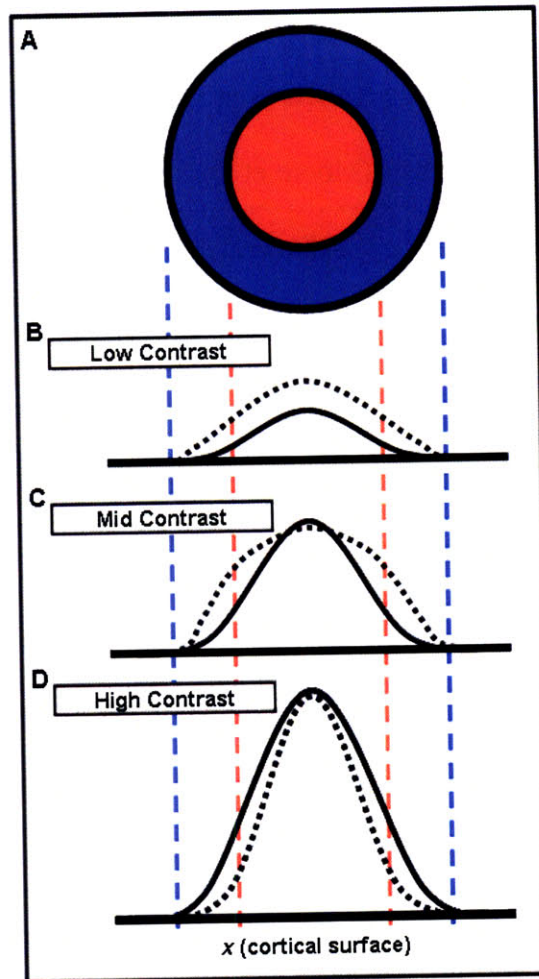
Fig. 3-9: Schematic summary of spatial macroscopic cortical response to FEF-EM. **(A)** The concentric circles correspond to regions on the two-dimensional cortical surface representation of a visual stimulus (c.f. Fig. 3-1D). Red / blue match the well / less well driven populations of *visual voxels* in Fig. 3-8. **(B, C, D)** Projecting this surface to one dimension yields three different activity profiles, depending on the stimulus contrast used (solid curve represents visual-only activation, dotted curve the combined response to visual stimulation and FEF-EM).

stimuli that produce smallest amounts of visual drive in cortical areas. High contrast stimuli, which produce the largest drive, were in general unaffected or reduced by FEF-EM.

3.5.1 Methodological Comparisons with Previous Studies

With respect to commonly-used attention models, such as contrast and response gain (Reynolds et al., 2000; Williford and Maunsell, 2006; Li et al., 2008), we note there are several key distinctions between the attention studies used to validate them and our own. Our subjects

- 129 -

performed a passive fixation task as we stimulated the FEF; hence, attention was not modulated here. While FEF stimulation has been shown to produce results that physiologically resemble spatial attention effects in visual cortex (Moore et al., 2003; Armstrong et al., 2006; Armstrong and Moore, 2007), exact correspondence with an attention task has not been established (that is, the behavioral and physiological results after FEF-EM in these studies were obtained in separate experiments). Second, the comparison most often made during attention tasks is to direct attention towards and away from (typically to the contralateral visual field) the stimulus of interest, to control for the difficulty in asking a subject to ignore a stimulus (Martinez-Trujillo and Treue, 2002a). Here, we compared visual responses during the presence and absence of FEF stimulation, which would more closely parallel an attention-on / attention-off design. Thus, our baseline condition at each contrast level was a visual-only response and is presumably lacking some of the higher order signals that would be present during an attend away condition. To match the attend-toward / attend-away design more typically used in behavioral spatial attention paradigms would require the non-trivial ability to stimulate both the left and right FEF in the same subject.

3.5.2 Comparison with previous CRFs

Both human imaging (Tootell et al., 1995; Buracas and Boynton, 2007; Li et al., 2008) and single unit studies [see [e.g.] Albrecht and Hamilton, (1982), Sclar et al., (1990), Reynolds et al., (2000) and Williford and Maunsell, (2006)] have measured CRFs in several early visual areas up to and including MT. Though the experimental designs, stimuli and contrast levels used vary across these studies, a rudimentary comparison is possible (Fig. 3-4). In areas V1, V2 and V4, we obtained relatively similar results to previous human fMRI studies. Particularly at lower contrasts, all the fMRI studies seem to systematically yield in V1 and V4 larger estimates of

normalized activity than single cell studies have measured. This observation suggests consistency when measuring CRFs with fMRI and that human and monkey contrast sensitivity may be relatively similar in striate and early extrastriate cortex. Both Tootell et al., (1995) and Buracas and Boynton, (2007) found that activity in human MT was essentially saturated at their lowest contrast stimuli (1.6% and 6.25% contrast, respectively), while we measured more of a sharply rising function that better matches single unit recordings of contrast response in MT (Sclar et al., 1990). Part of this discrepancy could be due to the difficulty in delineating human MT+ in fMRI data ([i.e.] human MT+ most likely consists of several areas, such as MT, MST, FST), but this comparison may also indicate a difference in contrast sensitivity between monkey MT and its human homologue.

Some further insight is possible from comparing model fit parameters, with the caveat that slightly different forms of the basic hyperbolic ratio model have been used in single cell and fMRI studies (Albrecht and Hamilton, 1982; Sclar et al., 1990; Li et al., 2008), and that species differences may add further variation as noted above. R_{max} values are difficult to equate because of technical differences, but c_{50} values should presumably be more comparable. In the regions they measured, Li et al. (2008) found V1 to be the least contrast sensitive, areas V2, V3 and V4 to be relatively similar and area V3A to be slightly less sensitive than these other extrastriate areas. We found a similar trend, though we measured a smaller c_{50} in area V1. Compared to values from the above two single unit studies, both fMRI studies measured much lower c_{50} terms in V1, while in area MT our value and the value found by Sclar et al. (1990) were not that discrepant (4.7% vs. 7%, respectively). In both species, these low c_{50} values indicate high contrast sensitivity likely due to a large proportion of input coming from the magnocellular

stream. By the same token areas MST and FST, in which we measured similar c_{50} values to MT, may also receive a large proportion of magnocellular-weighted input.

3.5.3 Modulation of CRFs by FEF-EM

In comparison with the canonical models used to describe the effects of attention on visual neural activity (Williford and Maunsell, 2006), we can make several general statements about the effects we observed when stimulating the FEF. The hallmark of a response gain effect is a proportional increase in response at all levels of activity, which is most readily apparent for high contrast stimuli. Under the conditions of our study, we did not observe such a scaling; instead, in many areas and in the overall response across visual cortex we saw a reduction in activity at high contrast. The principal characteristic of a contrast gain effect is a non-proportional increase in activity at intermediate contrasts, with little effect at baseline and saturation activity levels (Reynolds et al., 2000). We do observe some common features with this model, specifically at lower and intermediate contrasts. The correspondence is not perfect, however, particularly at high contrast. This divergence may be partly due to the methodological distinctions noted previously (attend-on / attend-off versus attend-toward / attend-away paradigms) and it may also indicate that FEF stimulation recruits only a part of the top-down network active during a true attention task.

On a mechanistic level, the pair of area V1 CRFs in Fig. 3-5A and the overall response schematic of Fig. 3-9 bear resemblance to a framework described previously for center-surround interactions in rat somatosensory cortex (Moore et al., 1999; Simons, 1985; Armstrong-James and Fox, 1987; Ghazanfar and Nicolelis, 1997). This framework was itself inspired by a model of contrast-dependent interactions mediated by horizontal connections in area V1 (Somers et al., 1998), which was later refined to include feedback connections from higher areas (Schwabe et

al., 2006). We speculate that by stimulating the FEF and presumably activating feedback connections to earlier visual areas, we are engaging this dynamical response: (i) at low levels of visual drive, the system acts to amplify all input and increase sensitivity, (ii) at high levels the system switches to a more discriminatory mode of operation that sharpens salient responses, and (iii) in between these extremes a hybrid mode exists. This hybrid mode of operation is consistent with our previous findings (Ekstrom et al., 2008), where we used chromatic stimuli with approximately 31% luminance contrast and observed increased fMRI responses around the stimulus margin and a slight suppression or no effect at the stimulus peak. Returning to models of covert attention, such a mechanism would seem easier to reconcile with a contrast gain response, provided the divergence at high contrast could be addressed.

Several predictions relating to the modulation of a stimulus representation and perception due to increased FEF output, either through EM in monkeys or transcranial magnetic stimulation (TMS) in humans (Grosbras and Paus, 2002; Ruff et al., 2006; Silvanto et al., 2006; Taylor et al., 2007), are possible from the operating schematic presented in Fig. 3-9. First, the representation of low contrast or faint stimuli in isolation should be uniformly amplified and perceived more readily. A number of attention experiments have exactly indicated this effect (Bashinski and Bacharach, 1980; Hawkins et al., 1990; Muller and Humphreys, 1991; Handy et al., 1996); given the present results, we predict largely similar behavioral effects following an artificial elevation of FEF output. A second prediction arises from the comparison of the mid and high contrast regimes. Specifically, a discrimination task using stimuli comprised of a central region and annulus, in which the discrimination must be made in the annular compartment, should be differentially impaired or facilitated by FEF output depending on the contrast used. Parallels of this prediction can be seen in recent work combining fMRI and TMS of human FEF (Ruff et al.,

2006). Using full-field stimuli that appear to be in our hypothesized mid-contrast regime, they measured topographic changes in the stimulus representation that largely match our prediction (Fig. 3-9C). Further, a subsequent psychophysical test in that study demonstrated a behavioral effect in line with our prediction and gives confidence that the results of the task outlined above should substantiate our results.

Regardless, we have strengthened further the observation (Rizzolatti et al., 1987; Corbetta et al., 1998; Moore and Armstrong, 2003; Cavanaugh and Wurtz, 2004; Ruff et al., 2006) that increased output from areas responsible for oculomotor control can modulate incoming visual activity. Additionally, we have found that the effective strength of this modulation is approximately inversely proportional to the underlying sensory drive. In general, our data support a non-proportional contrast gain rather than a response or activity gain following artificially increased output of the FEF.

Chapter 4

4 Effects of FEF Stimulation on Visual Features

This chapter is based upon:

Area-specific Changes in Feature Selectivity Due to Electrical Stimulation of the Macaque

Frontal Eye Field

(In preparation)

Leeland B. Ekstrom, Pieter R. Roelfsema, Timo van Kerkoerle, Hauke Kolster, Wim Vanduffel

Visual processing in the primate brain is commonly divided into two streams – a dorsal stream believed to code spatial location ('where' information) and a ventral stream more commonly involved in object recognition ('what' information) (Ungerleider and Mishkin, 1982; Goodale and Milner, 1992). Using stimuli matched to two of the more prominent functional specializations of these streams, we sought to test whether output from the FEF could produce shifts in stimulus selectivity within them. This pursuit was motivated by a number of reported observations of attention directed towards visual features and visual objects [see [e.g.] (Treue and Martinez-Trujillo, 1999; O'Craven et al., 1999)], in addition to spatial locations. Given the well known connections of FEF to some of the cortical areas that display these functional

- 135 -

specializations (Huerta et al., 1987; Schall et al., 1995) and a recent report of object-selective neurons in FEF (Peng et al., 2008), we reasoned that the FEF may have a role in influencing selectivity as well. This aim of this chapter was to examine the effects of increased FEF output on different stimuli classes placed at the same spatial location. The working hypothesis was that FEF-EM would particularly modulate the cortical areas known to be sensitive to the class of information contained within the stimulus.

4.1 Abstract

A number of studies in both humans and monkeys have shown that increased output from the Frontal Eye Field (FEF) can produce spatially specific modulations of visual activity in earlier cortical areas. Given a recent finding of object selective neurons in the FEF and the well-known connectivity of the FEF to other object selective visual regions, we sought to determine whether FEF output could also influence the relative selectivity between stimulus types in these other areas. Using cerebral blood volume (CBV)-weighted functional magnetic resonance imaging (fMRI), we measured the response in two awake, behaving monkeys to two very different types of stimuli (moving gratings and static monkey faces, respectively) positioned at the same retinotopic location in the visual field. Simultaneously, we applied electrical microstimulation (EM) to sites in the FEF with movement fields that were first aligned (congruent), and then unaligned (incongruent) with the stimulus locations. In early areas we observed little change in selectivity. We found in higher order visual areas though, that congruent FEF-EM shifted selectivity towards the stimulus preferred by that area and in some cases, this shift was mediated by the suppression of unfavored stimuli. When we switched to the unaligned stimulation paradigm, we found that these shifts in selectivity were often in the opposite direction. These results indicate that the effects of increased FEF output in visual

cortex depend not only on spatial location but also on the feature content of the stimulus presented.

4.2 Introduction

Converging lines of evidence suggest that a network of parieto-frontal areas send top-down signals towards visual cortex to modulate incoming sensory information (Rizzolatti et al., 1987; Kastner and Ungerleider, 2000; Corbetta and Shulman, 2002). The Frontal Eye Field (FEF), on the anterior bank of the arcuate sulcus, is one of the cortical structures in this network that has garnered particular interest in this respect (Moore et al., 2003; Hamker, 2005). Specifically, the FEF has been proposed as a source region for topographically-specific signals that indicate the 'behavioral relevance' of a *particular spatial location* in the visual field. Ample evidence exists that the FEF contains a topographic map (Bruce et al., 1985) and that this spatially specific information can be used to modulate visually driven activity during the deployment of spatial attention (see [e.g.] (Corbetta et al., 1998; Grosbras and Paus, 2002; Moore and Fallah, 2004)).

Our previous experiments [(Ekstrom et al., 2008) and (Ekstrom et al., In Prep.)], in which we used electrical microstimulation (EM) to artificially increase the output of specific sub-regions of the FEF, also showed topographically-specific modulation of functional magnetic resonance imaging (fMRI) activity in many visual areas in support of the above hypothesis. In general, the degree of modulation of visually driven activity induced by FEF-EM varied as a function of stimulus saliency: (i) effects were stronger for low compared to high luminance contrast stimuli presented within the movement field (MF) of the FEF site stimulated, and (ii) adding contralateral distractor stimuli (thereby, reducing the saliency of the MF or target stimulus) also increased the FEF-EM dependent modulation for targets within the FEF-MF. The

observed effects were spatially specific, since a retinotopic mismatch between the presentation of the visual stimulus and the stimulated MF decreased the modulation. Moore and Armstrong, (2003) observed a similar effect when stimulating FEF and recording V4 neuronal activity: the presence of distractor stimuli enhanced the observed modulations and a spatial mismatch between the stimulus and FEF-MF eliminated or even reversed them.

Recently, evidence has emerged that some neurons in the FEF can not only convey information concerning spatial locations but also about the shape of objects presented within their receptive field (Peng et al., 2008). Therefore, we hypothesized that this structure, which is well connected with many higher-order visual areas (Huerta et al., 1987; Schall et al., 1995), may also send feature or shape selective signals towards visual cortex. Presumably, these signals could modulate incoming visual information in a feature-specific manner, in addition to the above-described spatially-specific manner. If so, the FEF could play an important role during the deployment of both feature (Treue and Martinez-Trujillo, 1999; McAdams and Maunsell, 2000; Maunsell and Treue, 2006) and object selective attention (Roelfsema et al., 1998; O'Craven et al., 1999; Yantis and Serences, 2003), in addition to covert spatial attention.

To test this hypothesis, we collected cerebral blood volume (CBV)-weighted fMRI data from two awake monkeys (Vanduffel et al., 2001) while simultaneously stimulating the FEF (Ekstrom et al., 2008). We positioned two completely different types of stimuli at the same location within the MFs of the stimulated FEF sites: (i) low contrast moving gratings to primarily activate dorsal stream regions, and (ii) static, chromatic, high contrast face stimuli to activate more ventral stream areas. We first measured whether increased FEF output could differentially modulate stimulus selectivity in regions driven by these stimulus types. Then, using the incongruent paradigm of our previous study (Ekstrom et al., 2008), we sought to determine

whether the effects of FEF-EM were also feature-specific when the stimulus and MF location were not matched. In general, we found in early visual areas little and in some higher order areas profound feature-selective modulatory effects due to concurrent FEF stimulation in both the congruent and incongruent stimulation conditions.

4.3 Materials and Methods

Many of the details of the primate imaging and stimulation techniques used have been described previously [(Vanduffel et al., 2001; Ekstrom et al., 2008) and (Ekstrom et al., In Prep.); a brief summary will be given here, and any modifications noted. All procedures were approved by MGH's Subcommittee on Research Animal Care (Protocol #2003N000338) and MIT's Committee on Animal Care, and are in accordance with NIH guidelines for the care and use of laboratory animals.

4.3.1 Subject Preparation

In short, we prepared two male rhesus monkeys (*Macaca mulatta*; MM1 and MM2, 7-8 kg, 5-6 years old) for fMRI with surgical implantation of a MR compatible head post, and then trained them for a passive fixation task. Once the subjects achieved accurate fixation performance, we chronically implanted 26 intracortical microelectrodes in the right FEF, as previously described. After surgery, we verified the correct anatomical placement of the electrode tips in the FEF using T2-weighted images collected at 7.0 T. We also obtained behavioral verification, in the form of successfully induced saccadic eye movements, during a fixation task outside the scanner. These eye movements defined for the neurons surrounding each electrode the so-called MF and the stimulation threshold to evoke a saccade.

4.3.2 Anatomical and Functional MRI acquisition

High resolution, T1-weighted anatomical images and gradient-echo T2*-weighted echo-planar functional images were collected as previously described (Ekstrom et al., In Prep.). Prior to all experiments, we injected a bolus of Microcrystalline Iron Oxide Nanoparticles (MION; 8-12 mg/kg) in isotonic sodium citrate into the femoral or saphenous vein to increase the contrast-to-noise ratio compared to blood oxygen level dependent imaging (BOLD) (Vanduffel et al., 2001; Leite et al., 2002). Accordingly, we have flipped the polarity of all percent signal change values to account for the difference between MION CBV and BOLD activation maps (increased brain activation produces a decrease in MR signal in MION CBV maps).

4.3.3 Visual and electrical stimulation

We used a block design with 24 s long epochs (12 TRs) and 16 epochs per run, or time series, to measure fMRI activation during eight different conditions (Fig. 4-1A). The conditions we used were: (i) baseline Fixation-only (F), (ii) low contrast moving gratings (hereafter referred to as *motion* conditions and coded blue) without (V_m), with *congruent* (VEM_m) and with *incongruent* ($VEMI_m$) microstimulation of the FEF, (iii) FEF-EM only (EM), and (iv) high contrast, static face stimuli (hereafter referred to as *face* conditions and coded red) without (V_f), with *congruent* (VEM_f) and with *incongruent* ($VEMI_f$) microstimulation of the FEF. More detail on the different FEF-EM paradigms will be given below. In total, 21 312 functional volumes were collected from MM1 (5 sessions) and 20 736 functional volumes from MM2 (6 sessions), of which 4224 and 3456 volumes respectively, were used to generate the data shown. The other sessions were used to test the stimulation paradigm.

Fig. 4-1 (Next page): Stimulus conditions, stimulus locations and localizer example. **(A)** The eight stimulus conditions used: (i) baseline fixation-only (F), (ii) motion conditions without (V_m), with congruent (VEM_m) and with incongruent ($VEMI_m$) microstimulation of the FEF (grating luminance contrast has been doubled in this schematic for visualization purposes; actual grating contrast used was 6%), (iii) FEF-EM only (EM), and (iv) face conditions without (V_f), with congruent (VEM_f) and with incongruent ($VEMI_f$) microstimulation of the FEF. The average visual effect in the no-EM conditions (See 4.3.4 Statistical Analysis) was used as a localizer to identify a common population of visual voxels for further analysis. **(B, C)** Stimulus locations for MM1 and MM2, respectively. The stimuli were positioned at the endpoint of the saccade vector produced by stimulating each electrode above the threshold needed to elicit a saccade. The dotted white lines indicate the pair of stimulus locations used for that subject. The red dot in the center represents the fixation spot, which was visible in all conditions. **(D)** A thresholded t-score map ($P < 0.001$, uncorrected) of the localizer contrast ($V_m + V_f$ versus $2 \times F$) overlaid on the flattened representation of occipital cortex from MM1. Sulci are dark grey, and white and black solid lines indicate the representations of the vertical and horizontal meridians, respectively. Anatomical labels: Calc, Calcarine sulcus; CS, Central sulcus; IOS, Inferior Occipital sulcus; IPS, Intraparietal sulcus; LF, Lateral fissure; LuS, Lunate sulcus; OTS, Occipitotemporal sulcus; STS, Superior Temporal sulcus.

Visual stimulation was presented to the subjects at 1024 x 768 resolution and a 60 Hz refresh rate from a LCD projector (DLA-SX21, JVC; Yokohama, Japan) onto a translucent screen 51 cm from the animals' eyes. All visual stimuli were 6 visual degrees in diameter. *Motion* stimuli were monochromatic, clipped sine-wave gratings at 6% luminance contrast, where we defined contrast as the ratio between the difference and sum of luminance in the bright and dark regions (Michelson, 1927). The gratings had a spatial frequency of 0.5 cycles / degree and moved at 2 degrees / s in one direction along one of 2 axes (0 and 90 degrees), with mean luminance matched to that of the uniformly gray background (77 cd/m^2). *Face* stimuli consisted of 24 different chromatic images of monkey faces, surrounded by a scrambled background of the same luminance to augment the images to the required size. Stimulus location was matched to the MF of the pair of electrodes stimulated in that particular session (Moore and Armstrong, 2003; Ekstrom et al., 2008).
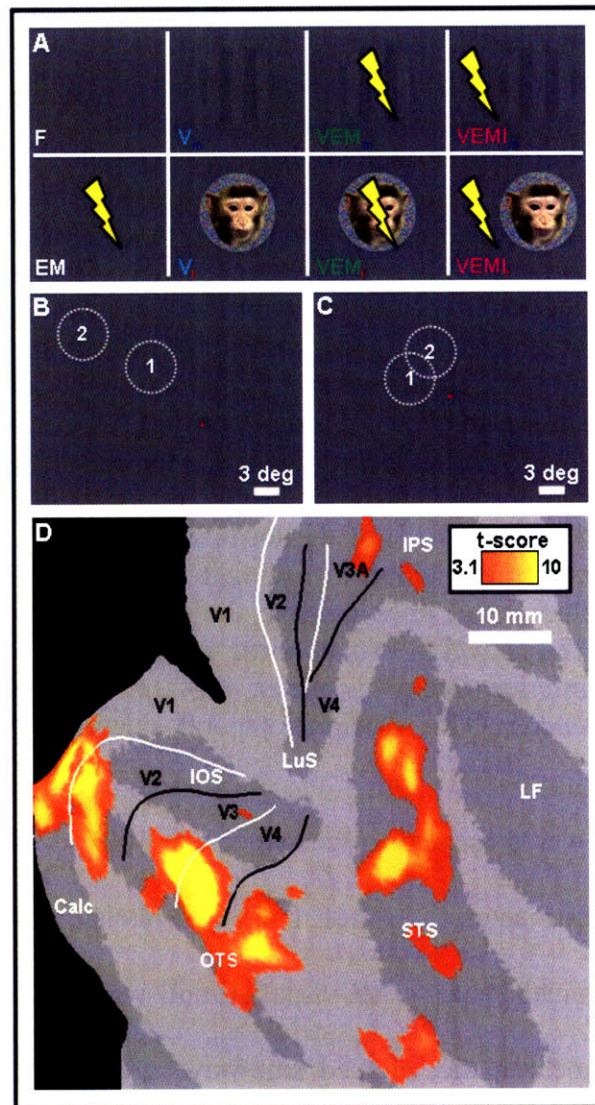
We used a pseudo-randomized design with multiple stimulus orders. In all the epochs with FEF-EM, we presented two visual stimuli and stimulated two electrodes sequentially within a TR (ISI = 1 s). A single visual stimulus was presented for 133 ms, followed by 250 ms of combined visual stimulation and FEF-EM and then 617 ms with neither, and this pattern was repeated twice. During *congruent* stimulation conditions, the visual stimulus was always matched to the MF of the FEF site stimulated. In other words, the stimulus appeared at location 1 while we stimulated at a sub-threshold level the electrode with a MF corresponding to that same location, and then the stimulus was moved to location 2 with accompanying FEF-EM (Fig.

4-1B and C). During *incongruent* stimulation conditions, the visual stimulus was always mismatched with the MF of the FEF site stimulated (MF separation in MM1 was 10.3 degrees and in MM2 4.1 degrees). In other words, the stimulus appeared at location 1 while we stimulated at a sub-threshold level the electrode with a MF corresponding to location 2, and then the stimulus was moved to location 2 while we stimulated the electrode corresponding to location 1 (Fig. 4-1B and C, see also (Ekstrom et al., 2008)). A central fixation point was continuously visible and the monkeys performed a passive fixation task throughout each run. Eye position was monitored at 120 Hz using an infrared pupil/corneal reflection tracking system (Iscan Inc.; Burlington, MA).

The EM signal was generated as previously described [(Ekstrom et al., 2008) and (Ekstrom et al., In Prep.)]. Prior to each fMRI experiment, we determined the threshold to elicit a saccade for each electrode by varying the EM amplitude until ~70% of stimulation trains induced a saccade from central fixation. A saccade vector was determined to identify the MF of the FEF site of interest for that experiment (see Fig. 4-1B for MM1's MFs and Fig. 4-1C for MM2's MFs used in the current study); a stimulation level of ~50% of this behaviorally-defined threshold was then used for the actual imaging experiment (Moore and Armstrong, 2003). At the beginning and end of each fMRI session, we measured the impedance of the stimulated channels with a 1V, 100 Hz reference signal to estimate the injected current. For MM1, mean impedance was 37 ± 1 kΩ and 34 ± 6 kΩ for the 2 electrodes used; for MM2, mean impedance was 38 ± 11 kΩ and 21 ± 12 kΩ (mean $\pm$ standard deviation across all sessions). Estimated stimulation amplitudes for the two FEF electrodes used in the present experiments were 39 μA and 153 μA in MM1, and 62 μA and 57 μA in MM2. We note that the current necessary to evoke saccades through chronic electrodes may be larger than with higher impedance acute electrodes. One

reason for this is the possible growth of a fibrous barrier between the electrodes and neural tissue over the 3-4 years between implantation and collection of this data (Bartlett et al., 2005).

4.3.4 Statistical analysis

We performed a voxel-based analysis with SPM99 as previously described [(Ekstrom et al., 2008) and (Ekstrom et al., In Prep.)]. We used the average visual effect across both features (that is, $V_m + V_f$ versus $2 \times F$, Fig. 4-1A) as a localizer to identify visually driven voxels for further analysis. t-score maps of this contrast from each session in each monkey were thresholded ($P < 0.05$, uncorrected) and overlaid on the common anatomical space defined by MM1's T1-weighed anatomical images as reconstructed by FreeSurfer (Dale et al., 1999). We created flattened cortical representations with Caret using the F99 atlas (http://brainmap.wustl.edu/caret, http://brainmap.wustl.edu:8081/sums/directory.do?id=636032) (Van Essen et al., 2001) (see Fig. 4-1D for an example of one session). The borders of thirteen visual areas were identified on this flattened cortical representation using retinotopic mapping data previously collected in three animals (Fize et al., 2003) and a Caret Atlas based on two previous studies (Felleman and Van Essen, 1991; Ungerleider and Desimone, 1986b). A fourteenth region, containing voxels driven by the *face* and *motion* stimuli, was selected in anterior infero-temporal cortex, rostral to area TEr. We extracted the population of voxels inside each area satisfying the above contrast and sampled the percent change in MR signal for each condition with SPM99. The first 3 TR in each epoch were excluded and an additional TR appended at the end to compensate for hemodynamic delay. We then concatenated the entire population of voxels in each area from both subjects to generate the plots shown.

To account for any head and eye movement-related fMRI activity, covariates of no-interest from six motion realignment parameters and the x and y eye trace components were

generated and included in the GLM analysis. Eye traces were thresholded at approximately 2 degrees, convolved with the MION hemodynamic response function, and sub-sampled to the TR. We performed several analyses to assess the potential effects of eye movements on the fMRI activation. First, for each run collected, we aligned the stimulation events across all *motion* conditions with FEF-EM to EM onset, as well as all *face* conditions. We then performed a *t*-test at each time point to identify any significant differences in eye position ($P < 0.05$, corrected for multiple comparisons across time points; two sample, two-tailed *t*-test across all trials in that run) between the congruent and incongruent paradigms. Any run with a significant difference at any time point for either feature was excluded from further analysis. Second, we performed a one-way ANOVA on the eye traces aggregated across both subjects to test for any significant differences in percent fixation, saccade rate, and eye position along the x and y axes between the eight conditions used (Table 4-1).

As a part of our analysis, we employed the scatter plot technique introduced in our earlier work to show the relationship between two particular stimulus conditions of interest (Ekstrom et al., 2008). To generate these scatter plots, we first normalized the signal change values in each condition by the peak or most active voxel in the unstimulated condition of the same stimulus type, to reduce the influence of any inter-subject variability. In other words, the most active voxel in the V_m condition was used to normalize all voxels in the V_m, VEM_m and $VEMI_m$ conditions, and similarly for *faces*. We normalized the EM-only condition values with the average of the peak response in the V_m and V_f conditions. As a measure of the average relationship between the two conditions plotted, we calculated the best fitting line in the least squares sense to each of these distributions. The y intercept in these fits was forced through the origin, so that the behavior of the distribution was characterized only by the slope, to facilitate

Table 4-1: Fixation behavior during fMRI runs. n is the number of independent fMRI runs collected from each subject. Percent fixation was calculated using a 2 degree × 2 degree window; σ_x & σ_y are the mean standard deviation of eye position along the x and y eye axes, across all repetitions of a condition within a given run. A one-way ANOVA on each condition pair showed no significant differences ($P > 0.05$) in any of the distributions.

Subject	n	Condition	% Fixation Median	P	Saccades / min Median	P	σ_x (deg) Median	P	σ_y (deg) Median	P
		F	83.9		11.9		0.21		0.32	
		EM	79.3		12.5		0.22		0.32	
		V_f	81.4		13.1		0.22		0.30	
MM1 & MM2	40	V_m	86.7	0.09	12.5	0.94	0.20	0.80	0.31	0.99
		VEM_f	79.9		15.0		0.21		0.31	
		VEM_m	84.4		13.8		0.20		0.32	
		$VEMI_f$	83.3		12.5		0.20		0.31	
		$VEMI_m$	84.2		12.5		0.21		0.31	

comparison. To estimate 95% confidence intervals for each of the fitted slopes we implemented a non-parametric bootstrap algorithm (Efron and Tibshirani, 1993). In a particular region, the visual voxel population was randomly sampled with replacement and the parameter for the best fitting line calculated for that particular sample. We repeated this sampling 10 000 times and determined the 2.5% and 97.5% quantile values from the resulting parameter distribution to estimate the confidence intervals.

4.4 Results

For each subject, we first identified a population of visual voxels for further analysis from the fMRI contrast defined by the mean visual effect across both object classes (that is, V_m + V_f versus 2 × F). This contrast identified voxels that were on average significantly activated by both stimuli with respect to the fixation-only condition. The use of possible alternative selection criteria (that is, *motion*-driven voxels determined by V_m versus F, or *face*-driven voxels

determined by V_f versus F) had little effect on the results shown here. Using this population, we extracted the percent change in MR signal with respect to that baseline F condition for each voxel in all the other stimulus conditions (Fig. 4-1A). For each cortical area of interest, we then concatenated the population of visual voxels extracted from each subject.

We first use three functional regions (V2, FST and TEr) as examples to explain our basic analysis, and then show a summary of these results for all areas sampled. In Fig. 4-2A to C, we present the initial stimulus selectivity in these three exemplar areas in the absence of microstimulation. To do so, we plotted the normalized percent change in MR signal in the motion (x axis) versus face (y axis) conditions for all visually driven voxels in that particular area (cyan data points). To capture the overall behavior of the voxel population, we then calculated the best fitting line and estimated 95% confidence intervals for it using a non-parametric bootstrap algorithm. In these plots, a slope of unity would indicate that the voxels responded equally well to the *motion* and *face* stimuli. As seen in Fig. 4-2A to C, the best fits to the cyan scatter plots lie below the diagonal indicating that the voxels within these three areas were better driven by *faces* compared to the low-contrast *motion* stimuli. Further, the best fitting (cyan) slopes decreased in areas FST and TEr compared to area V2, which indicates a higher sensitivity for *face* than motion stimuli in these higher-order areas while area V2 responded almost equally to both stimulus types.
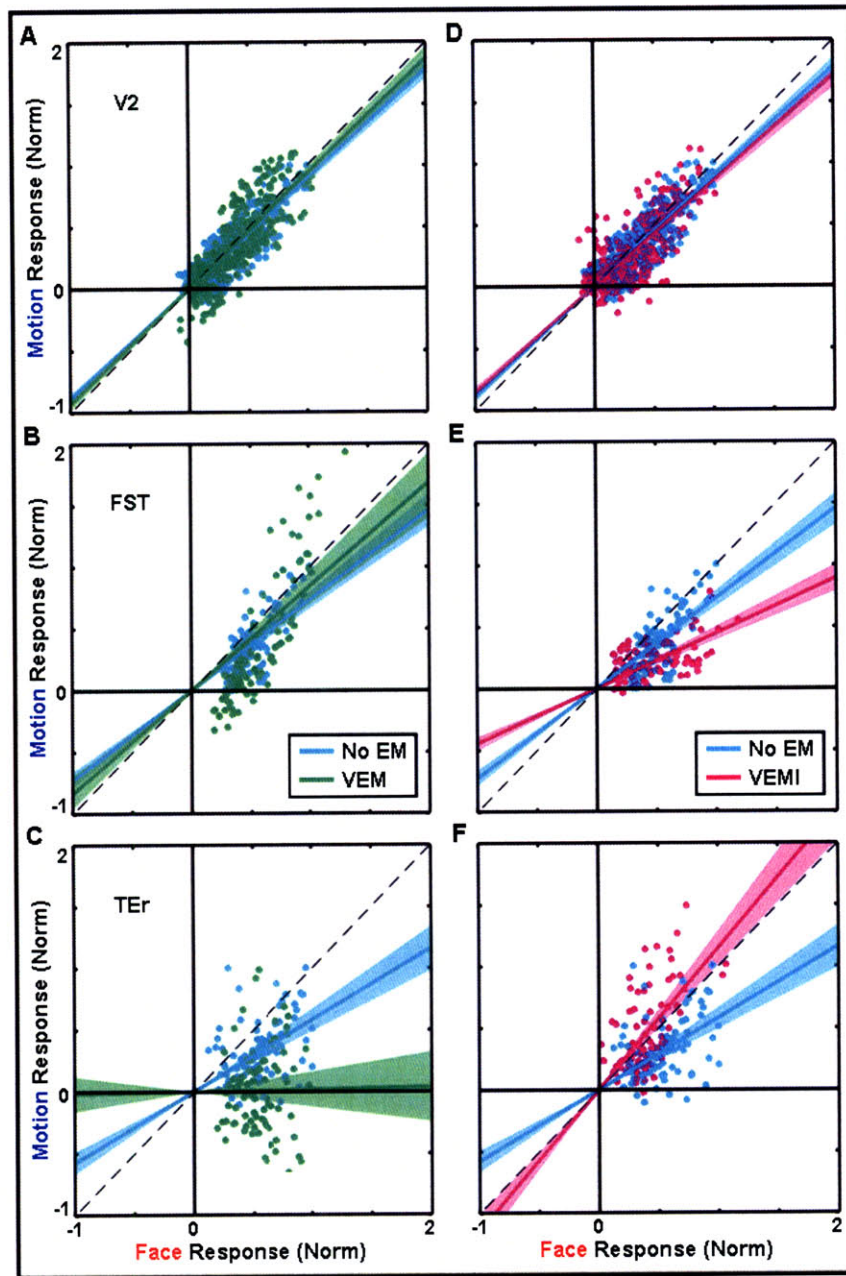
Fig. 4-2: Feature selectivity effects due to FEF-EM. **(A)** Scatter plot showing for each voxel in cortical area V2 the relationship between normalized percent change in MR signal for *motion* (*y* axis) and *face* (*x* axis) stimuli during the no (cyan) and *congruent* (green) FEF-EM conditions. Cyan and green lines are the best fit to the voxel distribution of the matching color; shaded regions indicate 95% confidence intervals for each fit, estimated by a non-parametric bootstrap algorithm. The black dashed line indicates unity slope in all panels. **(B)** and **(C)** present this same analysis for area FST (Fundus of superior temporal sulcus) and area TEr (Rostral temporal). **(D)**, Scatter plot showing in area V2 the relationship between normalized percent change in MR signal for *motion* and *face* stimuli during the no (cyan) and *incongruent* (pink) FEF-EM conditions. Lines of matching color and shaded regions are the same as A. **(E)** and **(F)** present this same analysis for areas FST and TEr.

If feedback signals originating in the FEF could only modulate visually driven activity in spatial terms, one would predict that FEF-EM should have little effect on these voxel distributions and the slopes of the best fit lines. In the other words, because the stimuli were presented at the exact same spatial location, the effects caused by FEF-EM should be identical for both the *face* and *motion* stimuli and depend only on the retinotopic position of the stimulus with respect to the location of the stimulated FEF-MF. As shown in Fig. 4-2A, this prediction holds true for early visual areas, such as V2. In green, we have plotted the normalized percent change in MR signal in the motion (*x* axis) versus face (*y* axis) conditions, but instead used the signal change values from the respective VEM, or *congruent* FEF-EM conditions. The fitted line and shaded region were determined in the same way as above. The green and cyan fitted lines, with associated confidence intervals, are nearly indistinguishable in V2, indicating that for this area the FEF-EM induced modulation of visually driven activity in this area does not depend on stimulus type. Surprisingly, however, in area TEr (Fig. 4-2C), artificially increased output from the FEF dramatically changed the relative sensitivity of these visually driven voxels in favor of the *face* stimuli. In essence, these voxels became much less responsive to the moving grating during increased FEF output; the end result is that TEr voxels show increased discriminability between the *face* and *motion* stimuli induced by congruent FEF-EM. In area FST (Fig. 4-2B), the opposite trend is apparent though less pronounced: voxels in this area became more sensitive to the *motion* compared to the *face* stimuli. Although its confidence interval still overlapped that of the unstimulated response (cyan), the green fitted line has shifted towards the diagonal and a substantial set of voxels were clearly more *motion* than *face* selective during *congruent* FEF-EM (green voxels above diagonal).

The previous analysis shows that the FEF-EM induced modulation of visually driven activity in higher order areas depends on both the position and type of the visual stimulus. In case of area TEr, *congruent* FEF-EM increased face selectivity while the opposite held true for area FST. This observation then raises the question as to what extent stimulus selectivity changes when a non-overlapping MF is stimulated (*i.e.* under *incongruent* visual and FEF-EM conditions). Based upon data from Moore et al., (2003) and our previous results (Ekstrom et al., 2008), one would predict that incongruent stimulation would reduce visually driven responses, irrespective of the stimulus used. In Fig. 4-2D to F, we now show the percent change in MR signal in the *incongruent*, VEMI conditions (pink) for comparison with the unstimulated conditions (cyan). Again, in area V2 (Fig. 4-2D) we see little change in selectivity; the fitted lines to the two distributions and confidence intervals are nearly indistinguishable. Thus, in early visual areas stimulus type has little effect on the modulation of visually driven activity by FEF-EM, be it congruent or incongruent. In agreement with our previous study (Ekstrom et al., 2008), however, activity in visually driven voxels was slightly enhanced under congruent compared to incongruent conditions, though irrespective of stimulus type. In higher-order areas, however, we again saw profound shifts in selectivity. In area FST (Fig. 4-2E), the visually driven voxels became relatively less sensitive to motion stimuli during *incongruent* FEF-EM, as indicated by the decrease in slope of the best fitting line (pink) compared to the unstimulated response (cyan). In area TEr, we observed the opposite trend: stimulating FEF sites when no stimulus was presented in the corresponding MF desensitized these voxels to the face stimuli, as seen by the increase in slope of the best fitting line (pink) compared to the no-EM conditions (cyan).

Extending this same analysis to all functional areas sampled, in Fig. 4-3 we present a summary of the best fit slopes characterizing the selectivity relationships in all three FEF-EM conditions (no-EM, *congruent*, and *incongruent*). In many areas, we found a slight preference to the *face* stimuli in the unstimulated condition (slopes of the cyan best fits less than unity). As expected, this bias was most profound in ventral stream areas (Fig. 4-3C), while in most dorsal areas we found no preference (confidence interval overlaps unity). That we did not observe a more pronounced bias to the *motion* stimuli in theses areas is likely because the *face* stimuli also drove these areas relatively well. The addition of *congruent* FEF-EM increased the relative *face* response in a number of areas, but particularly so in higher order ventral areas (compare cyan and green for STP, TEr and aTEr in Fig. 4-3C). Also in these areas, we observed particularly large effects in the opposite direction during *incongruent* FEF-EM, indicating a suppression of *face* activity under those conditions.

Another way to characterize the spatial dependency of FEF-EM and whether it is affected by stimulus type is to examine directly the relationship between *congruent* and *incongruent* stimulation, as in our previous study (Ekstrom et al., 2008). From that work and the analysis above, we expect larger fMRI responses when the stimulated MF directly overlaps the location at which a stimulus is presented than when there is a spatial mismatch [see also (Moore and Armstrong, 2003)]. In Fig. 4-4A to C, we measure this relationship directly by plotting percent change in MR signal in the *congruent* VEM (*y* axis) versus *incongruent* VEMI (*x* axis) conditions, for both the *face* and *motion* stimuli. For the *face* stimuli (red plots), we see in all three areas best fit lines that lie above the diagonal, which indicates a larger response when the stimulated MF and visual stimulus overlap, and that this enhancement is largest in area TEr (steepest slope). Looking at the *motion* responses (blue) confirms again our above assertion that

in higher visual areas the combination of spatial congruency and stimulus type determines the effect of increased FEF output. *Motion* stimuli in area FST were enhanced relatively more than *face* stimuli presented at the same location (compare blue and red in Fig. 4-4B), while in area TEr the *motion* responses were on average suppressed by *congruent* stimulation (Fig. 4-4C). We note that these opposite effects in FST and TEr cannot be explained simply by a difference in the drive of the two stimulus types, since in the no-EM conditions both areas were more face than motion selective (cyan slopes less than unity in Fig. 4-4B and C).

Again, extending this analysis to all functional areas sampled, we show in Fig. 4-5 a summary of the best fit slopes characterizing the relationship between *congruent* and *incongruent* FEF-EM for both stimulus types. We see in almost all areas that the *face* responses were relatively enhanced by *congruent* FEF-EM, as indicated by slope values that exceed unity by more than the 95% confidence intervals and that this enhancement was largest in the ventral stream areas (Fig. 4-5C). Looking at the *motion* responses, we see in the dorsal stream areas a similar effect, though only in areas MT and FST does the confidence interval not include unity. In some of the ventral areas, we observed a relatively large suppression of the moving gratings by congruent FEF-EM, as if increased FEF output blocks the processing of the unfavored motion stimuli in these regions.
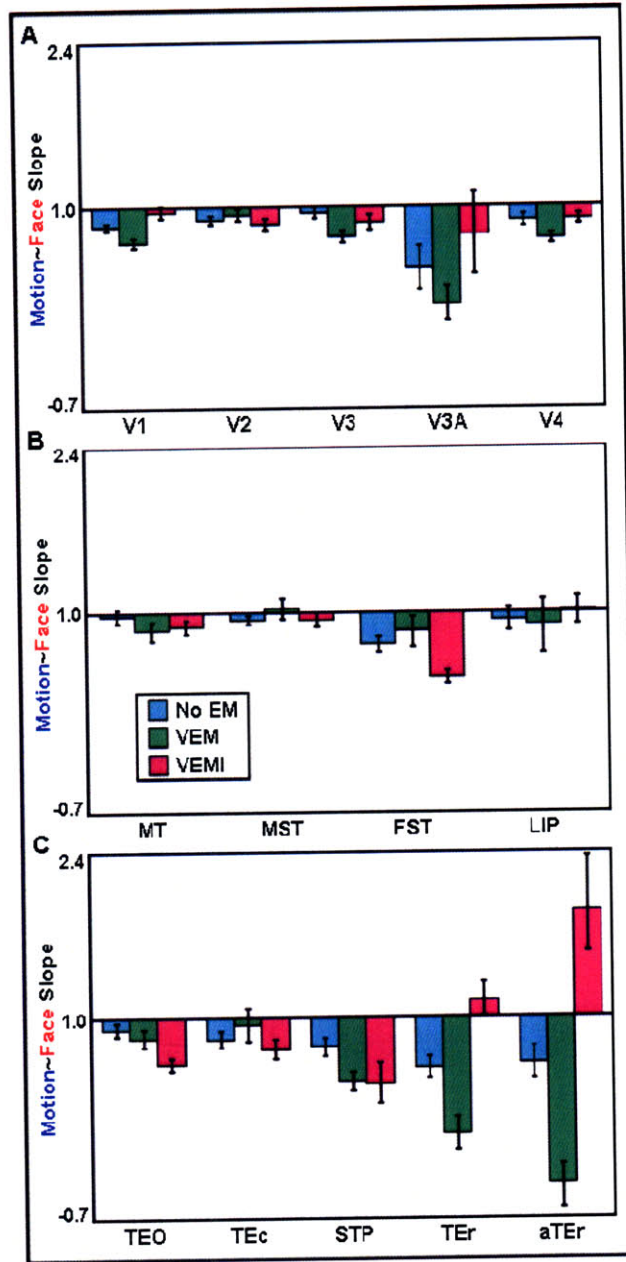
Fig. 4-3: Summary of selectivity effects across all areas. Best fitting slopes from voxel-wise scatter plots of the relationship between normalized percent change in MR signal for *motion* and *face* stimuli during the no (cyan), *congruent* (green) and *incongruent* (pink) FEF-EM conditions (Fig. 4-2). Error bars indicate 95% confidence intervals estimated from a non-parametric bootstrap algorithm. Areas have been grouped into early areas **(A)**, primarily dorsal stream areas **(B)** and primarily ventral areas **(C)**, and are ordered roughly by hierarchy. A positive value indicates that either the voxel distribution is on average more active in the *motion* conditions or suppressed in the *face* conditions. A negative value indicates the opposite: that either the voxel distribution is on average suppressed in the *motion* conditions or enhanced in the *face* conditions. Area labels: MT, Middle temporal; MST, Medial superior temporal; LIP, Lateral intraparietal; TEO, Temporo-occipital; TEc, Caudal temporal; STP, Superior temporal polysensory; aTEr, anterior to Rostral temporal.
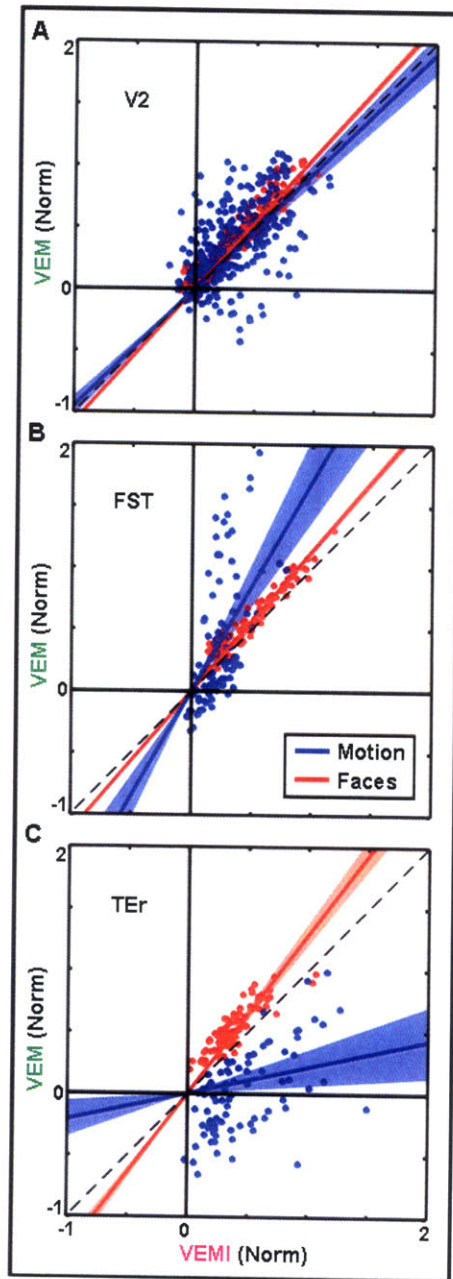
Fig. 4-4: FEF-EM congruency effects depending on stimulus type. **(A)**, Scatter plot showing for each voxel in area V2 the relationship between normalized percent change in MR signal during *congruent* (*y* axis) and *incongruent* (*x* axis) FEF-EM of *motion* (blue) and *face* (red) stimuli. Blue and red lines are the best fit to the *motion* and *face* distributions, respectively. Shaded blue and shaded red regions indicate 95% confidence intervals of the fit, estimated by a non-parametric bootstrap algorithm. The black dashed line indicates unity slope in both panels. **(B)** and **(C)** present this same analysis for areas FST and TEr.
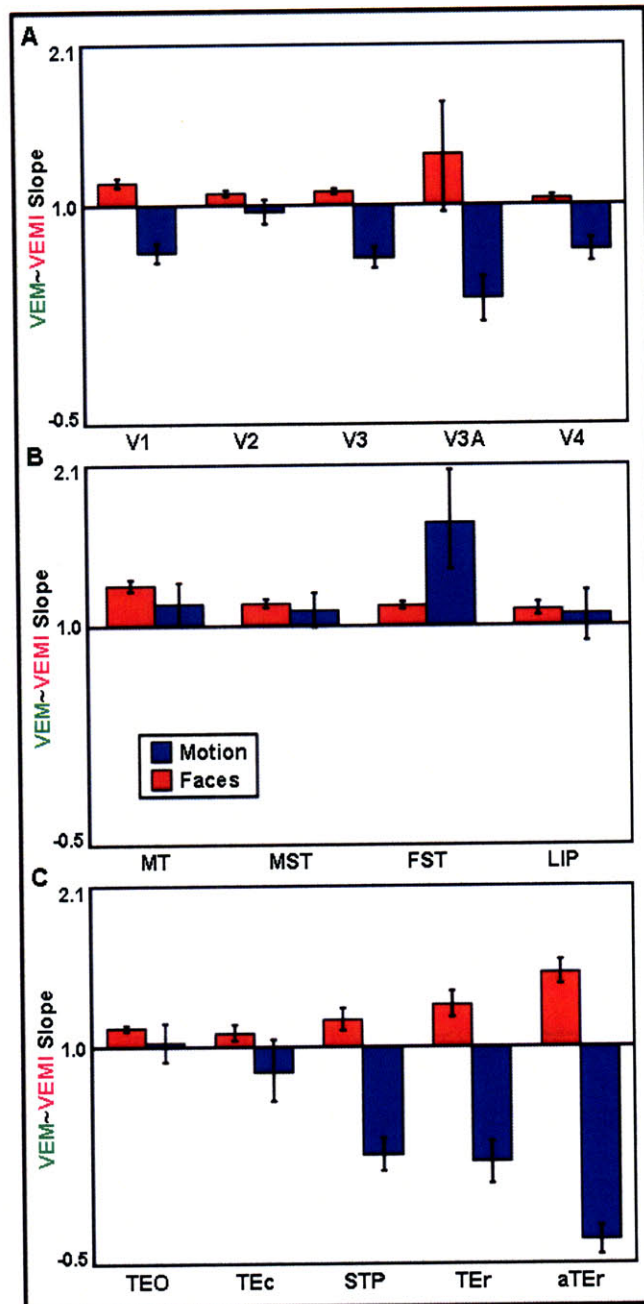
Fig. 4-5: Summary of congruency effects across all areas. Best fitting slopes from voxel-wise scatter plots of the relationship between normalized percent change in MR signal during *congruent* and *incongruent* FEF-EM of *motion* (blue) and *face* (red) stimuli (see Fig. 4-4). Error bars indicate 95% confidence intervals estimated from a non-parametric bootstrap algorithm. Areas have been grouped and ordered as in Fig. 4-3 – early areas **(A)**, primarily dorsal stream areas **(B)** and primarily ventral areas **(C)**. A positive value indicates that either the voxel distribution is on average enhanced in the *congruent* condition or suppressed in the *incongruent* condition. A negative value indicates the opposite: that either the voxel distribution is on average suppressed in the *congruent* condition or enhanced in the *incongruent* condition.

4.5 Discussion

Using CBV-weighted fMRI, we have measured the response to two very different visual stimulus types in fourteen defined functional areas of the macaque visual cortex, stretching across both the dorsal and ventral functional streams. We have observed how these responses were modulated by simultaneous stimulation of sites in the FEF that correspond retinotopically or not to the stimuli locations in the visual field. Specifically, we found in some higher cortical areas shifts in selectivity towards the presumably preferred stimulus in that cortical area, even though these different stimuli were presented at the same retinotopic location. When a non-overlapping MF was stimulated, we observed the opposite change – a shift away from the preferred stimulus type.

Our first two studies [(Ekstrom et al., 2008) and (Ekstrom et al., In Prep.)] demonstrated that increased output from the FEF could produce retinotopically specific modulations of stimulus representations throughout visual cortex and that these modulations depended on the underlying feedforward drive of the stimuli used. Here, by using disparate classes of *motion* and *face* object stimuli at identical retinotopic locations, we have shown that stimulus type, in addition to spatial location and stimulus strength, determine the effects of increased FEF output in visual cortex. Similar to past psychophysical (Vecera and Farah, 1994; Rossi and Paradiso, 1995), electrophysiological (Treue and Martinez-Trujillo, 1999; Roelfsema et al., 1998) and fMRI (Liu et al., 2003; O'Craven et al., 1999) studies of feature and object-based attention that show modulation of something other than spatial location, signals from the FEF can seemingly encode more than just spatial behavioral relevance but also relevance along at least two other stimulus dimensions. The utility of these multiple modes of modulation in the normal operating

state of the visual system is clear, given that the visual world consists of multiple possible cues, in addition to spatial location.

4.5.1 Suppression of Unwanted Stimuli

One of the most striking features of the modulations we observed, is that particularly in higher order ventral areas, the fMRI response from unwanted stimuli (that is, the *motion* stimuli in areas that respond more robustly to *faces*) was largely suppressed by congruent FEF-EM. The response to favored stimuli was relatively unchanged (see e.g. Fig. 4-2*C*). To enhance the relative visual response between two stimulus types for a generic downstream region to read out, two possible strategies could be used: (i) enhancement of favored stimuli, or (ii) suppression of unfavored stimuli. Both strategies yield the same result though – a larger relative difference between the two stimulus types. Speculatively, the strategy of increased inhibition of unfavored stimuli would demand less dynamic range in the population of neurons conveying this output, than the enhancement of favored stimuli would and potentially require less energy.

4.5.2 Modulation Strength as Function of Cortical Hierarchy

In their study of the deployment of attentional resources, Kastner et al., (1998) noted that the apparent modulations they observed seemed to increase with cortical hierarchy. In other words, modulatory influence was greater in regions located a larger number of synapses away from the retina. We too observed an apparent hierarchical effect, on two different organizational scales. First, early cortical areas for the most part showed smaller modulations than observed in higher order ventral areas (compare Fig. 4-3A and C, Fig. 4-5A and C). Second, within the presumptive ventral stream areas, we observed an increase in modulation with increasing hierarchy (particularly, compare TEO and TE with TEr and aTEr in Fig. 4-3C and Fig. 4-5C). To truly disentangle, however, how much of the observed modulation in each area is a direct

effect or the result of modulation from an earlier area being passed along would require the (non-trivial) ability to selective disable the presumptive feedback connections to a specific area [see e.g. (Herrero et al., 2008)].

Broadly, we have again strengthened the observation (Rizzolatti et al., 1987; Corbetta et al., 1998; Moore and Armstrong, 2003; Cavanaugh and Wurtz, 2004; Ruff et al., 2006) that increased output from areas responsible for oculomotor control can modulate incoming visual activity. Here, we have shown that stimulus type, in addition to spatial location and stimulus drive, determines the modulations produced by increased FEF output. Taken together with our previous studies, this set of observations shows that presumptive feedback from higher order areas plays a crucial role in generating visual representations and in some instances may be as important as the feed-forward activation. How these modulations ultimately affect perception and behavior becomes the next, and a very exciting, question.

Chapter 5

5 Conclusions

5.1 Summary of Major Contributions

The goals of this thesis were twofold: (i) to first develop methods extending the unique aspects of an awake, behaving primate functional imaging model by implementing simultaneous intracortical electrical microstimulation (EM) during fMRI acquisition, and (ii) to deploy those methods to understand how the nodes within a specific functional network interact. Specifically, the Frontal Eye Field (FEF), a node in the oculomotor control network on the anterior bank of the arcuate sulcus and a hypothesized source of modulatory signals during covert spatial attention, was targeted in this intervention.

In Chapter 2, the seminal technical innovations of this thesis were outlined in detail and used to measure the effects of increased FEF output in several visual conditions. Using a chronic implantation technique (Mioche and Singer, 1988), platinum-iridium microwires were inserted into the prearcuate cortex of two rhesus monkeys and verified by anatomical and behavioral measures to be located in the FEF. In a first experiment, the effects of stimulating the FEF below the threshold needed to evoke saccades were measured across the whole brain and found to be only in cortical and sub-cortical areas connected to the FEF. This stimulation map was

found to be largely in agreement with the known anatomical connectivity of the FEF (Huerta et al., 1986; Huerta et al., 1987; Schall et al., 1995; Stanton et al., 1988; Stanton et al., 1995) thus establishing, along with two other recent reports (Tolias et al., 2005; Moeller et al., 2008), this combined technique as a method for *in vivo* functional tractography or connectography.

Next, the ability of FEF output to modulate visual representations in occipital cortex was probed using small, high contrast, chromatic gratings placed in the movement fields (MFs), or at the saccadic endpoints (Moore and Armstrong, 2003), of the FEF sites stimulated. Sub-saccade-threshold stimulation of the FEF again produced fMRI activity in a number of cortical areas directly connected to the FEF, and in the presence of visual stimuli also in the earliest cortical visual areas. This effect was interpreted as a gating or enabling of FEF output by feedforward visual activation in these early areas, as had been predicted by several models (Fukushima, 1988; Grossberg, 1999; Roelfsema, 2006). The pattern of enhancive and suppressive modulation across the cortical surface was also measured, and found to be heterogeneous and present at a number of levels in the cortical hierarchy. Enhancements were primarily measured in voxels surrounding the most active visually driven regions, while the spatial peaks of these representations were unaffected or in some cases suppressed. In two additional control experiments, the specificity of these modulations was established and in area V4 their dependence upon strength of drive or visual intensity probed.

In Chapter 3, this investigation of visual intensity was expanded to twelve visual cortical areas. Using monochromatic stimuli varying in luminance contrast from 3% to 50%, the mean contrast response function (CRF) was measured for each of these regions fit using a common model based upon a hyperbolic ratio formulation (Naka and Rushton, 1966). In a subset of regions, these CRF were compared to existing data measured in monkeys using single cell

recording techniques (Albrecht and Hamilton, 1982; Sclar et al., 1990; Williford and Maunsell, 2006) and in humans using fMRI (Tootell et al., 1995; Buracas and Boynton, 2007; Li et al., 2008). Good agreement was found in early areas with past fMRI studies, while all fMRI-derived CRFs seemed to yield larger estimates of activity, particularly at low contrasts, than comparable single cell results. fMRI measurements of the CRF in monkey area MT were found to be more similar to single cell results than to human fMRI measurements in MT+, which saturated at the lowest contrast used. Further study is needed to determine whether this is a methodological artifact ([i.e.] due the difficulty in delineating human MT+) or a true species difference in contrast sensitivity in this region.

Next, modulation of the measured CRFs by sub-threshold stimulation of the FEF MFs overlapping the stimulus locations was assessed. Two recent models of neuronal modulation in area V4 during spatial attention deployment yield distinct predictions: (i) the contrast-gain model (Reynolds et al., 2000) predicts a non-proportional scaling or leftward shift of the CRF, while (ii) the response or activity-gain model (Williford and Maunsell, 2006) predicts a proportional scaling across all contrasts. Increased output from the FEF yielded CRF modulations more closely resembling an exaggerated contrast-gain effect. Significant positive interactions between visual stimulation and EM were measured for the lowest contrast stimuli in most areas, while no effect or even negative interactions were found at the highest contrasts used. Examining the spatial pattern across the cortical surface yielded a simple schematic that supported the observations of Chapter 2 and agreed with a similar study conducted with transcranial magnetic stimulation and fMRI in humans (Ruff et al., 2006). The schematic resembled a neural dynamics framework for center-surround interactions proposed in rat somatosensory cortex (Moore et al.,

1999), and presented several predictions testable in future psychophysical and electrophysiological experiments.

Lastly, in Chapter 4 the modulatory ability of increased FEF output on stimulus selectivity was assessed, with visual stimuli designed to match specific preferences in the dorsal (moving stimuli) and ventral (face stimuli) functional streams. These two different stimulus types were positioned at the exact same spatial locations in FEF MFs, which were then stimulated below the saccade threshold. In higher order areas in both functional streams, comparisons of the relative selectivity between the two stimulus types showed profound shifts with respect to the no-EM baseline that largely matched the underlying functional preference of these areas.

Broadly, this thesis has introduced an exciting new technique to the repertoire of primate imaging. It has used this technique to demonstrate a method of elucidating functional connections within a neural network. Further, this thesis has shown that increasing the activity of the FEF can induce modulations of visual stimulus representations at multiple levels of the visual system. In addition to spatial alignment, this thesis showed that form of modulation depended on both the strength of activation produced by a stimulus and the feature content contained within. In short, this thesis provides another compelling example of why, even in this age of non-invasive imaging techniques, the rhesus monkey remains an indispensable tool for neuroscientific discovery.

5.2 Proposed Future Directions

5.2.1 Additional Analyses of Current Data

This thesis has generated rich and unique data sets that could be used immediately in several additional analyses. The assumed form of the canonical hemodynamic response function

(HRF) is central to all general linear model (GLM) analysis of fMRI data. Some evidence exists of a conserved HRF across the primary sensory cortices of different modalities (Boynton et al., 1996; Josephs et al., 1997; Zarahn et al., 1997), but other evidence exists of variation in the HRF at higher cortical areas (Schacter et al., 1997). Given the strength of activation and diversity of cortical and sub-cortical areas activated in the initial FEF-EM only experiments, a straightforward analysis of HRF variation should be possible. How generalizable this analysis would be, particularly for human BOLD imaging, is admittedly open to debate given the use of the MION contrast agent. Comparison of how the MION CRF varies across the brain should at least yield a first order analysis, and inform whether repeating this experiment with BOLD contrast would be worthwhile.

A number of possible functional connectivity techniques were outlined in the Introduction (see Section 1.2.4). The FEF-EM only data set represents an almost ideal test bed to measure some of these techniques against, given the causal nature of microstimulation-induced activations. Particularly, the techniques employing Granger causality (Roebroeck et al., 2005), path analysis with Structural Equation modeling (McIntosh and Gonazlez-Lima, 1994), and functional correlation analysis (Biswal et al., 1995) could be tested to see how well they recapitulate the activity maps observed here. The original data set used to introduce Dynamic Causal Modeling (Buchel and Friston, 1997; Friston and Buchel, 2000) looked at the modulation of effective connectivity in an attention task, and maps well to the 2 × 2 design data set used in the bottom-up gating experiments. Applying DCM to this new data set could identify any changes in effective connectivity during FEF-EM, as is required by the gating interpretation, and would also serve as further validation of the DCM technique itself.

5.2.2 New Lines of Investigation

Stemming from this thesis are a number of possible lines of future study. The techniques presented here represent an operational platform for microstimulation during fMRI acquisition, but this platform is by no means optimized. A thorough parametric exploration of stimulation frequency, duration, amplitude with respect to saccade threshold and asynchrony with respect to visual stimulus onset could well yield a more effective prescription for measuring the effects of FEF output. Of perhaps slightly more interest would be the transfer of this now validated technique to other regions in the primate brain, for which the connectivity is unknown. One published report exists demonstrating this use to reveal new connectivity (Moeller et al., 2008), and several preliminary attempts have been made using the approach presented here (Frey et al., 2007). Other targets of interest and immediate clinical relevance include: (i) the sub-thalamic nucleus, currently targeted in deep brain stimulation treatment of Parkinson's disease (Benabid, 2003), (ii) cingulate white matter tracts near the genu of the corpus callosum, currently stimulated to treat intractable depression (Mayberg et al., 2005), and (iii) the thalamus, recently stimulated in improve patient responsiveness from a prolonged vegetative state (Schiff et al., 2007). In all cases, a first goal should be to assess the network of regions activated by these stimulation treatments. A critical, and yet unresolved, question in some of these examples and for generic regions is how to determine the level of stimulation when no obvious behavioral correlate exists, as in the FEF.

Diffusion-weighted MRI (DWI) has been recently and widely employed as a non-invasive, *in vivo* tract tracing tool, sensitive to white matter microstructure and changes to that microstructure in humans (Xue et al., 1999; Poupon et al., 2000; Wedeen et al., 2008) and rhesus monkeys (Tuch et al., 2005; Wedeen et al., 2008). Debate exists, however, on the exact relation between these diffusion-defined fibers and the underlying axonal tracts, and a systematic

validation of these methods is currently lacking (Tuch et al., 2005). Under the assumption that functional connection is facilitated by anatomical, FEF-EM and fMRI could increase the confidence placed in these techniques by determining if DWI-tractography could connect the so-called functional dots measured in the first EM-only experiments presented here. The multiple wave-vector fusion technique (Khachaturian et al., 2007b) for combining low angular resolution diffusion tensor data with high angular resolution q-Ball data or diffusion spectrum imaging (Wedeen et al., 2005) are two options that should yield sufficiently detailed fiber maps for this type of analysis. Further, data collection in an anesthetized primate subject (Khachaturian, 2007) should largely eliminate any motion artifacts and yield near optimal *in vivo* diffusion-weighted data. DWI tracts [for example, reconstructed using Probabilistic Tractography (Behrens et al., 2003) or TrackVis (Wedeen et al., 2008)] should be significantly more likely between two seed points in the network of areas identified by FEF-EM and fMRI than between one functionally defined seed point and points located increasingly outside of this network. In a further step, the combination of diffusion and functional tractography with a subsequent *ex vivo* validation in one or more primates using a traditional tracer approach (Huerta et al., 1987; Schall et al., 1995) would provide even more compelling support for DWI tractography measures.

A critical next step in evaluating the validity of the findings presented in this thesis is to combine this platform with a monkey performing a covert spatial attention task. In all the experiments presented here, the animals were passively fixating a central point. No direct control over endogenous attention was implemented, and therefore the conclusions are limited to modulations of fMRI-measured representations of visual activity with little indication of how this affects the animal's perception. Valid questions can certainly be raised as to if and how the animal's endogenous attention interacted with the stimuli and FEF stimulation, and whether the

observed modulations were behaviorally relevant. Further, the evidence presented here does not immediately imply that endogenous activation of the FEF in a spatial attention task will produce similar observations of visually driven modulation. Spatial attention has been shown to alter perception [see e.g. (Carrasco et al., 2004)], and the work of Moore and colleagues (Moore et al., 2003; Moore and Fallah, 2004; Armstrong et al., 2006; Armstrong and Moore, 2007) has established a line of evidence suggesting correspondence between increased FEF output and attention-like modulations of behavior and neuronal activity (albeit not simultaneously). These studies further motivate testing this platform behaviorally and with fMRI measurements.

In Chapter 3, several specific behavioral predictions were made regarding perceived changes of contrast in a center / annulus attention task combined with FEF-EM that should be evaluated. Preliminary evidence of the ability to implement an attention task during primate fMRI acquisition has been demonstrated (Vanduffel et al., 2004), and it should be straightforward, though perhaps not trivial, to combine with these methods. Of interest is the observed pattern of attentional modulation of a visual stimulus in occipital areas using sufficiently high resolution fMRI, and how this pattern is altered by FEF stimulation matched or mismatched with the stimulus location. Simultaneous behavioral measures of task improvement or decrement during congruent or incongruent stimulation would strengthen the argument that increased FEF output underlies attentional modulation.

To begin probing the local mechanisms of the visual modulations observed here or the potential pathways of their propagation could be done by combining inactivation techniques with this model. Cortical cooling (Payne et al., 1996; Khachaturian, 2007; Ponce et al., 2008) could be used to inactivate intermediate regions between the FEF and earlier areas in the visual cortex. Area LIP would be a first candidate, given the robust activity observed in it during the EM-only

experiments in both subjects, followed by any of the areas in the superior temporal sulcus that were identified. At the local level, one strategy would be to selectively inhibit feedback connections in a particular cortical area during FEF-EM. Herrero et al., (2008) recently demonstrated this approach using the muscarinic antagonist scopolamine to reduce attentional modulation in area V1 by presumably blocking feedback channels. One would predict that administering this agent or a similar one should attenuate observed modulations due to FEF-EM. The combination of multiple invasive techniques in both of these examples makes these experiments certainly exciting, but also more than a little challenging.

6 References

Afraz SR, Kiani R, Esteky H (2006) Microstimulation of inferotemporal cortex influences face categorization. Nature 442:692-695.

Albrecht DG, Hamilton DB (1982) Striate cortex of monkey and cat: contrast response function. J Neurophysiol 48:217-237.

Armstrong KM, Fitzgerald JK, Moore T (2006) Changes in visual receptive fields with microstimulation of frontal cortex. Neuron 50:791-798.

Armstrong KM, Moore T (2007) Rapid enhancement of visual cortical response discriminability by microstimulation of the frontal eye field. Proc Natl Acad Sci U S A 104:9499-9504.

Armstrong-James M, Fox K (1987) Spatiotemporal convergence and divergence in the rat S1 "barrel" cortex. J Comp Neurol 263:265-281.

Bartlett JR, DeYoe EA, Doty RW, Lee BB, Lewine JD, Negrao N, Overman WH, Jr. (2005) Psychophysics of electrical stimulation of striate cortex in macaques. J Neurophysiol 94:3430-3442.

Bashinski HS, Bacharach VR (1980) Enhancement of perceptual sensitivity as the result of selectively attending to spatial locations. Percept Psychophys 28:241-248.

Basser PJ, Pajevic S, Pierpaoli C, Duda J, Aldroubi A (2000) In vivo fiber tractography using DT-MRI data. Magn Reson Med 44:625-632.

Beaulieu C (2002) The basis of anisotropic water diffusion in the nervous system - a technical review. NMR Biomed 15:435-455.

Behrens TE, Woolrich MW, Jenkinson M, Johansen-Berg H, Nunes RG, Clare S, Matthews PM, Brady JM, Smith SM (2003) Characterization and propagation of uncertainty in diffusion-weighted MR imaging. Magn Reson Med 50:1077-1088.

Belliveau JW, Kennedy DN, Jr., McKinstry RC, Buchbinder BR, Weisskoff RM, Cohen MS, Vevea JM, Brady TJ, Rosen BR (1991) Functional mapping of the human visual cortex by magnetic resonance imaging. Science 254:716-719.

Benabid AL (2003) Deep brain stimulation for Parkinson's disease. Curr Opin Neurobiol 13:696-706.

Biswal B, Yetkin FZ, Haughton VM, Hyde JS (1995) Functional connectivity in the motor cortex of resting human brain using echo-planar MRI. Magn Reson Med 34:537-541.

Boussaoud D, Ungerleider LG, Desimone R (1990) Pathways for motion analysis: cortical connections of the medial superior temporal and fundus of the superior temporal visual areas in the macaque. J Comp Neurol 296:462-495.

Boynton GM, Engel SA, Glover GH, Heeger DJ (1996) Linear systems analysis of functional magnetic resonance imaging in human V1. J Neurosci 16:4207-4221.

Brewer AA, Press WA, Logothetis NK, Wandell BA (2002) Visual areas in macaque cortex measured using functional magnetic resonance imaging. J Neurosci 22:10416-10426.

Bruce CJ, Goldberg ME, Bushnell MC, Stanton GB (1985) Primate frontal eye fields. II. Physiological and anatomical correlates of electrically evoked eye movements. J Neurophysiol 54:714-734.

Buchel C, Friston KJ (1997) Modulation of connectivity in visual pathways by attention: cortical interactions evaluated with structural equation modelling and fMRI. Cereb Cortex 7:768-778.

Buracas GT, Boynton GM (2007) The effect of spatial attention on contrast response functions in human visual cortex. J Neurosci 27:93-97.

Buschman TJ, Miller EK (2007) Top-down versus bottom-up control of attention in the prefrontal and posterior parietal cortices. Science 315:1860-1862.

Carrasco M, Ling S, Read S (2004) Attention alters appearance. Nat Neurosci 7:308-313.

Cavanaugh J, Alvarez BD, Wurtz RH (2006) Enhanced performance with brain stimulation: attentional shift or visual cue? J Neurosci 26:11347-11358.

Cavanaugh J, Wurtz RH (2004) Subcortical modulation of attention counters change blindness. J Neurosci 24:11236-11243.

Chef d'hotel C, Hermosillo G, Faugeras O (2002) Flows of diffeomorphisms for multimodal image registration. In: IEEE International Symposium on Biomedical Imaging pp 753-756.

Cohen MR, Newsome WT (2004) What electrical microstimulation has revealed about the neural basis of cognition. Curr Opin Neurobiol 14:169-177.

Colby CL, Duhamel JR, Goldberg ME (1996) Visual, presaccadic, and cognitive activation of single neurons in monkey lateral intraparietal area. J Neurophysiol 76:2841-2852.

Connor CE, Preddie DC, Gallant JL, Van Essen DC (1997) Spatial attention effects in macaque area V4. J Neurosci 17:3201-3214.

Conturo TE, Lori NF, Cull TS, Akbudak E, Snyder AZ, Shimony JS, McKinstry RC, Burton H, Raichle ME (1999) Tracking neuronal fiber pathways in the living human brain. Proc Natl Acad Sci U S A 96:10422-10427.

Corbetta M, Akbudak E, Conturo TE, Snyder AZ, Ollinger JM, Drury HA, Linenweber MR, Petersen SE, Raichle ME, Van Essen DC, Shulman GL (1998) A common network of functional areas for attention and eye movements. Neuron 21:761-773.

Corbetta M, Shulman GL (2002) Control of goal-directed and stimulus-driven attention in the brain. Nat Rev Neurosci 3:201-215.

CRC Handbook (2006) CRC Handbook of Chemistry and Physics, 87th ed. Boca Raton, FL: CRC Press / Taylor and Francis Group.

Dale AM, Fischl B, Sereno MI (1999) Cortical surface-based analysis. I. Segmentation and surface reconstruction. Neuroimage 9:179-194.

De Poorter J, De Wagter C, De Deene Y, Thomsen C, Stahlberg F, Achten E (1995) Noninvasive MRI thermometry with the proton resonance frequency (PRF) method: in vivo results in human muscle. Magn Reson Med 33:74-81.

Denys K, Vanduffel W, Fize D, Nelissen K, Peuskens H, Van Essen D, Orban GA (2004a) The processing of visual shape in the cerebral cortex of human and nonhuman primates: a functional magnetic resonance imaging study. J Neurosci 24:2551-2565.

Denys K, Vanduffel W, Fize D, Nelissen K, Sawamura H, Georgieva S, Vogels R, Van Essen D, Orban GA (2004b) Visual activation in prefrontal cortex is stronger in monkeys than in humans. J Cogn Neurosci 16:1505-1516.

Desimone R, Duncan J (1995) Neural mechanisms of selective visual attention. Annu Rev Neurosci 18:193-222.

Durand JB, Nelissen K, Joly O, Wardak C, Todd JT, Norman JF, Janssen P, Vanduffel W, Orban GA (2007) Anterior regions of monkey parietal cortex process visual 3D shape. Neuron 55:493-505.

Efron B, Tibshirani R (1993) An Introduction to the Bootstrap. London: Chapman and Hall.

Ekstrom LB, Arsenault JT, Bonmassar G, Roelfsema PR, Vanduffel W (2007) The effect of FEF microstimulation on contrast response functions in visual cortex. In: Soc Neurosci Ann Mtg pp 229.2. Washington, DC.

Ekstrom LB, Bonmassar G, Tootell RB, Roelfsema PR, Vanduffel W (2005) FEF Microstimulate Modulates Visually Drive Activity In Cortex: Evidence From Awake Behaving Monkey fMRI. In: Soc Neurosci Ann Mtg pp 821.8. Washington, DC.

Ekstrom LB, Bonmassar G, Tootell RB, Roelfsema PR, Vanduffel W (2006) Investigating FEF microstimulation and distractor effects in visual cortex with awake monkey fMRI. In: Soc Neurosci Ann Mtg pp 703.8. Washington, DC.

Ekstrom LB, Roelfsema PR, Arsenault JT, Bonmassar G, Vanduffel W (2008) Bottom-up dependent gating of frontal signals in early visual cortex. Science 321:414-417.

Felleman DJ, Van Essen DC (1991) Distributed hierarchical processing in the primate cerebral cortex. Cereb Cortex 1:1-47.

Ferrier D (1874) The localization of function in brain. Proc R Soc Lond 22:229-232.

Fize D, Vanduffel W, Nelissen K, Denys K, Chef d'hotel C, Faugeras O, Orban GA (2003) The retinotopic organization of primate dorsal V4 and surrounding areas: A functional magnetic resonance imaging study in awake monkeys. J Neurosci 23:7395-7406.

Frey S, Petrides M, Pike GB, Khachaturian MH, Ekstrom LB, Arsenault JT, Vanduffel W (2007) Microstimulation and fMRI of areas 44 and 45 in the non-human primate. In: Soc Neurosci Ann Mtg pp 931.7. Washington DC.

Friston KJ, Buchel C (2000) Attentional modulation of effective connectivity from V2 to V5/MT in humans. Proc Natl Acad Sci U S A 97:7591-7596.

Friston KJ, Harrison L, Penny W (2003) Dynamic causal modelling. Neuroimage 19:1273-1302.

Friston KJ, Holmes AP, Worsley KJ, Poline JB, Frith C, Frackowiak RSJ (1995) Statistical Parametric Maps in Functional Imaging: A General Linear Approach. Hum Brain Mapp 2:189-210.

Fukushima K (1988) A Neural Network for Visual Pattern Recognition. IEEE Computer 21:65-75.

Gabriel C, Gabriel S, Corthout E (1996) The dielectric properties of biological tissues: I. Literature survey. Phys Med Biol 41:2231-2249.

Ghazanfar AA, Nicolelis MA (1997) Nonlinear processing of tactile information in the thalamocortical loop. J Neurophysiol 78:506-510.

Goodale MA, Milner AD (1992) Separate visual pathways for perception and action. Trends Neurosci 15:20-25.

Griswold MA, Jakob PM, Heidemann RM, Nittka M, Jellus V, Wang J, Kiefer B, Haase A (2002) Generalized autocalibrating partially parallel acquisitions (GRAPPA). Magn Reson Med 47:1202-1210.

Grosbras MH, Paus T (2002) Transcranial magnetic stimulation of the human frontal eye field: effects on visual perception and attention. J Cogn Neurosci 14:1109-1120.

Grossberg S (1999) How does the cerebral cortex work? Learning, attention, and grouping by the laminar circuits of visual cortex. Spat Vis 12:163-185.

Hadj-Bouziane F, Bell AH, Knusten TA, Ungerleider LG, Tootell RB (2008) Perception of emotional expressions is independent of face selectivity in monkey inferior temporal cortex. Proc Natl Acad Sci U S A 105:5591-5596.

Hamker FH (2005) The reentry hypothesis: the putative interaction of the frontal eye field, ventrolateral prefrontal cortex, and areas V4, IT for attention and eye movement. Cereb Cortex 15:431-447.

Handy TC, Kingstone A, Mangun GR (1996) Spatial distribution of visual attention: perceptual sensitivity and response latency. Percept Psychophys 58:613-627.

Hawkins HL, Hillyard SA, Luck SJ, Mouloua M, Downing CJ, Woodward DP (1990) Visual attention modulates signal detectability. J Exp Psychol Hum Percept Perform 16:802-811.

Heinze HJ, Mangun GR, Burchert W, Hinrichs H, Scholz M, Munte TF, Gos A, Scherg M, Johannes S, Hundeshagen H (1994) Combined spatial and temporal imaging of brain activity during visual selective attention in humans. Nature 372:543-546.

Herrero JL, Roberts MJ, Delicato LS, Gieselmann MA, Dayan P, Thiele A (2008) Acetylcholine contributes through muscarinic receptors to attentional modulation in V1. Nature 454:1110-1114.

Huerta MF, Krubitzer LA, Kaas JH (1986) Frontal eye field as defined by intracortical microstimulation in squirrel monkeys, owl monkeys, and macaque monkeys: I. Subcortical connections. J Comp Neurol 253:415-439.

Huerta MF, Krubitzer LA, Kaas JH (1987) Frontal eye field as defined by intracortical microstimulation in squirrel monkeys, owl monkeys, and macaque monkeys. II. Cortical connections. J Comp Neurol 265:332-361.

Hupé JM, James AC, Girard P, Lomber SG, Payne BR, Bullier J (2001) Feedback connections act on the early part of the responses in monkey visual cortex. J Neurophysiol 85:134-145.

Hupé JM, James AC, Payne BR, Lomber SG, Girard P, Bullier J (1998) Cortical feedback improves discrimination between figure and background by V1, V2 and V3 neurons. Nature 394:784-787.

Jarraya B, Arsenault JT, van Kerkoerle T, Ekstrom LB, Mandeville JB, Marota JJ, Vanduffel W (2007) Predictive reward value related fMRI activations in macaque. In: Soc Neurosci Ann Mtg pp 641.17. Washington, DC.

Josephs O, Turner R, Friston KJ (1997) Event-rleated fMRI. Hum Brain Mapp 5:243-248.

Juan CH, Shorter-Jacobi SM, Schall JD (2004) Dissociation of spatial attention and saccade preparation. Proc Natl Acad Sci U S A 101:15541-15544.

Kastner S, De Weerd P, Desimone R, Ungerleider LG (1998) Mechanisms of directed attention in the human extrastriate cortex as revealed by functional MRI. Science 282:108-111.

Kastner S, Ungerleider LG (2000) Mechanisms of visual attention in the human cortex. Annu Rev Neurosci 23:315-341.

Kayser C, Petkov CI, Augath M, Logothetis NK (2005) Integration of touch and sound in auditory cortex. Neuron 48:373-384.

Khachaturian MH (2007) Advances in MRI to Probe the Functional and Structural Network of the Macaque Brain. Massachusetts Institute of Technology.

Khachaturian MH, Arsenault JT, Ekstrom LB, Vanduffel W (2007a) V1 modulates visually-driven activity in several visual structures: an awake monkey fMRI study. In: Soc Neurosci Ann Mtg pp 451.5. Washington, DC.

Khachaturian MH, Wisco JJ, Tuch DS (2007b) Boosting the sampling efficiency of q-Ball imaging using multiple wavevector fusion. Magn Reson Med 57:289-296.

Kourtzi Z, Tolias AS, Altmann CF, Augath M, Logothetis NK (2003) Integration of local features into global shapes: monkey and human FMRI studies. Neuron 37:333-346.

Kwong KK, Belliveau JW, Chesler DA, Goldberg IE, Weisskoff RM, Poncelet BP, Kennedy DN, Hoppel BE, Cohen MS, Turner R, . (1992) Dynamic magnetic resonance imaging of human brain activity during primary sensory stimulation. Proc Natl Acad Sci U S A 89:5675-5679.

Leite FP, Tsao D, Vanduffel W, Fize D, Sasaki Y, Wald LL, Dale AM, Kwong KK, Orban GA, Rosen BR, Tootell RB, Mandeville JB (2002) Repeated fMRI using iron oxide contrast agent in awake, behaving macaques at 3 Tesla. Neuroimage 16:283-294.

Li X, Lu ZL, Tjan BS, Dosher BA, Chu W (2008) Blood oxygenation level-dependent contrast response functions identify mechanisms of covert attention in early visual areas. Proc Natl Acad Sci U S A 105:6202-6207.

Liu T, Slotnick SD, Serences JT, Yantis S (2003) Cortical mechanisms of feature-based attentional control. Cereb Cortex 13:1334-1343.

Logothetis NK, Guggenberger H, Peled S, Pauls J (1999) Functional imaging of the monkey brain. Nat Neurosci 2:555-562.

Logothetis NK, Pauls J, Augath M, Trinath T, Oeltermann A (2001a) Neurophysiological investigation of the basis of the fMRI signal. Nature 412:150-157.

Logothetis NK, Pauls J, Oeltermann A, Augath M, Trinath T (2001b) Studying connectivity with electrical microstimulation & fMRI. In: Soc Neurosci Ann Mtg pp 821.27. Washington, DC.

Logothetis NK, Pfeuffer J (2004) On the nature of the BOLD fMRI contrast mechanism. Magn Reson Imaging 22:1517-1531.

Lomber SG, Payne BR, Horel JA (1999) The cryoloop: an adaptable reversible cooling deactivation method for behavioral or electrophysiological assessment of neural function. J Neurosci Methods 86:179-194.

Luck SJ, Chelazzi L, Hillyard SA, Desimone R (1997) Neural mechanisms of spatial selective attention in areas V1, V2, and V4 of macaque visual cortex. J Neurophysiol 77:24-42.

Mandeville JB, Ekstrom LB, Marota JJ, Jenkins BG, Vanduffel W (2005) Contrast-enhanced fMRI of cocaine action in awake non-human primate. In: 13th Scientific Mtg of the Int Soc Magn Reson Med pp 1506. Miami, FL.

Mandeville JB, Jenkins BG, Chen YC, Choi JK, Kim YR, Belen D, Liu C, Kosofsky BE, Marota JJ (2004) Exogenous contrast agent improves sensitivity of gradient-echo functional magnetic resonance imaging at 9.4 T. Magn Reson Med 52:1272-1281.

Mandeville JB, Jenkins BG, Kosofsky BE, Moskowitz MA, Rosen BR, Marota JJ (2001) Regional sensitivity and coupling of BOLD and CBV changes during stimulation of rat brain. Magn Reson Med 45:443-447.

Martinez-Trujillo J, Treue S (2002a) Attentional modulation strength in cortical area MT depends on stimulus contrast. Neuron 35:365-370.

Martinez-Trujillo JC, Treue S (2002b) Attentional modulation strength in cortical area MT depends on stimulus contrast. Neuron 35:365-370.

Martinez-Trujillo JC, Treue S (2004) Feature-based attention increases the selectivity of population responses in primate visual cortex. Curr Biol 14:744-751.

Maunsell JH, Treue S (2006) Feature-based attention in visual cortex. Trends Neurosci 29:317-322.

Mayberg HS, Lozano AM, Voon V, McNeely HE, Seminowicz D, Hamani C, Schwalb JM, Kennedy SH (2005) Deep brain stimulation for treatment-resistant depression. Neuron 45:651-660.

McAdams CJ, Maunsell JH (1999a) Effects of attention on orientation-tuning functions of single neurons in macaque cortical area V4. J Neurosci 19:431-441.

McAdams CJ, Maunsell JH (1999b) Effects of attention on the reliability of individual neurons in monkey visual cortex. Neuron 23:765-773.

McAdams CJ, Maunsell JH (2000) Attention to both space and feature modulates neuronal responses in macaque area V4. J Neurophysiol 83:1751-1755.

McIntosh AR, Gonazlez-Lima F (1994) Structural Equation Modeling and Its Application to Network Analysis in Functional Brain Imaging. Hum Brain Mapp 2:2-22.

McNicol D (1972) A Primer of Signal Detection Theory. London: George Allen and Unwin.

Michelson AA (1927) Studies in Optics. Chicago: Univ. Chicago Press.

Mioche L, Singer W (1988) Long-term recordings and receptive field measurements from single units of the visual cortex of awake unrestrained kittens. J Neurosci Methods 26:83-94.

Moeller S, Freiwald WA, Tsao DY (2008) Patches with links: a unified system for processing faces in the macaque temporal lobe. Science 320:1355-1359.

Moore CI, Nelson SB, Sur M (1999) Dynamics of neuronal processing in rat somatosensory cortex. Trends Neurosci 22:513-520.

Moore T, Armstrong KM (2003) Selective gating of visual signals by microstimulation of frontal cortex. Nature 421:370-373.

Moore T, Armstrong KM, Fallah M (2003) Visuomotor origins of covert spatial attention. Neuron 40:671-683.

Moore T, Fallah M (2004) Microstimulation of the frontal eye field and its effects on covert spatial attention. J Neurophysiol 91:152-162.

Morel A, Bullier J (1990) Anatomical segregation of two cortical visual pathways in the macaque monkey. Vis Neurosci 4:555-578.

Muller HJ, Humphreys GW (1991) Luminance-increment detection: capacity-limited or not? J Exp Psychol Hum Percept Perform 17:107-124.

Munoz DP, Everling S (2004) Look away: the anti-saccade task and the voluntary control of eye movement. Nat Rev Neurosci 5:218-228.

Murphey DK, Maunsell JH (2007) Behavioral detection of electrical microstimulation in different cortical visual areas. Curr Biol 17:862-867.

Murphey DK, Maunsell JH (2008) Electrical microstimulation thresholds for behavioral detection and saccades in monkey frontal eye fields. Proc Natl Acad Sci U S A 105:7315-7320.

Naka KI, Rushton WA (1966) S-potentials from colour units in th retina of fish (Cyprinidae). J Physiol 185:536-555.

Nelissen K, Luppino G, Vanduffel W, Rizzolatti G, Orban GA (2005) Observing others: multiple action representation in the frontal lobe. Science 310:332-336.

Nelissen K, Vanduffel W, Orban GA (2006) Charting the lower superior temporal region, a new motion-sensitive region in monkey superior temporal sulcus. J Neurosci 26:5929-5947.

Nichols MJ, Newsome WT (2002) Middle temporal visual area microstimulation influences veridical judgments of motion direction. J Neurosci 22:9530-9540.

Nichols T, Brett M, Andersson J, Wager T, Poline JB (2005) Valid conjunction inference with the minimum statistic. Neuroimage 25:653-660.

Nir Y, Dinstein I, Malach R, Heeger DJ (2008) BOLD and spiking activity. Nat Neurosci 11:523-524.

Nir Y, Fisch L, Mukamel R, Gelbard-Sagiv H, Arieli A, Fried I, Malach R (2007) Coupling between neuronal firing rate, gamma LFP, and BOLD fMRI is related to interneuronal correlations. Curr Biol 17:1275-1285.

O'Craven KM, Downing PE, Kanwisher N (1999) fMRI evidence for objects as the units of attentional selection. Nature 401:584-587.

Ogawa S, Tank DW, Menon R, Ellermann JM, Kim SG, Merkle H, Ugurbil K (1992) Intrinsic signal changes accompanying sensory stimulation: functional brain mapping with magnetic resonance imaging. Proc Natl Acad Sci U S A 89:5951-5955.

Orban GA, Fize D, Peuskens H, Denys K, Nelissen K, Sunaert S, Todd J, Vanduffel W (2003) Similarities and differences in motion processing between the human and macaque brain: evidence from fMRI. Neuropsychologia 41:1757-1768.

Orban GA, Van Essen D, Vanduffel W (2004) Comparative mapping of higher visual areas in monkeys and humans. Trends Cogn Sci 8:315-324.

Payne BR, Lomber SG, Villa AE, Bullier J (1996) Reversible deactivation of cerebral network components. Trends Neurosci 19:535-542.

Penfield W, Boldrey E (1937) Somatic motor and sensory representation in the cerebral cortex of man as studied by electrical stimulation. Brain 60:389-443.

Peng X, Sereno ME, Silva AK, Lehky SR, Sereno AB (2008) Shape selectivity in primate frontal eye field. J Neurophysiol 100:796-814.

Petkov CI, Kayser C, Steudel T, Whittingstall K, Augath M, Logothetis NK (2008) A voice region in the monkey brain. Nat Neurosci 11:367-374.

Pinsk MA, DeSimone K, Moore T, Gross CG, Kastner S (2005a) Representations of faces and body parts in macaque temporal cortex: a functional MRI study. Proc Natl Acad Sci U S A 102:6996-7001.

Pinsk MA, Moore T, Richter MC, Gross CG, Kastner S (2005b) Methods for functional magnetic resonance imaging in normal and lesioned behaving monkeys. J Neurosci Methods 143:179-195.

Ponce CR, Lomber SG, Born RT (2008) Integrating motion and depth via parallel pathways. Nat Neurosci 11:216-223.

Posner MI, Snyder CR, Davidson BJ (1980) Attention and the detection of signals. J Exp Psychol 109:160-174.

Poupon C, Clark CA, Frouin V, Regis J, Bloch I, Le Bihan D, Mangin J (2000) Regularization of diffusion-based direction maps for the tracking of brain white matter fascicles. Neuroimage 12:184-195.

Preuss TM, Goldman-Rakic PS (1991) Myelo- and cytoarchitecture of the granular frontal cortex and surrounding regions in the strepsirhine primate Galago and the anthropoid primate Macaca. J Comp Neurol 310:429-474.

Reilly JP (1998) Excitation Models. In: Applied Bioelectricity: From Electrical Stimulation to Electropathology pp 105-147. New York: Springer-Verlag.

Reynolds JH, Chelazzi L (2004) Attentional modulation of visual processing. Annu Rev Neurosci 27:611-647.

Reynolds JH, Chelazzi L, Desimone R (1999) Competitive mechanisms subserve attention in macaque areas V2 and V4. J Neurosci 19:1736-1753.

Reynolds JH, Pasternak T, Desimone R (2000) Attention increases sensitivity of V4 neurons. Neuron 26:703-714.

Reynolds JH, Sundberg KA (2007) A Simple Model Reconciles Attention-Dependent Contrast- and Response-Gain Modulation. In: Soc Neurosci Ann Mtg pp 177.9. Washington, DC.

Rizzolatti G, Riggio L, Dascola I, Umilta C (1987) Reorienting attention across the horizontal and vertical meridians: evidence in favor of a premotor theory of attention. Neuropsychologia 25:31-40.

Robinson DA, Fuchs AF (1969) Eye movements evoked by stimulation of frontal eye fields. J Neurophysiol 32:637-648.

Roebroeck A, Formisano E, Goebel R (2005) Mapping directed influence over the brain using Granger causality and fMRI. Neuroimage 25:230-242.

Roelfsema PR (2006) Cortical algorithms for perceptual grouping. Annu Rev Neurosci 29:203-227.

Roelfsema PR, Lamme VA, Spekreijse H (1998) Object-based attention in the primary visual cortex of the macaque monkey. Nature 395:376-381.

Romo R, Hernandez A, Zainos A, Salinas E (1998) Somatosensory discrimination based on cortical microstimulation. Nature 392:387-390.

Rossi AF, Paradiso MA (1995) Feature-specific effects of selective visual attention. Vision Res 35:621-634.

Ruff CC, Blankenburg F, Bjoertomt O, Bestmann S, Freeman E, Haynes JD, Rees G, Josephs O, Deichmann R, Driver J (2006) Concurrent TMS-fMRI and psychophysics reveal frontal influences on human retinotopic visual cortex. Curr Biol 16:1479-1488.

Salzman CD, Britten KH, Newsome WT (1990) Cortical microstimulation influences perceptual judgements of motion direction. Nature 346:174-177.

Sasaki Y, Rajimehr R, Kim BW, Ekstrom LB, Vanduffel W, Tootell RB (2006) The radial bias: a different slant on visual orientation sensitivity in human and nonhuman primates. Neuron 51:661-670.

Schacter DL, Buckner RL, Koutstaal W, Dale AM, Rosen BR (1997) Late onset of anterior prefrontal activity during true and false recognition: an event-related fMRI study. Neuroimage 6:259-269.

Schall JD (1995) Neural basis of saccade target selection. Rev Neurosci 6:63-85.

Schall JD (1997) Visuomotor Areas of The Frontal Lobe. In: Cerebral Cortex (Rockland SKJ, ed), pp 527-638. New York: Plenum Press.

Schall JD (2002) The neural selection and control of saccades by the frontal eye field. Philos Trans R Soc Lond B Biol Sci 357:1073-1082.

Schall JD, Morel A, King DJ, Bullier J (1995) Topography of visual cortex connections with frontal eye field in macaque: convergence and segregation of processing streams. J Neurosci 15:4464-4487.

Schiff ND, Giacino JT, Kalmar K, Victor JD, Baker K, Gerber M, Fritz B, Eisenberg B, Biondi T, O'Connor J, Kobylarz EJ, Farris S, Machado A, McCagg C, Plum F, Fins JJ, Rezai AR (2007) Behavioural improvements with thalamic stimulation after severe traumatic brain injury. Nature 448:600-603.

Schiller PH, Sandell JH, Maunsell JH (1987) The effect of frontal eye field and superior colliculus lesions on saccadic latencies in the rhesus monkey. J Neurophysiol 57:1033-1049.

Schwabe L, Obermayer K, Angelucci A, Bressloff PC (2006) The role of feedback in shaping the extra-classical receptive field of cortical neurons: a recurrent network model. J Neurosci 26:9117-9129.

Sclar G, Maunsell JH, Lennie P (1990) Coding of image contrast in central visual pathways of the macaque monkey. Vision Res 30:1-10.

Segraves MA, Goldberg ME (1987) Functional properties of corticotectal neurons in the monkey's frontal eye field. J Neurophysiol 58:1387-1419.

Sereno ME, Trinath T, Augath M, Logothetis NK (2002) Three-dimensional shape representation in monkey cortex. Neuron 33:635-652.

Shmuel A, Augath M, Oeltermann A, Logothetis NK (2006) Negative functional MRI response correlates with decreases in neuronal activity in monkey visual area V1. Nat Neurosci 9:569-577.

Silvanto J, Lavie N, Walsh V (2006) Stimulation of the human frontal eye fields modulates sensitivity of extrastriate visual cortex. J Neurophysiol 96:941-945.

Simons DJ (1985) Temporal and spatial integration in the rat SI vibrissa cortex. J Neurophysiol 54:615-635.

Smirnakis SM, Brewer AA, Schmid MC, Tolias AS, Schuz A, Augath M, Inhoffen W, Wandell BA, Logothetis NK (2005) Lack of long-term cortical reorganization after macaque retinal lesions. Nature 435:300-307.

Somers DC, Todorov EV, Siapas AG, Toth LJ, Kim DS, Sur M (1998) A local circuit approach to understanding integration of long-range inputs in primary visual cortex. Cereb Cortex 8:204-217.

Sommer MA, Wurtz RH (1998) Frontal eye field neurons orthodromically activated from the superior colliculus. J Neurophysiol 80:3331-3335.

Sperling G, Melchner MJ (1978) The attention operating characteristic: examples from visual search. Science 202:315-318.

Stanton GB, Bruce CJ, Goldberg ME (1995) Topography of projections to posterior cortical areas from the macaque frontal eye fields. J Comp Neurol 353:291-305.

Stanton GB, Goldberg ME, Bruce CJ (1988) Frontal eye field efferents in the macaque monkey: I. Subcortical pathways and topography of striatal and thalamic terminal fields. J Comp Neurol 271:473-492.

Suzuki H, Azuma M (1983) Topographic studies on visual neurons in the dorsolateral prefrontal cortex of the monkey. Exp Brain Res 53:47-58.

Taylor PC, Nobre AC, Rushworth MF (2007) FEF TMS affects visual cortical activity. Cereb Cortex 17:391-399.

Tehovnik EJ (1996) Electrical stimulation of neural tissue to evoke behavioral responses. J Neurosci Methods 65:1-17.

Tehovnik EJ, Sommer MA, Chou IH, Slocum WM, Schiller PH (2000) Eye fields in the frontal lobes of primates. Brain Res Brain Res Rev 32:413-448.

The Deep-Brain Stimulation For Parkinson's Disease Study Group (2001) Deep-brain stimulation of the subthalamic nucleus or the pars interna of the globus pallidus in Parkinson's disease. N Engl J Med 345:956-963.

Thompson KG, Bichot NP, Schall JD (1997) Dissociation of visual discrimination from saccade programming in macaque frontal eye field. J Neurophysiol 77:1046-1050.

Tolias AS, Smirnakis SM, Augath MA, Trinath T, Logothetis NK (2001) Motion processing in the macaque: revisited with functional magnetic resonance imaging. J Neurosci 21:8594-8601.

Tolias AS, Sultan F, Augath M, Oeltermann A, Tehovnik EJ, Schiller PH, Logothetis NK (2005) Mapping cortical activity elicited with electrical microstimulation using FMRI in the macaque. Neuron 48:901-911.

Tootell RB, Reppas JB, Kwong KK, Malach R, Born RT, Brady TJ, Rosen BR, Belliveau JW (1995) Functional analysis of human MT and related visual cortical areas using magnetic resonance imaging. J Neurosci 15:3215-3230.

Tootell RB, Tsao D, Vanduffel W (2003) Neuroimaging weighs in: humans meet macaques in "primate" visual cortex. J Neurosci 23:3981-3989.

Treue S, Martinez-Trujillo JC (1999) Feature-based attention influences motion processing gain in macaque visual cortex. Nature 399:575-579.

Tsao DY, Freiwald WA, Knutsen TA, Mandeville JB, Tootell RB (2003a) Faces and objects in macaque cerebral cortex. Nat Neurosci 6:989-995.

Tsao DY, Freiwald WA, Tootell RB, Livingstone MS (2006) A cortical region consisting entirely of face-selective cells. Science 311:670-674.

Tsao DY, Vanduffel W, Sasaki Y, Fize D, Knutsen TA, Mandeville JB, Wald LL, Dale AM, Rosen BR, Van Essen DC, Livingstone MS, Orban GA, Tootell RB (2003b) Stereopsis activates V3A and caudal intraparietal areas in macaques and humans. Neuron 39:555-568.

Tuch DS, Wisco JJ, Khachaturian MH, Ekstrom LB, Kotter R, Vanduffel W (2005) Q-ball imaging of macaque white matter architecture. Philos Trans R Soc Lond B Biol Sci 360:869-879.

Ungerleider LG, Desimone R (1986a) Cortical connections of visual area MT in the macaque. J Comp Neurol 248:190-222.

Ungerleider LG, Desimone R (1986b) Projections to the superior temporal sulcus from the central and peripheral field representations of V1 and V2. J Comp Neurol 248:147-163.

Ungerleider LG, Mishkin M (1982) Two cortical visual systems. In: The analysis of visual behavior (Ingle DJ, Mansfield RJW, Goodale MA, eds), pp 549-586. Cambridge, MA: MIT Press.

Van Essen DC, Drury HA, Dickson J, Harwell J, Hanlon D, Anderson CH (2001) An integrated software suite for surface-based analyses of cerebral cortex. J Am Med Inform Assoc 8:443-459.

Vanduffel W, Fize D, Mandeville JB, Nelissen K, Van Hecke P, Rosen BR, Tootell RB, Orban GA (2001) Visual motion processing investigated using contrast agent-enhanced fMRI in awake behaving monkeys. Neuron 32:565-577.

Vanduffel W, Fize D, Peuskens H, Denys K, Sunaert S, Todd JT, Orban GA (2002) Extracting 3D from motion: differences in human and monkey intraparietal cortex. Science 298:413-415.

Vanduffel W, Payne BR, Lomber SG, Orban GA (1997) Functional impact of cerebral connections. Proc Natl Acad Sci U S A 94:7617-7620.

Vanduffel W, Wardak C, Nelissen K, Orban GA (2004) Spatial attention in monkeys investigated using fMRI. In: Soc Neurosci Ann Mtg pp 717.11. Washington DC.

Vecera SP, Farah MJ (1994) Does visual attention select objects or locations? J Exp Psychol Gen 123:146-160.

Vogels R, Orban GA (1994) Activity of inferior temporal neurons during orientation discrimination with successively presented gratings. J Neurophysiol 71:1428-1451.

Wedeen VJ, Hagmann P, Tseng WY, Reese TG, Weisskoff RM (2005) Mapping complex tissue architecture with diffusion spectrum magnetic resonance imaging. Magn Reson Med 54:1377-1386.

Wedeen VJ, Wang RP, Schmahmann JD, Benner T, Tseng WY, Dai G, Pandya DN, Hagmann P, D'Arceuil H, de Crespigny AJ (2008) Diffusion spectrum magnetic resonance imaging (DSI) tractography of crossing fibers. Neuroimage 41:1267-1277.

Williford T, Maunsell JH (2006) Effects of spatial attention on contrast response functions in macaque area V4. J Neurophysiol 96:40-54.

Winkowski DE, Knudsen EI (2006) Top-down gain control of the auditory space map by gaze control circuitry in the barn owl. Nature 439:336-339.

Worsley KJ, Marrett S, Neelin P, Vandal AC, Friston KJ, Evans AC (1996) A unified statistical approach for determining significant signals in images of cerebral activation. Hum Brain Mapp 4:58-73.

Xue R, van Zijl PC, Crain BJ, Solaiyappan M, Mori S (1999) In vivo three-dimensional reconstruction of rat brain axonal projections by diffusion tensor imaging. Magn Reson Med 42:1123-1127.

Yantis S, Serences JT (2003) Cortical mechanisms of space-based and object-based attentional control. Curr Opin Neurobiol 13:187-193.

Yarbus AL (1961) Eye movements during the examination of complicated objects. Biofizika 6(2):52-56.

Zarahn E, Aguirre G, D'Esposito M (1997) A trial-based experimental design for fMRI. Neuroimage 6:122-138.